

**Hydraulic fracture monitoring: Integrated analysis of DAS, pumping
information, microseismicity and PKN modelling**

by

Ana Karen Ortega Perez

A thesis submitted in partial fulfillment of the requirements for the degree of

Master of Science

in

Geophysics

Department of Physics
University of Alberta

© Ana Karen Ortega Perez, 2022

Abstract

Well-monitoring before, during and after hydraulic fracturing treatment is essential to accomplish a successful fracture completion program. By knowing the geometry, orientation, and propagation of the hydraulic fractures, we can identify potential completion issues during fracturing operations and help in the design of more efficient unconventional reservoir completions. Distributed Acoustic Sensing (DAS) is an emerging technology in hydraulic fracture monitoring that enables continuous, real-time measurements along the entire length of a fiber optic cable. The low-frequency band of DAS records strain perturbations of the medium, due to fracture propagation, which provides critical constraints on hydraulic fracture geometry.

In this study, the low-frequency DAS strain fronts was analyzed, with their corresponding pumping curves, for one hydraulic fracturing treatment to obtain information of the hydraulic fractures like fracture azimuth, propagation speed, number of fractures created during each stage and re-stimulation of pre-existent fractures. Then, the microseismicity of the treatment was analyzed to obtain information on hydraulic fractures like length, height, trajectory and cloud growth over time. The microseismicity was also projected onto the strain fronts to study the development of the events with respect to the fracture signal and to find correlations between the strain changes and the microseismic events. Finally, the PKN model was computed using parameters from the stimulation treatment and the DAS strain fronts to forecast anticipated fracture lengths against observations. The PKN modeling results were compared to the microseismic and DAS results to find stages where the hydraulic fractures did not grow or propagate as expected.

The low-frequency DAS is able to obtain information on hydraulic fractures that would need extra processing or might not be picked up using other records as microseismicity. However, the spatial constraint of the measurements in DAS needs to be taken into consideration. This spatial constraint can be addressed by the integration of other records. In general, there is good agreement between the LF DAS data, the pumping information, the microseismic data and the PKN model. But when they do not agree on a stage, that gives us an indication that something unexpected happened during injection. Models describing the expected behavior of the different records analyzed in this research were created to explain some possible scenarios of fracture propagation. Most stages in this treatment fall within one of these models.

Preface

This dissertation is submitted for the degree of Master of Science in Geophysics at the University of Alberta. The research described herein is original, and neither this nor any substantially similar dissertation was or is being submitted for any other degree or other qualification at any other university.

"It was the best of times, it was the worst of times, it was the age of wisdom, it was the age of foolishness, it was the epoch of belief, it was the epoch of incredulity, it was the season of light, it was the season of darkness, it was the spring of hope, it was the winter of despair."

- Charles Dickens

To God, who all my life has been faithful and good to me.

To my parents, who gave everything they had so that I could accomplish my dreams.

To my brother, who always supported me unconditionally.

To Rafael, who was light in dark times.

Acknowledgements

I would like to express my gratitude to my supervisor, Dr. Mirko van der Baan for his support, patience, motivation and kindness. I will always be grateful to him for believing in me and giving me this amazing opportunity. He taught me so much during the course of my MSc and helped me further develop my abilities and skills. I couldn't have had a better supervisor.

I would like to acknowledge the members of my final examination committee, Juliana Leung, Vadim Kravchinsky, and Wojciech Rozmus, as well as Bruce Sutherland for their valuable feedback on my thesis.

I would like to thank the Sponsors of the Microseismic Industry Consortium for their financial support and the anonymous company that gave me permission to use and display the data for my thesis.

I would also like to express my appreciation to all my friends and colleagues from Geophysics and Physics at the University of Alberta. Specially to Shreyaa and Lucia, who were always there for me as friends, sisters, cheerleaders and therapists.

Finally, I am deeply grateful to my family; my dad, my mom, my brother, and my Rafael. They have supported me, encouraged me, loved me and made many sacrifices to help me accomplish my goals. Without them, this achievement wouldn't have been possible.

Table of Contents

1	Introduction	1
1.1	Hydraulic fracturing background	1
1.1.1	Hydraulic fractures	2
1.2	Site geological background	4
1.3	Motivation	5
1.4	Objectives	5
1.5	Outline	6
	References	8
2	Low-frequency DAS analysis	10
2.1	DAS Background	10
2.2	Pumping information background	18
2.3	Methodology	20
2.3.1	DAS strain fronts characteristics	20
2.3.2	Fracture and pumping characteristics	21
2.4	Results and Discussion	24
2.4.1	Characteristics in strain fronts and engineering curves	25
2.4.2	Propagation speeds	30
2.4.3	Fracture connection map	32
2.4.4	Characteristic distribution per stage	33
2.5	DAS analysis conclusions	37
	References	39
3	Microseismic analysis	42
3.1	Microseismic monitoring of hydraulic fractures	42
3.1.1	Microseismic Spatio-temporal evolution and integration with pumping information and DAS	44
3.2	Methodology	49
3.2.1	Microseismic cloud analysis	50

3.2.2	Microseismic data integration with DAS and pumping information	54
3.3	Results and Discussion	56
3.3.1	Microseismic cloud analysis results	56
3.3.2	Microseismic cloud growth patterns and MS-DAS integration results	63
3.4	Microseismic analysis conclusions	76
	References	78
4	PKN modelling analysis	80
4.1	2D Hydraulic fracturing models	80
4.1.1	KGD model	80
4.1.2	PKN model	81
4.2	Methodology	83
4.2.1	Fracture half-length at the end of injection and at the DAS hit time	83
4.2.2	PKN integration with DAS to compare to the microseismic cloud (PKN vs MS plots)	86
4.3	Results and Discussion	88
4.3.1	Fracture half-length at the end of injection	88
4.3.2	Fracture half-length at the DAS hit time	89
4.3.3	PKN vs MS plots	90
4.3.4	PKN results	95
4.3.5	PKN modelling conclusions	97
	References	100
5	Discussion	101
5.1	Integrated scenarios	101
5.1.1	Scenario 1 - Expected stage	104
5.1.2	Scenario 2 - Re-stimulation of a pre-existent fracture	114
5.1.3	Scenario 3 - Re-stimulation of a pre-existent fracture with new hydraulic fracture	118
5.1.4	Scenario 4 - Fracture deviation	122
5.1.5	Scenario 5 - MS cloud longer than expected	125
	References	130
6	Conclusions	132
6.1	Suggested future research	135

List of Tables

4.1	Geomechanical and completion parameters for the PKN fracture propagation model.	84
5.1	Correlations between the expected characteristics.	114

List of Figures

1.1	Schematic illustration of cased and open-hole completion methods. a) For a cased well the casing is perforated creating points that allow the entrance of fluids into the formation. b) For an open wellbore, a sliding sleeve is placed and then a ball is pumped inside a liner. When the ball seats onto the sliding sleeve assembly the port opens and allows fluid to enter the formation (Eaton, 2018).	2
1.2	Wells geometry, upper (a) and side (b) view. Treated well analyzed in this thesis is represented by the blue line. The monitoring well with the fiber optic cable is the black line. The wells spacing is 150 m and both wells are located in the Middle Montney formation.	5
2.1	Fiber optic sensing configurations. Single point sensors have only one sensor at the end of the fiber. Multiplexed point sensors have multiple sensors distributed along the cable. Distributed sensors use the fiber as the sensor. Modified from Hartog (2017).	11
2.2	Components of the scattered light. Brillouin and Raman scattering are the inelastic scattering of light in a medium caused by acoustic or optical phonons, respectively. The backscattered light can have shorter (anti-Stokes) or longer (Stokes) wavelength than the incident light. Rayleigh scattering is the elastic scattering of light caused by much smaller particles. The backscattered light preserves the same wavelength as the incident light. Modified from Molenaar and Cox (2013).	12
2.3	Principle of operation of Distributed Acoustic Sensors: a pulse travels along an optical fiber, and the phase of the Rayleigh backscattered light that returns to the interrogator is recorded. Retrieved from Fernandez-Ruiz et al. (2020).	13

2.4	Hypothetical strain and cable responses of a propagating hydraulic fracture. Times T1 and T2 show the response of a fracture approaching the monitor well with the fiber optic cable. Time T3 displays the signal when the fracture intercepts the monitoring well. Time T4 shows the strain pattern just after the stimulation ends. Modified from Liu et al. (2020) and Ugueto et al. (2019)	15
2.5	DAS Strain Front of one stage from an offset well with some characteristics pointed. The x-axis is time, and the y-axis is measured depth. Red indicates extension and blue compression strain. Second row shows the pumping information of the stage; Slurry rate times 10 (m^3/min) is the red curve, Bottom-hole pressure (MPa) is the blue curve, and Bottom-hole concentration (kg/m^3) is the purple curve. The treatment clusters and the fracture hits projected onto the MD of the monitoring well are shown on the left in green triangles and red circles respectively.	17
2.6	Idealized diagram of two possible types of pressure behavior during fracture treatment depending upon various underground conditions. a) FBP is higher than the fracture propagation pressure. b) There is no distinct FBP. Modified from Hubbert and Willis (1957).	20
2.7	DAS strain front of one stage with picked strain front characteristics and the start of the Relaxation zone represented by a black line. See Figure 2.5 for detailed description of the legend and other symbols.	21
2.8	DAS strain front of one stage with all its fracture and pumping characteristics picked out. Start of injection, yellow line. FBP, blue line. Frac hit time, green line. The Frac MDs are the red circles on the left. End of the injection, pink line. Legend and symbols as in Figure 2.5.	22
2.9	Unexpected behavior in engineering curves and strain fronts. a) Engineering curves show a stage with no noticeable FBP peak. The concave portion of the curve before it flattens was selected as the FBP. b) Strain front shows a dragonfly with no heart-shaped tip. The frac hit time was selected as the convergence of the blue wings. The frac hit MD was the midrange of the top and bottom depth of the wings. See Figure 2.5 for full legend.	23
2.10	Upper view of treated well (blue) and monitoring well (black) with the perforation clusters (blue dots) and the frac hits (red dots). Stage 1 cluster is connected to the Stage 1 frac hit with a red line that shows the deviation angle of the fracture propagation direction (Frac azimuth).	24

2.11	Strain front and engineering curves of Stage 13 with its characteristics picked out.	27
2.12	Strain front and engineering curves of Stage 26 with its characteristics picked out. Multiple dragonflies are visible in the strain front.	27
2.13	Strain front of Stage 34 with its characteristics picked out. Two dragonflies are visible, the first fracture stops propagating mid injection meanwhile the second one continues until the end of injection.	28
2.14	2 cases of Stages with antennas in strain fronts. a) Stage 36 was stimulated twice, the second time the dragonfly does not present the hear-shaped tip. b) Stage 6 has an antenna but also a heart-shaped tip, the antenna is a fracture from Stage 5 being reopened but the injection also created a new fracture as the hear-shaped tip is present.	28
2.15	Chart with the DAS characteristics; heart tip, antenna and multiple fractures, and engineering curves characteristic; FBP, distribution across all stages. Blue means stages have that characteristic and red means they do not.	29
2.16	Fracture propagation speed for every stage using DAS strain fronts. The average speed is 21.13 m/min. Speeds above 45 m/min were considered outliers and eliminated. Trendline (dotted blue line) and best fit linear equation are displayed. Upper and lower boundaries of the data are represented by the red lines.	31
2.17	Time difference between the end of injection and the start of the Relaxation zone. The average time difference which is 52 seconds. Trendline (dotted blue line) and best fit linear equation are displayed. Upper and lower boundaries of the data are represented by the red lines.	31
2.18	Fracture connection map for all stages, with original wells geometry See Figure 2.10 for full legend. Displays the direction of fracture propagation. The stimulation started on the right in Stage 1 (toe of the well) and finished on the left in Stage 38 (heel of the well).	32
2.19	Fracture connection map for all stages, with original wells geometry. See Figure 2.18 for full legend. The dots represent characteristics present in each stage. Green means the presence of a heart-shaped tip, purple means the presence of an antenna, yellow means multiple frags, cyan means clear FBP peak, and the pink arrows mark the stages that did not propagate perpendicular from the treated well.	35
2.20	Stage 18 strain front and engineering curves. This stage is an example of a stage that has a heart-shaped tip, no FBP peak, and an antenna.	36

2.21	Stage 23 strain front and engineering curves. This stage is an example of a stage that has a heart-shaped tip, no FBP peak, and no antenna, but the tail of the previous stage was reopened during treatment. . . .	36
3.1	Example of an r-t plot. Distances of the MS events from the center of the injection interval versus their occurrence times. Dotted lines denote the expected distance of diffusion-controlled microseismicity (Equation (3.1)) for three different diffusivities $D= 0.5, 1, \text{ and } 2 \text{ m}^2/\text{s}$. Retrieved from Shapiro et al. (1997).	45
3.2	Schematic of three different scenarios of microseismicity rates (grey area) relative to the engineering curves; bottom-hole pressure (blue), injection rate (red), and proppant concentration (purple). a) High MS concentration at the beginning of injection indicates fracture initiation. b) Constant MS during injection means consistent fracture growth. c) High MS concentration towards the end of injection indicates fracture blockage or fault activation. Modified from Maxwell (2014).	48
3.3	Various scenarios based on pressure and microseismic activity rates during the injection. Scenarios 1 to 5 display the behavior that shows uniform fracture growth, formation hardening, formation weakening, fracture resistance, and fracture compliance, respectively. Modified from Maxwell (2014).	49
3.4	Fracture connection map with microseismic cloud and its linear regression for one stage. The microseismic events are the blue stars and the linear regression of the MS clouds is the long red line with confidence boundaries being the dotted red lines.	51
3.5	Front view of the wells with the microseismic cloud represented by the blue stars. The treated well is at the origin ($x=0$) represented by the cyan dot and the monitoring well is 150 meters apart from the treated well represented by the black dot. The MS cloud length was calculated by measuring the distance between the treated well and the last event on the right. The height of the cloud was estimated by the difference in depths between the shallowest and deepest events.	52
3.6	Horizontal schematic of the wells. The treated well is the blue line and the monitoring well is the black one. The MS cloud length for one stage is represented by the pink line which is placed at the stage cluster position. Fracture trajectory direction was not considered. . . .	52

3.7	Stage r-t plot that shows the distance of the microseismic event from the injection point over time. MS events on the NE of the treated well are represented by the black stars, and the MS events on the SW are represented by the red stars. DAS characteristics and FBP are depicted by the same vertical lines and colors as in the strain fronts in Chapter 2.	53
3.8	Steps to plot MS events on top of strain fronts. a) Filtering, eliminating MS events (blue stars) on the SW of the treated well (blue line). b) Projecting MS events onto the monitoring well (black line) to get their measured depth. Projected MS events are the black stars. c) Using their measured depth we plotted the MS events (black stars) on top of the strain fronts as a function of time.	55
3.9	Microseismic events plotted as a function of their magnitude and the time of their occurrence.	55
3.10	Horizontal plane of the wells with the microseismic clouds of all stages. The blue line is the treated, and the black line is the monitoring well. The microseismic clouds are shown in different colors depending on the stage. Microseismic events are propagating mostly towards the northeast.	57
3.11	Horizontal plane of the wells with the microseismic clouds for: a) Stages 1 - 4. b) Stages 5 - 8. c) Stages 9 - 12. d) Stages 13 - 16.	58
3.12	Horizontal plane of the wells with the microseismic clouds for: a) Stages 17 - 20. b) Stages 21 - 24. c) Stages 25 - 28. d) Stages 29 - 32.	59
3.13	Horizontal plane of the wells with the microseismic clouds for: a) Stages 33 - 36. b) Stages 37 and 38.	60
3.14	Horizontal schematic of the wells. The microseismic cloud lengths for all stages are represented by the pink lines placed at the stage cluster position. Purple arrows represent the stages where the MS cloud propagated mainly towards the SW.	62
3.15	Graph that shows the measured height for all microseismic clouds which represents the fracture height for every stage. The average height is 162.8 meters.	62
3.16	Stage 31. a) r-t plot with normal development pattern. Black stars are MS events propagating towards NE and red towards the SW. DAS characteristics and FBP are depicted as well. b) DAS-MS plot with microseismicity (black stars) on the strain front, and with the DAS characteristics and FBP depicted.	65

3.17	Stage 18. a) r-t plot with "halted growth" development pattern. b) DAS-MS plot. The MS events are on top of the dragonfly and happen continuously. See Figure 3.16 for the full legend.	66
3.18	Stage 25 a) r-t plot and b) DAS-MS plot. The r-t plot uncovers a separate cluster of events from the main MS growth (orange circle). The new injection might have caused stress changes at the old location and opened a previous fracture. This stage also has two different diffusive patterns (blue and yellow arrows).	69
3.19	Stage 14 a) r-t plot and b) DAS-MS plot. There are clearly MS events still occurring at the previous stage which is why there is microseismicity happening immediately after the start of injection (orange circle). This stage presents fault/fracture reactivation in the middle of injection most likely due to stress changes rather than fluids (green circle).	70
3.20	Stage 6 a) DAS-MS plot and b) r-t plot. The MS events travel to the toe of the well during injection in the strain front (orange circle). The r-t plot presents linear MS growth around the same time (orange circle). This can be interpreted as fluids moving into pre-existing fractures or faults and reactivating them.	71
3.21	Plot with the strain front of Stage 2 with overlaying microseismicity at the top. This stage shows behavior present in the first stages of the treatment where MS occurs mostly when the proppant enters as seen on the engineering curves.	73
3.22	2 cases of Stages with increased microseismicity activity after the end of the injection. a) Stage 9 increase in MS might be due to increased sensitivity resulting from the pumping ending. b) Stage 23 presents the BH pressure spike characteristic of the water hammer effect, so the increase in MS might be due to that.	73
3.23	Fracture connection map for all stages, with original wells geometry. See Figure 2.18 for full legend. The squares represent characteristics present in each stage. Pink means that the fracture propagated mostly towards the SW, green means "normal" pattern in the r-t plots, orange="halted growth", cyan="reactivation", grey="stress transfer" and the brown ones mean that the MS is not on top of the dragonfly.	76

4.1	Illustration of the fracture geometry of the two main 2D hydraulic fracturing models. a) KGD fracture model, where height > length. b) PKN fracture model, where height < length. Modified from Xiao et al. (2017).	82
4.2	Fracture half-length evolution during injection for one stage. The fracture half-length at the end of injection and at the DAS hit time are marked in the curve with a red and pink asterisk respectively.	85
4.3	Horizontal schematic of the wells. See Figure 3.6 for full legend. a) The fracture half-length at the end of injection for one stage is represented by the steel-blue line which is placed at the stage cluster position. b) The fracture half-length at the DAS hit time for one stage (orange line) placed at the stage cluster position.	86
4.4	Horizontal plane of the wells with the PKN and microseismic fracture half-length for one stage. The steel blue line is the PKN fracture half-length at the end of injection (1146.7 m) and the pink line is the microseismic fracture half-length (886.6 m).	87
4.5	Diagram that shows the integration of the PKN fracture half-length with the DAS frac azimuth. The fracture azimuth of the stage was extended to the PKN half-length maintaining the angle of propagation to create the PKN fracture.	87
4.6	PKN vs MS plot. Fracture connection map with microseismic cloud, its linear regression for one stage and the PKN fracture (green line). See Figure 3.4 for full legend.	88
4.7	Horizontal plane of the wells with the fracture half-lengths at the end of injection for all stages (steel blue lines). See Figure 3.6 for full legend. Fractures are smaller in later stages compared to earlier ones.	89
4.8	Horizontal plane of the wells, (See Figure 3.6 for full legend), with the fracture half-lengths at the DAS hit time represented by the orange lines. The range of good agreement is placed at ± 50 meters showed by the dotted cyan lines. Most fractures are within the range of good agreement and the ones that are not show that something unexpected happened during the injection.	90
4.9	PKN vs MS plots for: a) Stages 1 - 5. b) Stages 6 - 10. c) Stages 11 - 15. d) Stages 16 - 20. PKN fractures are the solid lines and the linear regressions of the MS clouds are represented by the dotted lines.	92

4.10	PKN vs MS plots for: a) Stages 21 - 25. b) Stages 26 - 30. c) Stages 31 - 35. d) Stages 36 - 38. PKN fractures are the solid lines and the linear regressions of the MS clouds are represented by the dotted lines.	93
4.11	Example of good agreement between trajectories. PKN vs MS plot of Stage 10. See Figure 4.6 for full legend.	94
4.12	Example of bad agreement between trajectories. PKN vs MS plot of Stage 28. See Figure 4.6 for full legend.	94
4.13	Stages 5 (black circles) and 6 (blue stars) microseismic clouds with the wells, with the linear regression of the MS cloud and the PKN fracture of Stage 6. See Figure 3.4 for full legend. The PKN fracture and MS cloud of Stage 6 had a similar trajectory until the pink circle where the MS seems to migrate towards Stage 5.	95
4.14	Horizontal plane of the wells, (see Figure 3.6 for full legend), with the PKN fracture half-lengths at the end of injection (steel blue) and the microseismic cloud lengths side by side (pink). The green arrows represent stages where the MS propagated SW. The orange circles show stages where the fracture half-length at the DAS hit time was longer than expected, the yellow circles show the stages where it was shorter.	97
5.1	Figures 2.19, 3.23, and 4.14 that present the results from Chapters 2, 3, and 4 respectively. See those figures for full legend.	102
5.2	Characteristics table for all stages. Blue means the stage presents that characteristic and red that it does not have it. The "R" next to the stage number means that the stage was re-stimulated. In the r-t front propagation, R = "reactivation" pattern, ST = "stress transfer" pattern, H = "halted growth" pattern, and C = the MS change patterns. In the MS overlay, characteristic "t" means the MS events travel to previous stages. In the PKN-DAS agreement row, "S" means the fracture length is shorter than expected, and "L" means the fracture length is longer than expected. In the PKN-MS agreement, "MS" means that the microseismic cloud is longer than the PKN fracture.	103
5.3	Definition of the parameters to determine if a stage has or does not have a characteristic.	104
5.4	Schematic of the expected characteristics displayed in the LF DAS, engineering curves, microseismicity and PKN analyses for Scenario 1.	105
5.5	Schematic showing the stresses created by a planar propagating hydraulic fracture. Modified from Eyre and van der Baan (2018).	106

5.6	Relationship between hydraulic fracture opening and propagation directions relative to the in situ principal stresses in a horizontal well. Modified from Eberhardt and Amini (2018).	108
5.7	Schematic showing the stresses created by a planar propagating hydraulic fracture and the associated microseismicity. Modified from Cipolla and Wright (2002) and Eyre and van der Baan (2018).	109
5.8	Expected characteristics table for all stages. Blue means the stage presents that characteristic and red that it does not have it. See Figure 5.2 for the full legend.	113
5.9	Schematic of the expected characteristics displayed in the LF DAS, engineering curves, microseismicity and PKN analyses for Scenario 2.	115
5.10	Re-stimulation of Stage 25: a) DAS-MS plot. b) r-t plot. Fracture signal in strain front does not have a heart-shaped tip and the r-t plot shows "reactivation" and "stress transfer" patterns.	116
5.11	Stage 11: a) Strain front with DAS-MS plot. b) r-t plot. The fracture signal does not have a heart-shaped tip and presents the "reactivation" pattern. But there are multiple fractures propagating so the stage is not a failed one.	117
5.12	Stage 9: a) strain front and b) fracture half-length at the DAS hit time (orange line) in the schematic of the wells. The hydraulic fracture propagated faster than expected but has a heart-shaped tip.	118
5.13	Schematic of the expected characteristics displayed in the LF DAS, engineering curves, and PKN analysis for Scenario 3.	119
5.14	Stage 15: a) strain front and b) fracture half-length at the DAS hit time (orange line) in the schematic of the wells. The hydraulic fracture has an antenna and propagated slower than expected	121
5.15	Stage 13: a) strain front and b) fracture half-length at the DAS hit time (orange line) in the schematic of the wells. The hydraulic fracture has an antenna and propagated as expected.	122
5.16	Fracture connection map for all stages, with original wells geometry See Figure 2.10 for full legend. Displays the direction of fracture propagation.	123
5.17	Schematic of the expected characteristics displayed in the fracture connection map, and PKN analysis for Scenario 4.	123
5.18	Stage 20: a) strain front and b) the fracture half-length at the DAS hit time.	125
5.19	Schematic of the expected characteristics displayed in the PKN vs MS comparison, DAS-MS plot, and r-t plot for Scenario 5.	126

5.20 Schematic of the well with the PKN fracture (blue line) and the microseismic cloud (pink line) lengths side by side. 127

5.21 Stage 6: a) DAS-MS plot, b) r-t plot and c) Stages 5 (black circles) and 6 (blue stars) microseismic clouds with the wells, the linear regression of the MS cloud and the PKN fracture of Stage 6. Orange and pink circles in the three figures highlight the microseismicity moving to the previous stage. 128

5.22 Stage 34: a) DAS-MS plot, and b) r-t plot, orange circle highlights the fracture/fault reactivation happening in the stage which seems to be at the same measured depth as the fractures created in Stage 34. 129

Abbreviations

BH Bottom-hole.

DAS Distributed Acoustic Sensing.

FBP Formation Breakdown Pressure.

KGD Kristianovich-Geertsma-de Klerk.

LF DAS Low-Frequency Distributed Acoustic Sensing.

MD Measured Depth.

MS Microseismic.

PKN Perkins-Kern-Nordgren.

TVD True Vertical Depth.

Chapter 1

Introduction

1.1 Hydraulic fracturing background

Unconventional reservoirs are oil or gas-bearing units with very low permeability and porosity so that the resources are trapped there with little to no ability to flow through the rock and into a wellbore. In order to produce from these reservoirs stimulation treatments, like hydraulic fracturing, are needed to help these resources flow and so make them economically viable (Alberta Energy Regulator, n.d.).

Hydraulic fracturing is a multistage well-stimulation technique employed to extract hydrocarbons from unconventional reservoirs by increasing their permeability and productivity with the creation of fractures (Kim et al., 2014). This is accomplished by injecting large quantities of fluid into the formation at high pressures, when the pumping pressure exceeds the strength of the rock formation the rock breaks and fractures are created (API HF1., 2009; Jalili & Ahangari, 2017; Nolen, 2013). As the injection continues the fractures grow and proppant is pumped in the formation along with the fluid. These proppants are usually solid and are used to keep the fracture open after the injection stops, creating a path for the hydrocarbons to flow from the reservoir into the wellbore (Jalili & Ahangari, 2017).

Well completion mode selection is a very important component of unconventional reservoir completions. There are multiple types of well completion modes, but there are two main techniques commonly used in the gas industry: open hole (OH) and

cased hole (CH). The most suitable completion mode is selected depending on the type and properties of the reservoir (Djabelkhir, 2020).

In the cased hole completion, the wells are cased and cemented through the entire length of the well and then perforated through the casing and cement with a perforating gun that creates small holes, also known as clusters. The clusters provide an entrance to the formation to the fracturing fluids and are isolated by plugs between stages (Figure 1.1a). This method is called Plug and Perf. For open hole completion, the reservoir is completely exposed, there is no casing in the target zone. Open-hole packers are used for isolation between stages and sleeves with ports that can be opened are placed within specific intervals. To activate the port to open the sleeve, and create a flow path for the fracturing fluid, a ball is "dropped" inside a liner and when the ball seats onto the sleeve assembly the sleeve opens and activates (Figure 1.1b). This type of method is called Sliding Sleeve and typically has one opening (cluster) per stage, but a much larger area of the formation is exposed to the fluids meaning it can exploit pre-existing joints and weaknesses in the formation (Belyadi et al., 2019; Djabelkhir, 2020; Eaton, 2018).

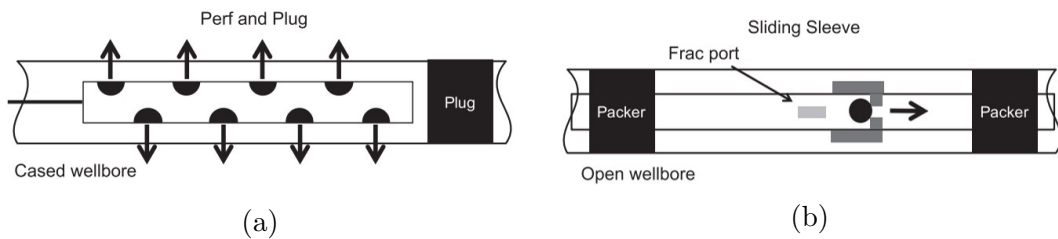


Figure 1.1: Schematic illustration of cased and open-hole completion methods. a) For a cased well the casing is perforated creating points that allow the entrance of fluids into the formation. b) For an open wellbore, a sliding sleeve is placed and then a ball is pumped inside a liner. When the ball seats onto the sliding sleeve assembly the port opens and allows fluid to enter the formation (Eaton, 2018).

1.1.1 Hydraulic fractures

The fractures created during hydraulic fracturing are called hydraulic fractures. The orientation and propagation direction of these fractures are controlled by the in-situ

stress field, defined by three principal compressive stresses, which are perpendicular to each other; vertical stress (Sv), maximum horizontal stress ($SHmax$), and minimum horizontal stress ($Shmin$) (Nolen, 2013). Depending on the magnitude and orientation of these stresses there are three in-situ stress regimes which are normal faulting ($Sv > SHmax > Shmin$), strike-slip faulting ($SHmax > Sv > Shmin$), and reverse faulting ($SHmax > Shmin > Sv$) stress regime. Studies have shown that hydraulic fractures propagate perpendicular to the minimum horizontal stress, which is usually perpendicular to the wellbore axis (Jalili & Ahangari, 2017). However, when there are discontinuities or weakness planes in the reservoir the propagation might change. This can create complex fracture geometries and may divert fracture propagation from being completely perpendicular to the wellbore axis (Ugueto et al., 2019; Wang, 2019).

Understanding the geometry, orientation, and propagation of hydraulic fractures is very important in order to design successful unconventional reservoir completions. For example, the length and height of hydraulic fractures give information on how to optimize the well spacing and job size. On the other hand, the width contains information on proppant transportation and fracture permeability. Furthermore, density is important to optimize cluster spacing. This information helps identify the factors that affect well production and in doing so, more efficient unconventional reservoir completions can be designed, which will help to reduce treatment costs and enhance production performance (Jin & Roy, 2017).

There are many techniques that can be used to monitor hydraulic fractures during treatment, such as; microseismic monitoring, pressure monitoring in offset wells, fluid and proppant traces, tiltmeters, and fiber optics. They all have their advantages and disadvantages, the techniques should be selected depending on the type of information and quality needed. However, no single technology is enough on its own to provide the information needed to fully understand and optimize fracturing treatments. That is why it is important to integrate multiple of these technologies to obtain a more

detailed and complete diagnostic (Jin & Roy, 2017, 2019; Mahmoud et al., 2021).

1.2 Site geological background

The data set was provided by an anonymous company and included; distributed acoustic sensing, microseismicity, injection information, triaxial tests, and wireline logs. The study well analyzed in this project was the second to last fractured well, part of a four horizontal well fracturing operation with open-hole ball drop completion. Figure 1.2 shows the wells geometry of the site. The study well ("Treated well") is the blue line and the well with the fiber optic cable ("Monitoring well") is represented by the black line. The fracturing operation had 38 fracturing stages, represented by the blue circles. Both wells are in the middle Member of the Montney Formation, the separation between them is 150 meters and they both are drilled in the direction of minimum principal stress.

The Triassic Montney Formation is located in northeast British Columbia and northwest Alberta. It is one of the most active plays in Western Canada and one of the most prolific hydrocarbon resources in North America (Davies, 1997; Kendall, 1999). The Montney Formation is subdivided into three Members; Upper, Middle, and Lower, and is bound, top and base, by the Coplin and sub-Jurassic unconformities and the Permian-Triassic unconformity respectively (Davies et al., 1997). The Middle Montney Member was deposited during the Smithian stage (Davies et al., 1997; Kendall, 1999) and includes the D1, D2, D3, and D4 horizons (Prenoslo et al., 2018).

The Montney Formation in the data area is considered tight gas due to its low matrix permeability and low porosity; it produces gas and liquid hydrocarbons (Davey, 2012; Duenas et al., 2014; Smith et al., 2009). The regional stress regime in this area is strike-slip, where the two horizontal principal stresses are the maximum and minimum stress magnitudes and the vertical stress is the intermediate one (Davey, 2012).

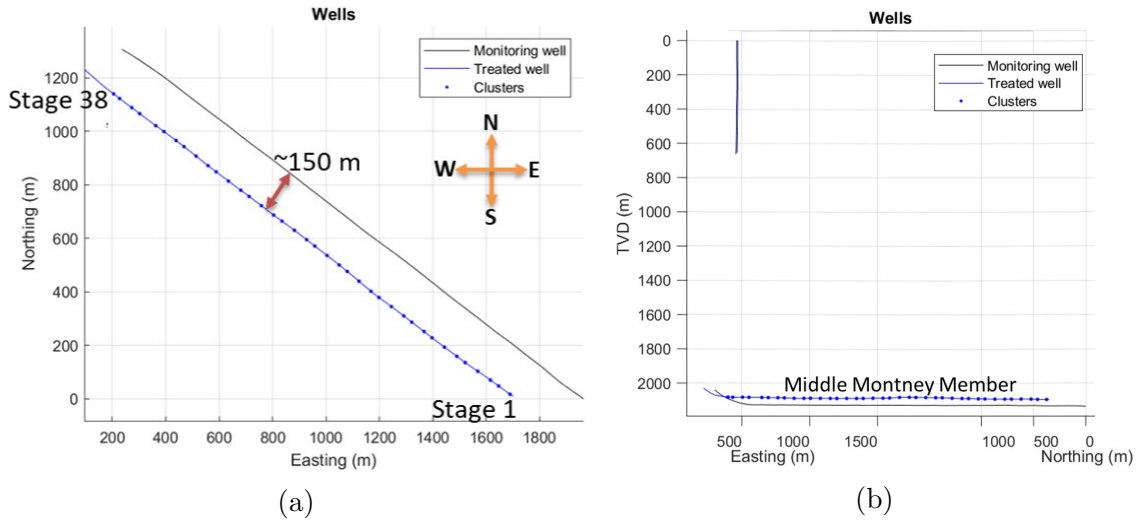


Figure 1.2: Wells geometry, upper (a) and side (b) view. Treated well analyzed in this thesis is represented by the blue line. The monitoring well with the fiber optic cable is the black line. The wells spacing is 150 m and both wells are located in the Middle Montney formation.

1.3 Motivation

The aim of this thesis is to study hydraulic fracture propagation at temporal and spatial scales by analyzing low-frequency DAS, pumping information, and microseismicity of one hydraulic treatment and comparing the results with a numerical model. Different data types hold different information, and this integrated analysis could give us a more complete interpretation of the treatment, help identify completion issues, and so, help in the design of more efficient unconventional reservoir completions. There is particular interest in the comparison of DAS and microseismicity as it is rarely done but could provide much insight into what happens during hydraulic fracturing treatments.

1.4 Objectives

The objectives of this thesis are:

- The interpretation of LF DAS strain fronts for one hydraulic fracturing treatment

- The determination of the fracture network between the treated and monitoring well.
- The comparison between LF DAS, pumping curves, microseismicity records and PKN fracture modelling.

The purpose of doing all this is to gain insight into the relationship between strain changes, injection rates, microseismic events, and hydraulic fractures, and also to identify properties and/or characteristic features of failed stages across all these analyses and see if they converge in some cases.

1.5 Outline

The thesis is structured into 5 main chapters as follows:

Chapter 2 covers the theoretical background of distributed acoustic sensing, low-frequency DAS, and pumping curves. This chapter also describes the methodology used for the analysis of low-frequency DAS data and pumping information. Finally, the results of this analysis are shown and the discoveries are discussed.

Chapter 3 provides a description of the background on microseismic monitoring. Then, it describes the methodology used for the analysis of the microseismic cloud and the comparison of microseismic events with the low-frequency DAS data. At the end of the Chapter, the results are shown and discussed.

Chapter 4 presents the theory of the PKN model. It also shows the methodology for the PKN modeling and the use as a diagnostic tool for the low-frequency DAS data and the microseismic analysis. In the end, the results of these analyses are presented and discussed.

Chapter 5 presents a summary of the significant results (from the hydraulic fracturing treatment and the different analyses) and describes the expected characteristics displayed in the different observations. Then a statistical analysis is run over these

expected observations to try and find correlations among them. Finally, the results are presented and discussed.

Finally, **Chapter 6** discusses the conclusions of the thesis and suggests possible directions for future research.

References

- Alberta Energy Regulator. (n.d.). *Hydraulic Fracturing* [accessed on 2022-04-12]. <https://www.aer.ca/providing-information/by-topic/hydraulic-fracturing>
- API HF1. (2009). Hydraulic Fracturing Operations, Well Construction and Integrity Guidelines. *American Petroleum Institute*, 36.
- Belyadi, H., Fathi, E., & Belyadi, F. (2019). Chapter Eleven - Horizontal well multistage completion techniques. In H. Belyadi, E. Fathi, & F. Belyadi (Eds.), *Hydraulic Fracturing in Unconventional Reservoirs (Second Edition)* (Second Edition, pp. 177–189). Gulf Professional Publishing. <https://doi.org/https://doi.org/10.1016/B978-0-12-817665-8.00011-4>
- Davey, H. (2012). *Geomechanical characterization of the Montney Shale northwest Alberta and northeast British Columbia, Canada* (Doctoral dissertation). Colorado School of Mines.
- Davies, G. R. (1997). The Triassic of the Western Canada Sedimentary Basin: Tectonic and Stratigraphic Framework, Paleogeography, Paleoclimate and Biota. *Bulletin of Canadian Petroleum Geology*, 45, 434–460.
- Davies, G. R., Moslow, T. F., & Sherwin, M. D. (1997). The Lower Triassic Montney Formation, West-Central Alberta. *Bulletin of Canadian Petroleum Geology*, 45, 474–505.
- Djabelkhir, N. (2020). *Simulation Of Notch Driven Hydraulic Fracture In Open Hole Completion* (Doctoral dissertation). University of North Dakota.
- Duenas, C., Davis, T., & Damico, D. (2014). *Understanding Rock Quality Heterogeneity Using Combined Multicomponent Seismic Inversion and Well Log Cluster Analysis. Montney Shale Reservoir, Pouce Coupe Field, Alberta, Canada*. <https://doi.org/10.15530/urtec-2014-1921332>
- Eaton, D. W. (2018). Stress Measurement and Hydraulic Fracturing. *Passive Seismic Monitoring of Induced Seismicity: Fundamental Principles and Application to Energy Technologies* (pp. 95–126). Cambridge University Press. <https://doi.org/10.1017/9781316535547.005>
- Jalili, S., & Ahangari, K. (2017). Effects of different stress regimes on hydraulic fracture geometry: a particle flow code approach. *Innovative Infrastructure Solutions*, 2, 6. <https://doi.org/10.1007/s41062-017-0096-1>
- Jin, G., & Roy, B. (2017). Hydraulic-fracture geometry characterization using low-frequency DAS signal. *The Leading Edge*, 36, 975–980.
- Jin, G., & Roy, B. (2019). Using Distributed Acoustic Sensing to Monitor Hydraulic Fracturing Operations, 5.
- Kendall, D. R. (1999). Sedimentology and stratigraphy of the lower triassic Montney formation, Peace River basin, subsurface of northwestern Alberta. <https://doi.org/10.11575/PRISM/10182>
- Kim, J., Um, E., & Moridis, G. (2014). Fracture Propagation Fluid Flow and Geomechanics of Water Based Hydraulic Fracturing in Shale Gas Systems and Electromagnetic Geophysical Monitoring of Fluid Migration, 18. <https://doi.org/10.2118/168578-MS>

- Mahmoud, A., Gowida, A., Aljawad, M., Al R., M., & Ibrahim, A. (2021). Advancement of Hydraulic Fracture Diagnostics in Unconventional Formations. *Geofluids*, 2021, 17. <https://doi.org/10.1155/2021/4223858>
- Nolen, R. (2013). Elements of hydraulic fracturing. *Oilfield Review*, 25, 51–52.
- Prenoslo, D., Furlong, C. M., Gingras, M., Playter, T., & Zonneveld, J. (2018). The sedimentology, stratigraphy and reservoir characteristics of the Montney D1 and D2 horizons in the Greater Pouce Coupe area. *Bulletin of Canadian Petroleum Geology*, 66, 338–358.
- Smith, T. M., Sayers, C. M., & Sondergeld, C. H. (2009). Rock properties in low-porosity/low-permeability sandstones. *The Leading Edge*, 28(1), 48–59. <https://doi.org/10.1190/1.3064146>
- Ugueto, G., Todea, F., Daredia, T., Wojtaszek, M., Huckabee, P., Reynolds, A., Laing, C., & Chavarria, J. (2019). Can You Feel the Strain? DAS Strain Fronts for Fracture Geometry in the BC Montney, Groundbirch. *Proceedings of SPE Annual Technical Conference and Exhibition*, 15. <https://doi.org/10.2118/195943-MS>
- Wang, H. (2019). Hydraulic fracture propagation in naturally fractured reservoirs: Complex fracture or fracture networks. *Journal of Natural Gas Science and Engineering*, 68, 14. <https://doi.org/10.1016/j.jngse.2019.102911>

Chapter 2

Low-frequency DAS analysis

2.1 DAS Background

Since the introduction of the fiber optic sensors to the oil and gas industry, they have been increasingly used as more applications have been discovered (Kavousi et al., 2018; Mellors et al., 2019). This technology presents a promising prospect for different applications in geophysics due to the characteristics of the fiber optic, as it can measure almost all of the physical properties, like, temperature, pressure flow, vibration, strain, velocity, among others. It also can withstand extreme environmental conditions and the same cable can be used to measure more than one property simultaneously (Becker et al., 2020; Lee et al., 2006).

Optical fiber sensors use light to sense information of the medium and typically consist of an interrogator unit, an optical cable, and a sensor. They are classified in two groups: point sensors and distributed sensors. The main difference between these two groups is that the first one measures at a finite number of discrete locations whereas with the second you can obtain a measurement at every point in the fiber (Hartog, 2017). Point sensors use an optical fiber cable to conduct light to and from a remote sensor to an interrogator unit. There could be only one single sensor or multiple sensors sharing the same fiber, also known as multiplexed point sensors or quasi-distributed sensors. For distributed sensors, the entire length of the optic cable is the sensor so there are no additional transducers (Figure 2.1) (Molenaar & Cox,

2013; Parker et al., 2014).

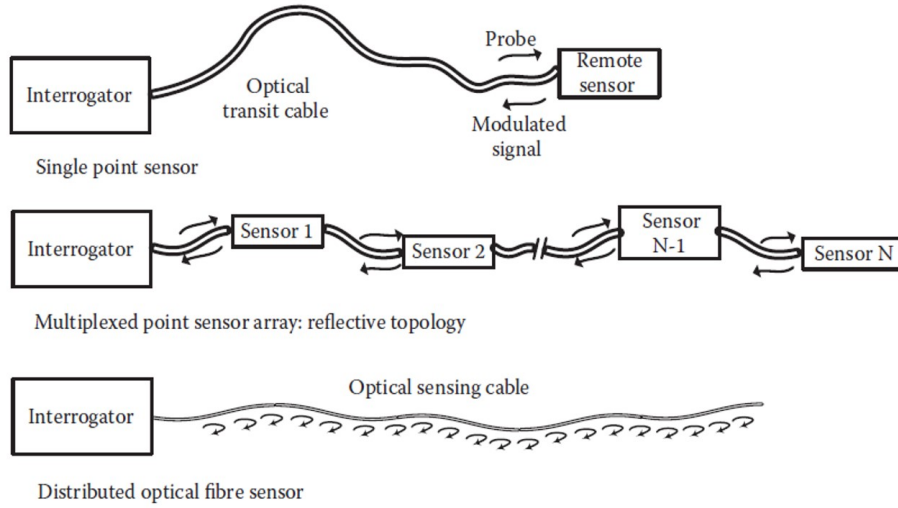


Figure 2.1: Fiber optic sensing configurations. Single point sensors have only one sensor at the end of the fiber. Multiplexed point sensors have multiple sensors distributed along the cable. Distributed sensors use the fiber as the sensor. Modified from Hartog (2017).

As the distributed sensors use light to convey the information they sense, the principle of operation of these sensors is based on the natural scattering processes inherent to optical cables: Brillouin, Raman, and Rayleigh scattering (Figure 2.2) (Fernandez-Ruiz et al., 2020). Brillouin and Raman scattering are inelastic processes, meaning that the energy of the scattering particles changes. The difference between these two is that in Raman scattering photons are scattered by molecular vibrations, while Brillouin scattering results from the interactions between light and acoustic phonons. The backscattered light in these processes can have a frequency either lower (Stokes) or higher (anti-Stokes) than the incident light, longer or shorter wavelength respectively (Muanenda et al., 2019). Rayleigh scattering is an elastic process, the incident energy is preserved, where the light is scattered by particles much smaller than the wavelength of the incident light. In this process, the backscattered light has the same frequency and wavelength as the incident light, as it neither loses nor gains energy (Paschotta, n.d.). Depending on the scattering process used in the sensor, or the combination of more than one, they create different sensors with different specific

features. Particularly, using Rayleigh scattering creates the system used in this thesis, distributed acoustic sensors (Fernandez-Ruiz et al., 2020).

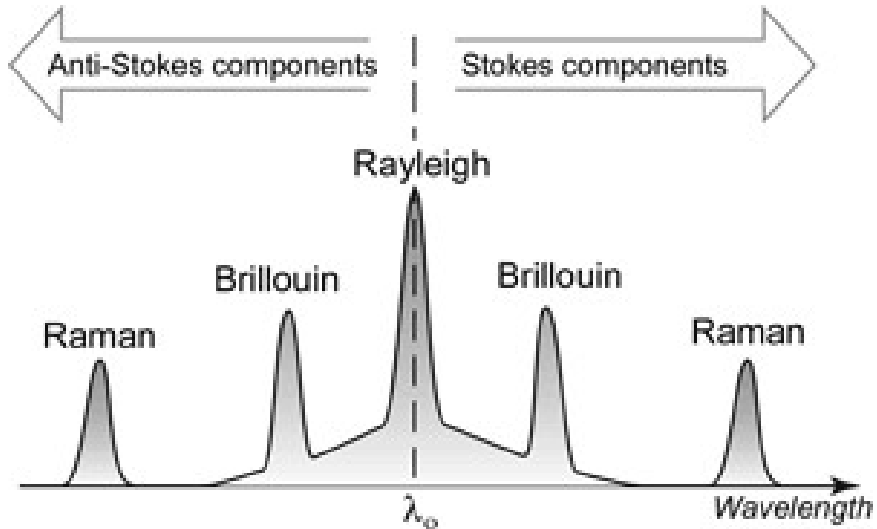


Figure 2.2: Components of the scattered light. Brillouin and Raman scattering are the inelastic scattering of light in a medium caused by acoustic or optical phonons, respectively. The backscattered light can have shorter (anti-Stokes) or longer (Stokes) wavelength than the incident light. Rayleigh scattering is the elastic scattering of light caused by much smaller particles. The backscattered light preserves the same wavelength as the incident light. Modified from Molenaar and Cox (2013).

The distributed acoustic sensors operate by sending coherent laser pulses from the interrogator unit to the fiber cable at constant intervals. These pulses of light experience scattering by interacting with small, natural inhomogeneities present in the cable. This scattered light returns to the interrogator unit, where the phase is measured. This process is also known as backscattering (Figure 2.3). Any vibroacoustic disturbance that affects the optic cable produces variations in the phase of the backscattered light. These phase variations in the returned signal provide measurements of the strain the fiber cable is subjected to, and, by recording the time of its arrival, it determines the position at which each component of the backscattered light was generated (Fernandez-Ruiz et al., 2020; Yu et al., 2019).

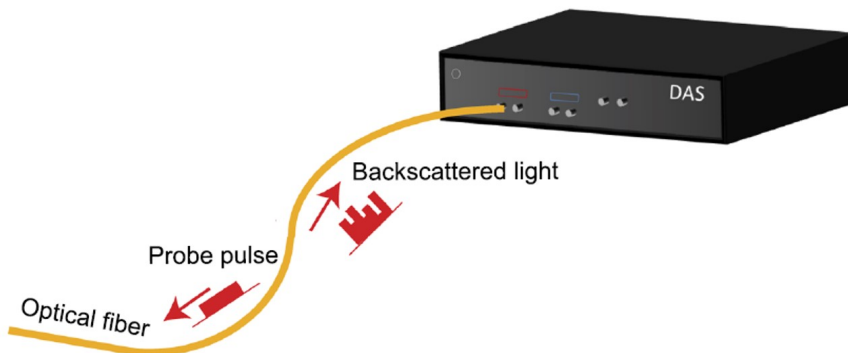


Figure 2.3: Principle of operation of Distributed Acoustic Sensors: a pulse travels along an optical fiber, and the phase of the Rayleigh backscattered light that returns to the interrogator is recorded. Retrieved from Fernandez-Ruiz et al. (2020).

Distributed acoustic sensing is a technology that has been used in wells by the oil and gas industry for more than a decade. It has presented a steady growth for the past few years and is expected to surpass \$2 bn by 2025 (Lellouch et al., 2020; Muanenda, 2018). It has been mostly used to monitor hydraulic fracturing operations, as it is very sensitive to dynamic strain, and stimulation effects can be clearly identified like; the opening and closing of fractures in response to pumping and injection, and microseismicity. These types of data help to monitor and diagnose potential completion issues during stimulation and to optimize parameters and design for the following operations (Becker et al., 2020; Hartog, 2017; Richter et al., 2019).

Most of the testing and applications of DAS during hydraulic fracturing have been on the high-frequency bands (> 1 Hz) of the DAS data. However, recent studies have demonstrated that DAS data in the low-frequency band provides information on hydraulic fracture geometry. Depending on the specific DAS bandwidth used there can be different applications (Becker et al., 2018; Jin & Roy, 2017). The DAS signal at very high-frequency bands (> 1 kHz) can be used to estimate fluid and proppant allocation as these bands focus on the energy throughput of injecting high-rate fluids through perforations (White et al., 2020). This can be done by correlating each of the cluster's DAS signal intensity to the slurry rate and downhole concentration (Grubert et al., 2020; Jin & Roy, 2019). With these correlations, an evaluation of the cluster

efficiency in the hydraulic fracturing operations can be carried out. At mid-frequency bands (10 Hz - 1 kHz) the DAS signal can be used to monitor microseismic activity (Karrenbach et al., 2017; Webster et al., 2013b), as in these bands is where the high-frequency acoustic data is mostly concentrated (Sharma et al., 2020). This is achieved by recording the microseismic waveforms during treatment and then inverting them to get the event locations and moment tensors. Finally, the low-frequency bands (< 0.1 Hz) of the DAS signal can be used to monitor hydraulic fracture, growth, geometry, and propagation during injection, as this band is sensitive to mechanical strain changes. The strain fronts obtained from this band can be analyzed to obtain information on hydraulic fractures (Jin & Roy, 2017, 2019).

Jin and Roy (2017) demonstrated that the low-frequency DAS data can be used to measure small and gradual variations along the fiber caused by the opening, closing, and propagation of fractures during hydraulic stimulation of a well. In this case, the data can be used to constrain hydraulic fractures geometry; length, density, width, propagation speed, and azimuth, by analyzing the DAS strain front patterns (Becker et al., 2018; Jin & Roy, 2017; Mellors et al., 2019; Ugueto et al., 2019). As mentioned before, understanding the geometry of hydraulic fractures is important in order to design successful unconventional reservoir completions. That is why DAS is a very attractive technique as it allows to monitor the hydraulic fractures during injection inside the formation.

To use low-frequency DAS to monitor hydraulic fracture geometry during stimulation the fiber is installed and cemented in a monitor well close to the well being treated. This well is usually horizontal, same as the treated well (Jin & Roy, 2019). During hydraulic fracturing treatment, strain perturbations in the formation are generated by the opening, propagation, and closing of hydraulic fractures (Jin & Roy, 2017). Figure 2.4 shows the hypothetical strain and cable responses of a propagating hydraulic fracture, as observed in a monitoring horizontal well. In the figure, we can observe at times T1 and T2 how the fracture is approaching the monitoring well with

the fiber. The closer it gets the narrower the extending strain rate front gets and the extension region detected by the cable gradually decreases but the magnitude becomes larger. This happens because as the fracture propagates the rock ahead of the fracture tip is under strain as it resists to crack.

At time T3 the fracture has intercepted the monitoring well. This creates, right at the point where the fracture intercepts the well, a narrow extending strain pattern surrounded by a compressing region that decreases in magnitude as it gets farther from the intercept zone. At this time, the cable on the fracture path is still extended and the cable sections on both sides of the fracture path are compressed as the formation is trying to accommodate the new feature. Time T4 shows the strain response after the stimulation of the treated well ends, the regions that were extending during treatment are now compressing and vice versa. This happens because the fracture is trying to close after the pumping of fluid ends and the rock deformation starts decreasing (Liu et al., 2020; Ugueto et al., 2019; Webster et al., 2013).

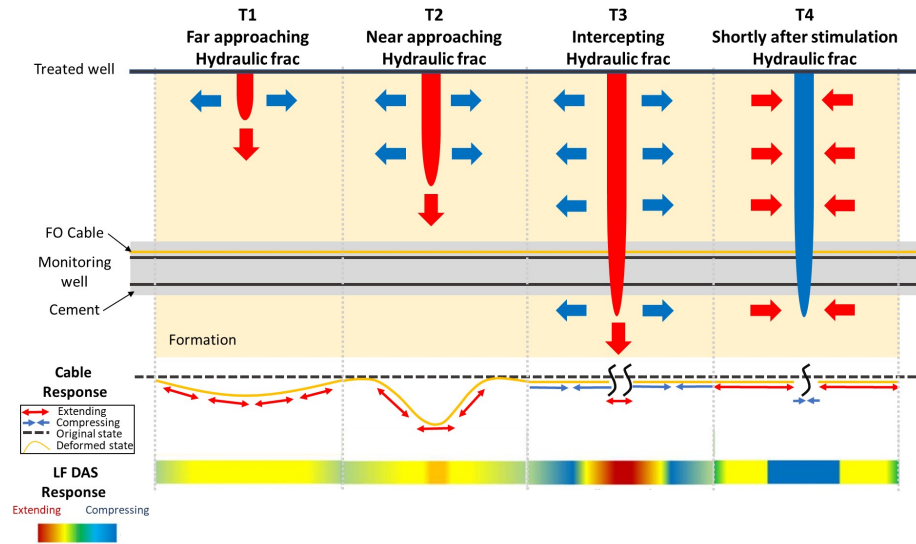


Figure 2.4: Hypothetical strain and cable responses of a propagating hydraulic fracture. Times T1 and T2 show the response of a fracture approaching the monitor well with the fiber optic cable. Time T3 displays the signal when the fracture intercepts the monitoring well. Time T4 shows the strain pattern just after the stimulation ends. Modified from Liu et al. (2020) and Ugueto et al. (2019)

Figure 2.5 is a real-life example of the low-frequency DAS response for one hydraulic fracture, acquired from a single treatment stage during well stimulation, as recorded in the monitoring well. This is called a DAS strain front; the y-axis is measured depth and the x-axis is time, on the right side, the port depth of the packers from the treatment well were projected onto the monitoring well by minimum distance, we call them clusters. The red dots on the left represent the places where the fractures intercepted the monitoring well (Frac hits). For both triangles and dots, the filled ones correspond to the current stage and the unfilled ones to other stages. In the strain fronts, the red color indicates extension while the blue indicates compression. The fracture signal resembles the shape of a dragonfly with a red heart-shaped tip, that represents the fracture hit and blue wings on the sides also known as the stress shadow. The extensional strain comes from the fracture causing local extension as it opens. Fracture opening causes local compression in the surrounding rock, visible as compressing strain (Ugueto et al., 2019; Webster et al., 2013). It is assumed that each fracture hit is created by a single fracture since the spatial resolution of DAS (1 m) cannot differentiate between closely spaced multiple fractures (Jin & Roy, 2017; Ugueto et al., 2019). Some dragonflies present an extending signal that shows almost at the start of injection, they were named the antennas for this thesis and they represent the reopening of a pre-existing fracture. As the fracture propagates past the well there may be areas with alternating compression and extension until the injection stops, likely due to the generation of multiple hydraulic fractures within the Frac-Zone-Domain or to the opening and closing of the fracture, due to poroelastic effects caused by the injection of fluid in the formation (Grubert et al., 2020). During the injection sometimes small compression-extension signals out of the main Frac-Zone-Domain appear, we call them blips but we don't really know what causes them. We believe they could be signals of the cable slipping.

When the stimulation ends, the strain pattern reverses almost immediately: regions that were extending are now compressing and those compressing in the surrounding

stress shadow area are now starting to relax and extend. This happens because the fracture starts to close and the surrounding rock relaxes, this zone is known as the Relaxation zone (Grubert et al., 2020). The end part of the dragonfly after the strain pattern reverses were named tails for this thesis.

We plot the engineering curves that present the pumping information of the stage underneath the DAS strain fronts. In this case, the slurry rate which is the red curve, the bottom-hole pressure information is the blue curve, and the bottom-hole concentration which is the purple line are shown.

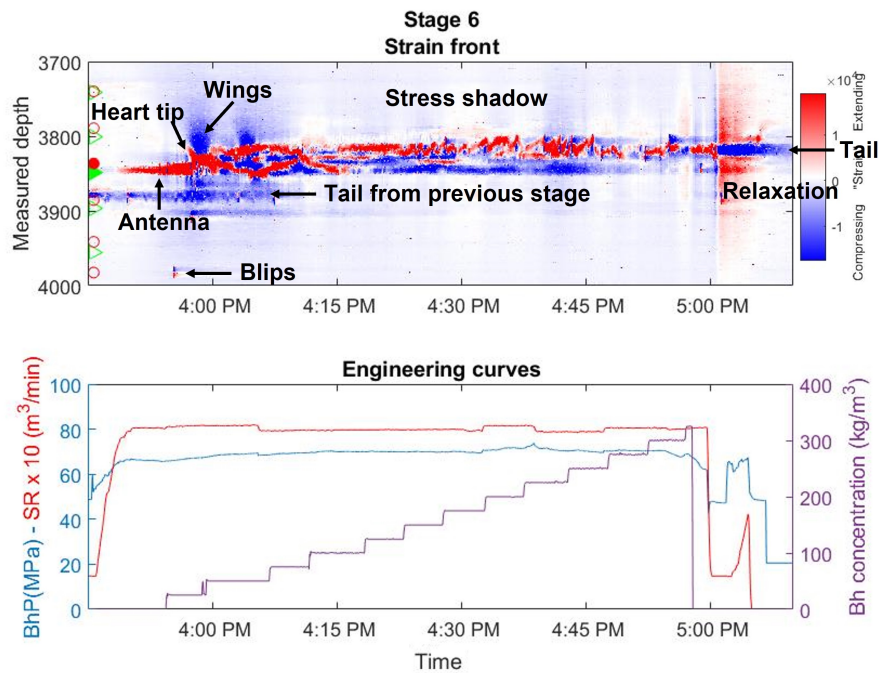


Figure 2.5: DAS Strain Front of one stage from an offset well with some characteristics pointed. The x-axis is time, and the y-axis is measured depth. Red indicates extension and blue compression strain. Second row shows the pumping information of the stage; Slurry rate times 10 (m^3/min) is the red curve, Bottom-hole pressure (MPa) is the blue curve, and Bottom-hole concentration (kg/m^3) is the purple curve. The treatment clusters and the fracture hits projected onto the MD of the monitoring well are shown on the left in green triangles and red circles respectively.

2.2 Pumping information background

Hydraulic fracture treatments are designed based on data obtained during drilling and from nearby wells drilled in the same or similar formations. This information helps to perfect the fracturing fluid, select the best proppant for the job, and calculate the hydraulic pressures necessary to fracture formation. During the fracturing treatment, injection pressure, slurry rate, and proppant concentration, among other pumping data, are all continuously monitored and compared to anticipated conditions. This is done to verify the treatment is proceeding as expected or to assess unexplained deviations from the anticipated design conditions and made the corrections needed before continuing operations. The monitoring also helps gather more information about the formation which can be used to refine future operations (Asgarpour, 2013).

As mentioned before, the pumping information of the stages is usually displayed at the bottom of the strain fronts on the same time scale, when presented as curves they are called the engineering curves. This helps to make correlations between strain changes and injection characteristics during the stimulation process in the stage, as well as to obtain information on the timing and extent of communication between the treated and monitored well (Cole et al., 2017; Karrenbach et al., 2017). For example, the time difference between the time of the formation breakdown pressure and the time of the fracture hit can be used to calculate the fracture propagation speed. Or the delay between the end of injection and the start of the Relaxation zone might tell us about fluid communication between the wells.

For this work, the slurry rate, the bottom-hole concentration, and the bottom-hole pressure information are used for hydraulic fracture monitoring. The slurry rate (m^3/min) is the total rate combined of fluid, chemicals, and proppant that is injected at high speeds into a formation to create hydraulic fractures (Ballotpedia, n.d.). The Bottom-hole concentration (kg/m^3) is the proppant concentration measured at the bottom of the hole (Oil and gas overview, n.d.). The bottom-hole pressure (MPa) is

the pressure measured at the bottom of the hole, it is calculated as the sum of the different pressures acting downhole (Trenchless pedia, n.d.).

The pressure behavior during injection gives us information on fracture creation, propagation, closure, and some other formation information. There are two possible idealized types of pressure behavior during fracture treatment as described by Hubbert and Willis (1957). In the first case, Figure 2.6a, the formation breakdown pressure (FBP) is considerably higher than the fracture propagation pressure. They thought this corresponded to either the formation of a horizontal fracture or to the formation of a vertical fracture under conditions in which the two horizontal principal stresses were nearly equal. In the second case, Figure 2.6b, there is no noticeable FBP, this indicates that the pressure required to start the fracture is less than or equal to the fracture propagation pressure. This would correspond to a horizontal or vertical fracture starting from a pre-existing opening. However, the absence of the FBP peak does not necessarily mean the opening of a preexisting fracture. The FBP value can be lowered in the presence of initial cracks, these cracks help to open the hydraulic fractures with little resistance (Lavrov, 2016). Another reason for the pressure curve to not exhibit expected breakdown behavior is that the breakdown pressure is less than or equal to the minimum principal stress, in this case no peak is observed in the pressure curve (Zoback et al., 1982).

The formation breakdown pressure is a very important parameter, it is at this pressure that the rock of the formation fractures and allows fluids to flow inside (Schlumberger, n.d.). It is at this moment that a new hydraulic fracture is created. Usually, it is the maximum pressure reached early during the injection. After the FBP the pressure drops due to the fracture propagation, at this stage the fluid in the fracture reaches a pressure equilibrium referred to as the fracture propagation pressure. When the injection stops the pressure drops abruptly, sometimes it is followed by a slower pressure decay (Dutler et al., 2020).

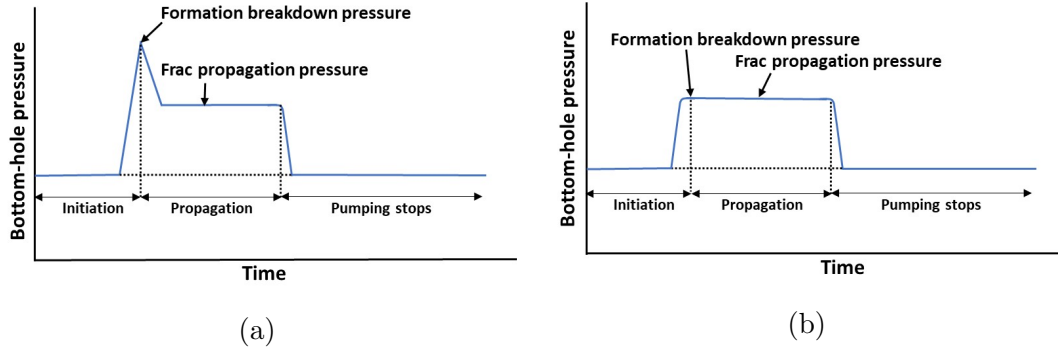


Figure 2.6: Idealized diagram of two possible types of pressure behavior during fracture treatment depending upon various underground conditions. a) FBP is higher than the fracture propagation pressure. b) There is no distinct FBP. Modified from Hubbert and Willis (1957).

2.3 Methodology

For the analysis of LF DAS and the pumping information we looked at DAS strain fronts for fracture and pumping characteristics; start of injection, FBP, frac hits, end of injection, the start of the Relaxation zone, propagation direction, and propagation speed.

2.3.1 DAS strain fronts characteristics

As previously mentioned, the DAS strain fronts present the strain perturbations in the medium caused by the propagation of hydraulic fractures during fracturing treatment. The changes in strain polarity and the shapes of the fracture signal (dragonfly) might uncover fracture characteristics or information about the formation.

First, heart-shaped tips, wings, and tails were counted per stage as the presence of more than one of these features indicates that the stage created multiple fractures and can give an estimation of the number of fractures created during the stages. Next, antennas were identified in the strain fronts, as they are indicators of re-stimulation of previous stages. Finally, the start of the Relaxation zone was selected. The Relaxation zone starts when the strain pattern reverses after the end of the injection. It is

identified on the strain fronts when the regions that were extending during treatment are now compressing and vice versa. Figure 2.7 shows the strain front of one stage with the start of the Relaxation zone represented by a black line and the other strain front characteristics pointed out.

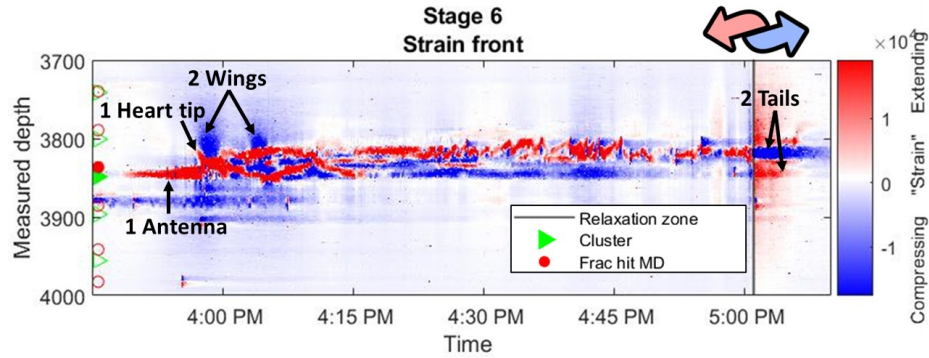


Figure 2.7: DAS strain front of one stage with picked strain front characteristics and the start of the Relaxation zone represented by a black line. See Figure 2.5 for detailed description of the legend and other symbols.

2.3.2 Fracture and pumping characteristics

Fracture and pumping characteristics in both the strain fronts and the engineering curves were selected. Figure 2.8 shows a strain front for one stage with all its fracture and pumping characteristics picked out.

First, the start and end of injection (yellow and pink line respectively) were picked from the pumping information of the stages. Then, the FBP (blue line) was identified using the bottom-hole pressure curve as the first peak before the curve becomes continuous. If there is no identifiable peak, the concave portion of the curve before it flattens was selected as shown in Figure 2.9a. Finally, the fracture hits, or frac hits, time and measure depth were identified. The frac hit time (green line) is the time when the fracture intercepts the monitoring well and is identified as the bottom of the heart-shaped tip of the dragonfly, where the wings converge. When there was no visible heart-shaped tip the convergence of the blue wings was used as the frac hit time as shown in Figure 2.9b. Only the first arriving heart-shaped tip was considered.

The frac hit measured depth (red circles on the left) is the place in the cable where the fracture intercepted the monitoring well. To calculate the frac hit MD we selected the top and bottom depths of the hearth shaped tip and calculated the midrange between those values. When there was no visible heart-shaped tip the top and bottom depths of the blue wings were used to calculate the frac hit MD as shown in Figure 2.9b. Plotting the clusters and frac hits MD on the same side of the well can help to see if the fractures propagated perpendicular to the treated well.

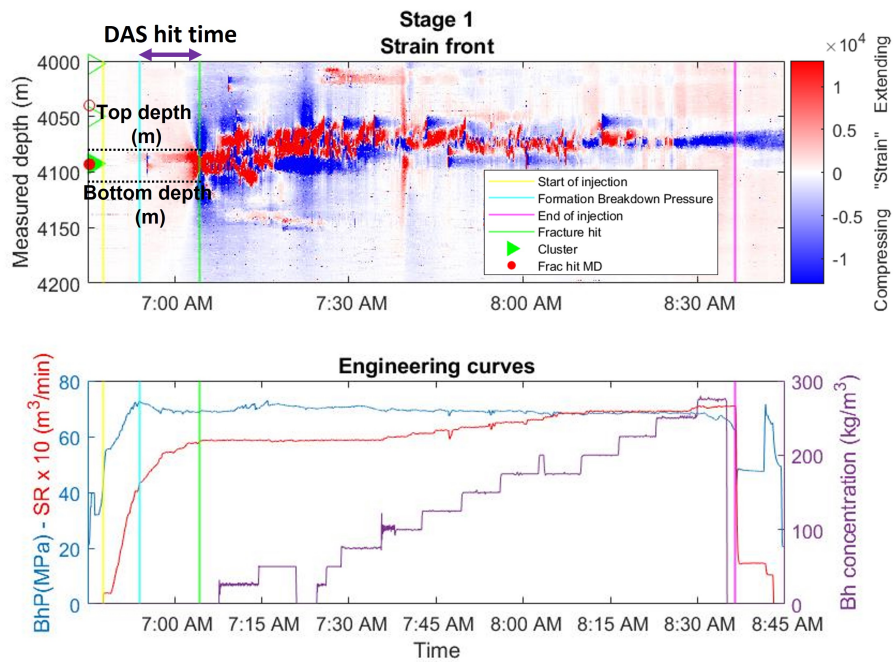
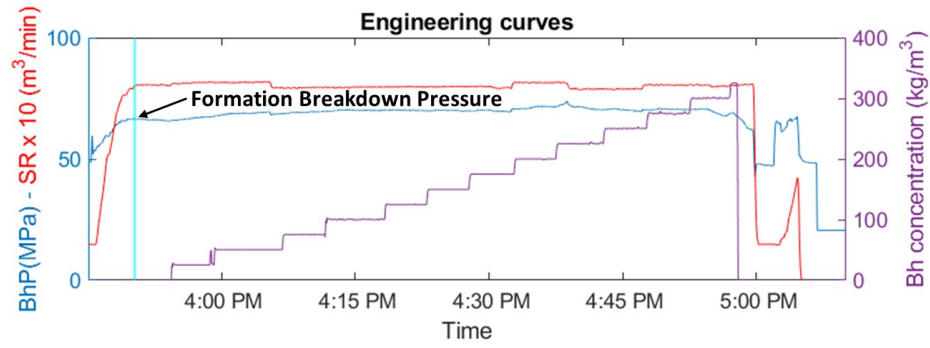
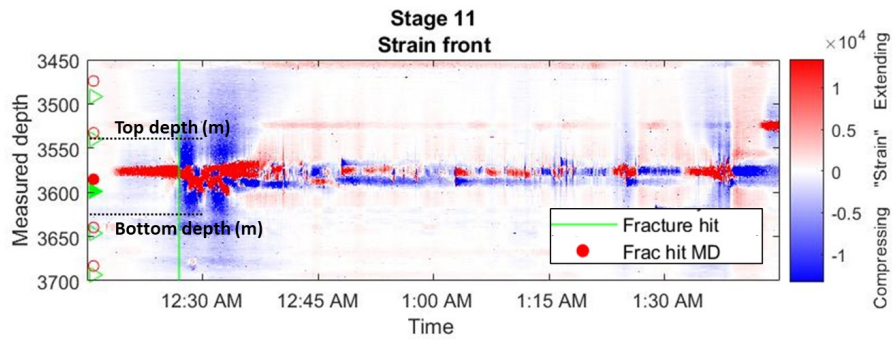


Figure 2.8: DAS strain front of one stage with all its fracture and pumping characteristics picked out. Start of injection, yellow line. FBP, blue line. Frac hit time, green line. The Frac MDs are the red circles on the left. End of the injection, pink line. Legend and symbols as in Figure 2.5.



(a)



(b)

Figure 2.9: Unexpected behavior in engineering curves and strain fronts. a) Engineering curves show a stage with no noticeable FBP peak. The concave portion of the curve before it flattens was selected as the FBP. b) Strain front shows a dragonfly with no heart-shaped tip. The frac hit time was selected as the convergence of the blue wings. The frac hit MD was the midrange of the top and bottom depth of the wings. See Figure 2.5 for full legend.

Propagation speed

To calculate the minimum fracture propagation speed, the minimal projected distance between the treated well and the monitoring well (150 m) is divided by the time difference between the FBP and the Frac hit, also known as DAS hit time (Figure 2.8).

Propagation direction - Fracture connection map

It is important to know the propagation direction of the hydraulic fractures created during the injection. The fractures are expected to propagate perpendicular to the treated well because of its orientation with respect to the maximum horizontal stress,

but sometimes this is not the case. Fracture connection maps illustrate the fracture network between the treated and the monitoring well. They provide information on the direction of fracture propagation (Jin & Roy, 2017; Ugueto et al., 2019).

To determine the propagation direction the frac hits measured depth are plotted on the monitoring well and connected them to their corresponding cluster in the treated well with a line, as shown in Figure 2.10. The lines connecting these two points show the deviation angle of the fracture propagation direction. Doing this for all stages creates the fracture connection map.

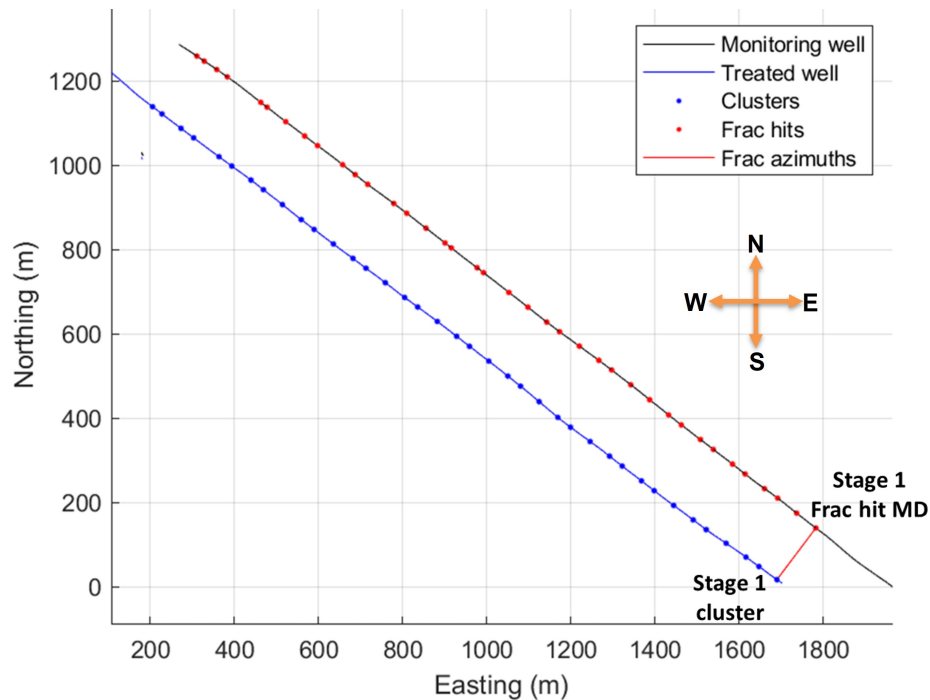


Figure 2.10: Upper view of treated well (blue) and monitoring well (black) with the perforation clusters (blue dots) and the frac hits (red dots). Stage 1 cluster is connected to the Stage 1 frac hit with a red line that shows the deviation angle of the fracture propagation direction (Frac azimuth).

2.4 Results and Discussion

In this section, the results of the DAS and pumping information analysis are introduced and discussed. Some multi-stage results are presented but due to the nature of the study, not all strain fronts can be shown.

2.4.1 Characteristics in strain fronts and engineering curves

Figure 2.11 shows the strain front and engineering curves for Stage 13, this stage is considered a good example as all the DAS fracture, and pumping characteristics are visible. The dragonfly signal presents one heart-shaped tip, one pair of wings, one antenna, two tails, and the start of the Relaxation zone is easily identified (black line). Due to there being two visible tails it is possible that more than one fracture was created during the injection but the full dragonfly signal of the second fracture was suppressed by the stress shadow of the first fracture as they might have been created very close to each other. The start of injection is represented by the yellow line. Then there is a nice FBP identified by the blue line. The frac hit time is represented by the green line, and the frac hit MD is identified by the red-filled circle on the left side of the plot. Finally, the end of the injection is represented by the pink line.

Figure 2.12 shows the strain front and engineering curves for Stage 26, this stage shows multiple dragonfly signals, which means that multiple hydraulic fractures are propagating during injection with enough spacing between them as to not suppress the complete fracture signal. All the characteristics are picked out as well with the same line colors as Figure 2.11. In stages that present indications of multiple fractures created the competition between them can be seen in the strain patterns. In a scenario with two close propagating fractures, one dragonfly signal might close before the end of injection while the other continues to propagate until the injection stops.

In Figure 2.13 Stage 34 is presented, in the beginning, there was only one propagating fracture, and a bit later in the injection, another fracture was created. The first fracture closed around 10:52 am while the second one stayed open. One thing noticed in this analysis, and that can be observed in Stage 26 (Figure 2.12), is that if there are multiple fractures created during one stage they open towards the heel of the well, away from the stress shadow of the previous stage. This is unexpected since we would anticipate them moving towards the toe were there are new fractures.

While analyzing the strain fronts, we noticed some stages do not present the heart-shaped tip, they just have a line that appears shortly after the start of injection, which we named the antenna. The answer to why this happens came from three stages where the same stage was re-stimulated after a first injection. Figure 2.14a shows Stage 36, which was one of the three stages that were stimulated twice. During the first injection, there is a dragonfly with a heart-shaped tip. After the end of the injection, the pattern reverses and stays that way until the re-stimulation starts. For the reopening of the stages, the dragonflies do not present a heart-shaped tip, there is just the antenna. Knowing that a fracture had been open previously at the same place, we concluded that the absence of the heart-shaped tip most probably means that the fracture was already there. The re-stimulated stages also do not display the expected shape of the wings. There is compression surrounding the fracture, but the region extends longer in time.

There are other stages that present antennas but they also have heart-shaped tips happening later, like in Stage 6 (Figure 2.14b). Here, the antenna comes from a fracture stimulated in Stage 5, but the injection also created a hydraulic fracture, as we have a heart-shaped tip happening later in the injection. The antennas can come from the re-stimulation of either a natural fracture or a hydraulic fracture created in the treatment of the current well or past wells.

The antenna usually disappears after the heart-shaped tip of the new hydraulic fracture intercepts the monitoring well, but we have cases where the antenna signal keeps showing even after the new hydraulic fracture reaches the monitoring well. In the first case it seems like the pre-existent fracture reopens due to a fluid pulse at the start of the injection, causing the antenna, and then the fluid breaks the rock and it starts moving through the new hydraulic fracture, the pre-existent fracture does not seem to receive more of the fluids. In the second case, the pre-existent fracture is being re-stimulated for most of the injection, so its signal is visible in the strain fronts past the arrival of the new hydraulic fracture.

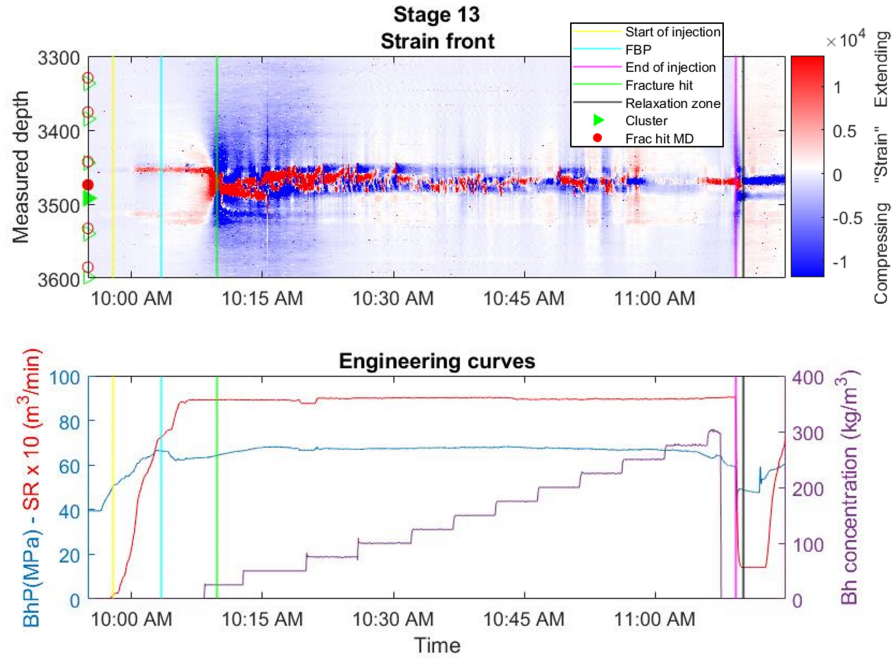


Figure 2.11: Strain front and engineering curves of Stage 13 with its characteristics picked out.

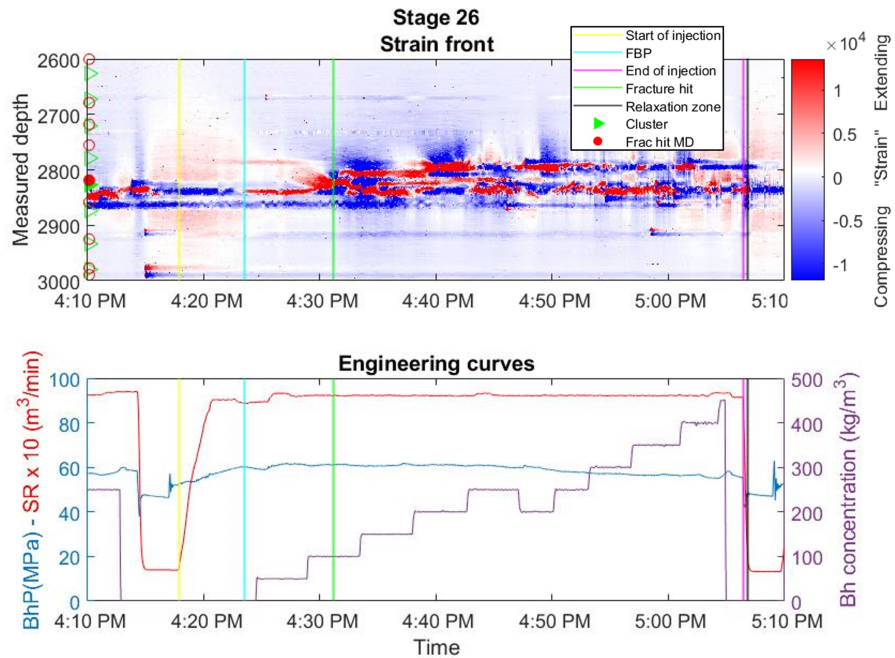


Figure 2.12: Strain front and engineering curves of Stage 26 with its characteristics picked out. Multiple dragonflies are visible in the strain front.

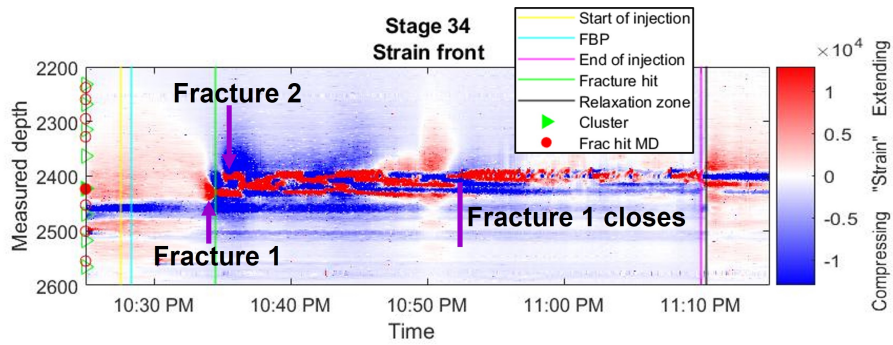


Figure 2.13: Strain front of Stage 34 with its characteristics picked out. Two dragonflies are visible, the first fracture stops propagating mid injection meanwhile the second one continues until the end of injection.

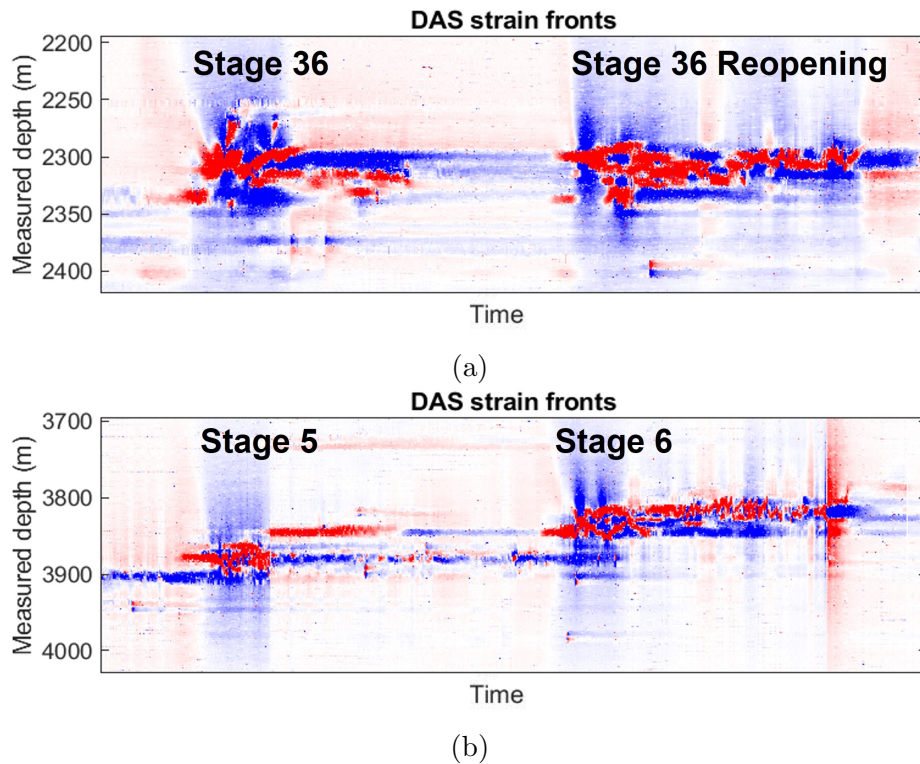


Figure 2.14: 2 cases of Stages with antennas in strain fronts. a) Stage 36 was stimulated twice, the second time the dragonfly does not present the hear-shaped tip. b) Stage 6 has an antenna but also a heart-shaped tip, the antenna is a fracture from Stage 5 being reopened but the injection also created a new fracture as the hear-shaped tip is present.

Figure 2.15 displays a chart with the DAS strain fronts and engineering curves characteristics distribution across all stages. The blue columns mean the characteristic is present and red means it is not. Most stages present the expected heart-shaped tip. Most stages present some sort of antenna. Also, most stages present characteristics of having created multiple fractures which would be that they present; multiple dragonflies, heart tips, wings, and/ or tails. Another thing noticed in this analysis is that almost 60 percent of the stages do not present noticeable FBP peaks even though the strain fronts show that new fractures are being created (presence of heart-shaped tips). Possible explanations for this behavior include the presence of initial cracks in the formation that lower the FBP and makes it easier to create hydraulic fractures with little resistance, or the FBP is less than or equal to the minimum principal stress which does not create the characteristic peak in the pressure curves.

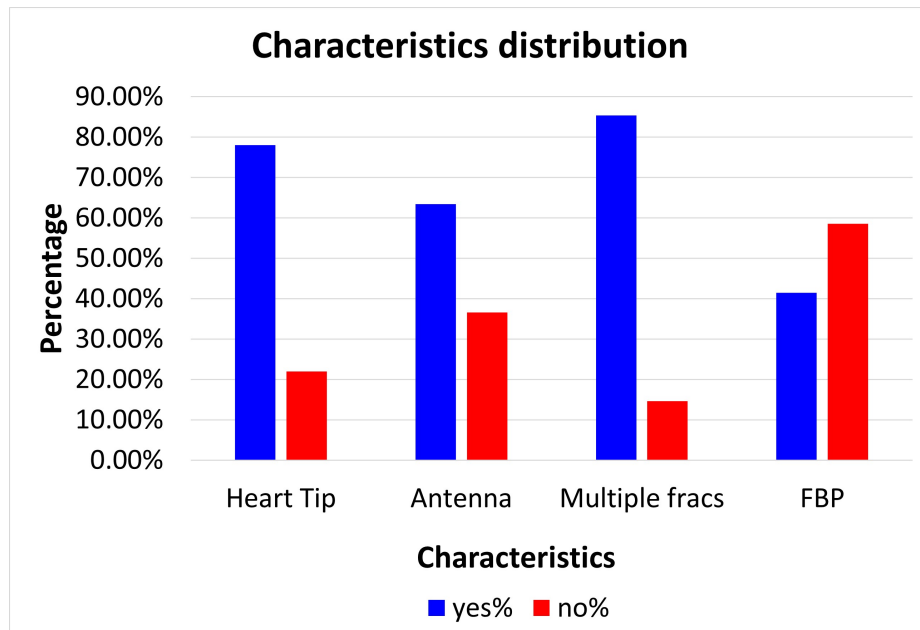


Figure 2.15: Chart with the DAS characteristics; heart tip, antenna and multiple fractures, and engineering curves characteristic; FBP, distribution across all stages. Blue means stages have that characteristic and red means they do not.

2.4.2 Propagation speeds

The minimum fracture propagation speed per stage, assuming that fractures propagate perpendicular to the treated well is shown in Figure 2.16. Stages with speeds above 45 m/min were deemed outliers and eliminated. I did not remove speeds with low rates. The plot has the data trendline (blue dotted line), best fit linear equation, lower and upper boundaries of the data (red lines). The boundaries are lines parallel to the original trendline with ± 35 percent the average of the original line. Values outside these boundaries could be anomalies. The average speed of fracture propagation in this well is 21.13 meters per minute. We see how the speed increases in the later stages. This could be because the injection rate was increased systematically and/or the formation closer to the heel may be more fractured which allows the fractures to propagate more easily.

On the strain fronts, there is a time difference between the end of the injection and the start of the Relaxation zone, which shows how long it takes the fractures to start closing after the end of the injection. Figure 2.17 shows a graph with this time difference among the stages. Once again, the plot has the data trendline (blue dotted line), best fit linear equation, lower and upper boundaries of the data (red lines). The boundaries this time were set to ± 75 percent the average of the original line because of the dispersion of the data. Values outside these boundaries could be anomalies. The time difference goes from as little as 10 seconds to as long as 2 minutes and 30 seconds, as seen in Figure 2.17. The average time difference is 52 seconds across all the treatment. As mentioned before, this delay might tell us about fluid communication inside the well. The only pattern found was that the time difference decreases with stages, which could mean the pressure and fluids are more easily dispersed and leaked into the formation as it is more fractured. Another explanation could be that the cumulative stress shadows from the previous stages induce an accelerated fracture closure upon end of injection because of fluid build up

with associated increased volumetric strain.

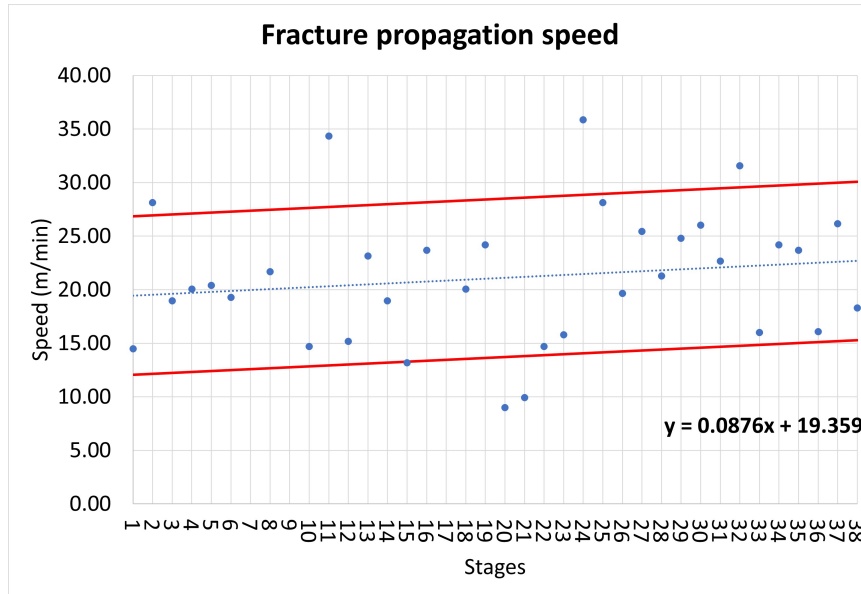


Figure 2.16: Fracture propagation speed for every stage using DAS strain fronts. The average speed is 21.13 m/min. Speeds above 45 m/min were considered outliers and eliminated. Trendline (dotted blue line) and best fit linear equation are displayed. Upper and lower boundaries of the data are represented by the red lines.

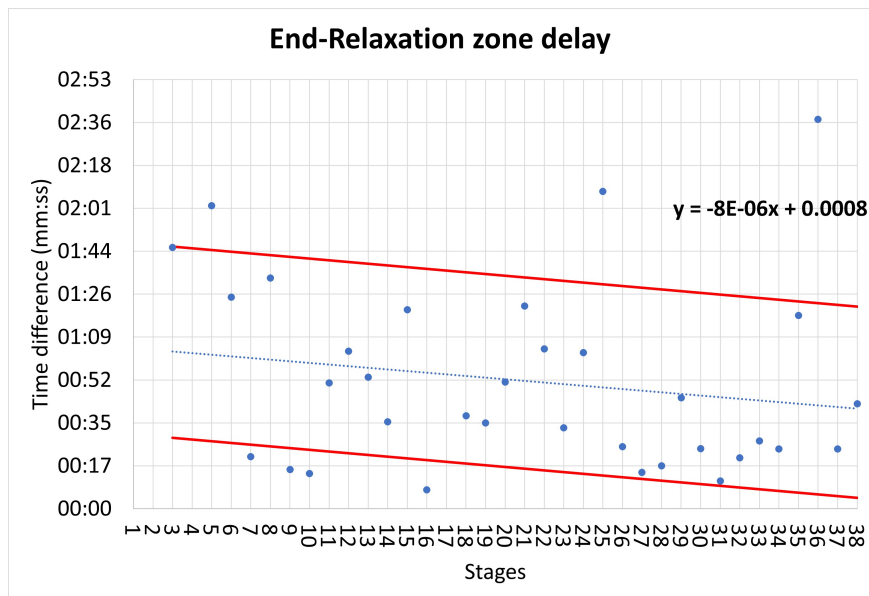


Figure 2.17: Time difference between the end of injection and the start of the Relaxation zone. The average time difference which is 52 seconds. Trendline (dotted blue line) and best fit linear equation are displayed. Upper and lower boundaries of the data are represented by the red lines.

2.4.3 Fracture connection map

Figure 2.18 shows the final fracture connection map with original geometry of the wells. The blue line is the treated well, the blue dots are the clusters for every stage, the black line is the monitoring well with the fiber, the red dots are the fracture hits and the red lines are the inferred fracture azimuths. The fractures propagate towards the North-East, perpendicular to the treated well, as expected given that the maximum horizontal stress is perpendicular to the well orientation. However, some paths have a steep inclination angle. This could be because there are other fractures in the formation that diverted the hydraulic fracture or something unexpected happened during the injection. The PKN model, introduced in Chapter 4, might be able to cast some light on why the fractures deviated from the perpendicular by comparing expected propagation speeds according to the parameters of the treatment to the speeds obtained from the DAS strain fronts.

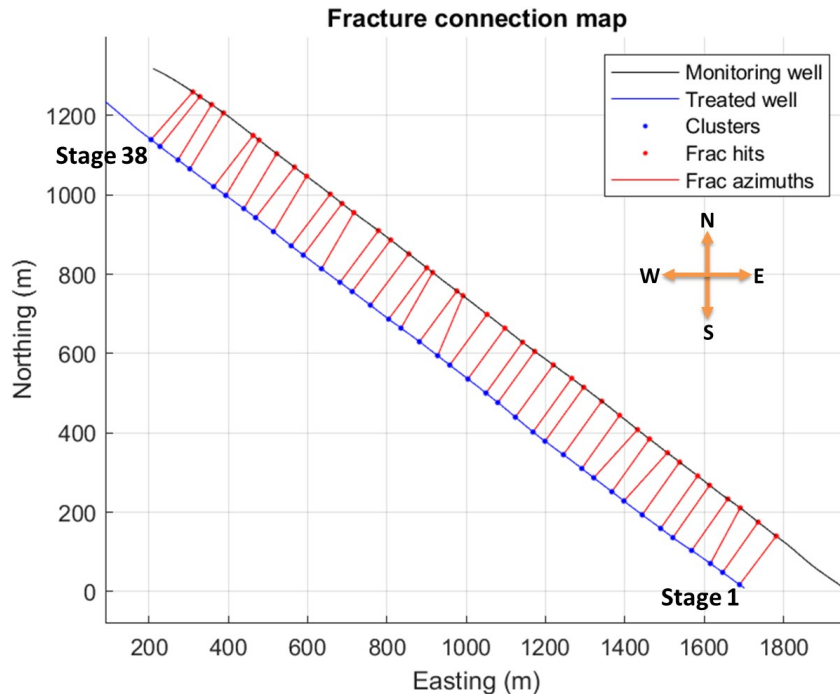


Figure 2.18: Fracture connection map for all stages, with original wells geometry See Figure 2.10 for full legend. Displays the direction of fracture propagation. The stimulation started on the right in Stage 1 (toe of the well) and finished on the left in Stage 38 (heel of the well).

2.4.4 Characteristic distribution per stage

Figure 2.19 shows the fracture connection map (Figure 2.18) with different color dots on top of the fracture azimuths that stand for different characteristics present in that stage. The green dots mean that the first dragonfly signal in the stage presents a heart-shaped tip. Purple dots symbolize the presence of antennas in the dragonfly signals. The yellow dots represent the presence of multiple fractures in the stage, meaning there are multiple heart-shaped tips, wings, tails, and/or dragonfly signals in the strain front. Cyan dots mean that the bottom-hole pressure curve in the stage presents the formation breakdown pressure peak. The pink arrows mark the stages that present a deviated azimuth. They did not propagate perpendicularly from the treated well, and they show the direction of the deviation, NE or SE.

This plot makes it easier to notice some patterns in the characteristic distribution among the stages. For example, the presence of a heart-shaped tip does not necessarily mean there is an FBP peak. In most of the stages that have this combination, a heart-shaped tip - no FBP, also present antennas like Stage 18 shown in Figure 2.20. The antennas indicate that there were initial cracks close to the injection point, and they helped to open the new hydraulic fractures with less resistance, which lowered the FBP value. Other stages that do not present antennas, but have the heart-shaped tip - no FBP combination, present the reopening of the previous stage tail or of a pre-existent fracture (either natural or from past fracturing treatments, the signal is not traced to a previous stage). Although it is clearly separated from the heart-shaped tip and so, not considered an antenna like Stage 23 shown in Figure 2.21.

Stages that have antennas but do not present heart-shaped tips, like Stage 11 (Figure 2.9b, might seem like stages where the injection did not create a fracture. However, all these stages also present indications that multiple fractures were created, like Stage 11, that presents two pairs of wings and two tails. The stress shadow of the re-opened fracture responsible for the antenna might have suppressed the heart-

shaped tip of the new hydraulic fracture.

The azimuth deviation happens mostly towards the heel of the well and in the later stages, which is not expected, as we would assume they will deviate towards the toe of the well where it's fractured. It seems like the fractures are going away from the stress shadow of previous stages. Another reason could be that they are intercepting fractures created from previously fractured wells (this was the third fractured well).

Chapter 3 presents the analysis of the propagation and characteristics of the microseismic clouds. This will provide information on what happened in other parts of the formation that are not seen by the DAS cable. The integration of the DAS data and the microseismicity will provide a wider picture of what happened during the fracturing treatment.

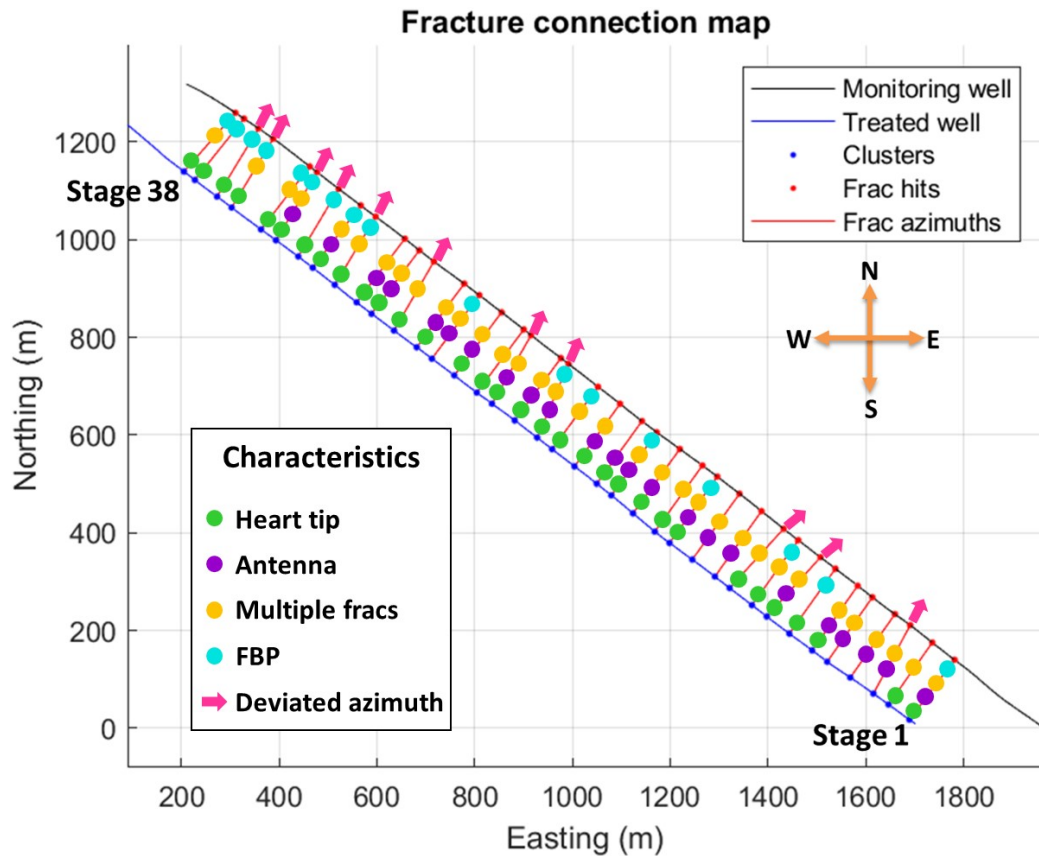


Figure 2.19: Fracture connection map for all stages, with original wells geometry. See Figure 2.18 for full legend. The dots represent characteristics present in each stage. Green means the presence of a heart-shaped tip, purple means the presence of an antenna, yellow means multiple fracs, cyan means clear FBP peak, and the pink arrows mark the stages that did not propagate perpendicular from the treated well.

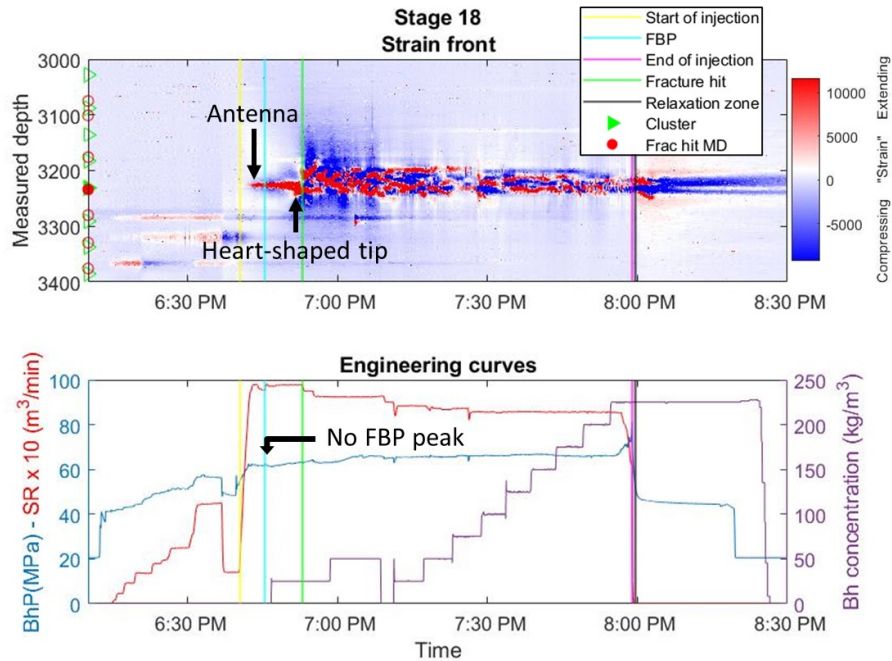


Figure 2.20: Stage 18 strain front and engineering curves. This stage is an example of a stage that has a heart-shaped tip, no FBP peak, and an antenna.

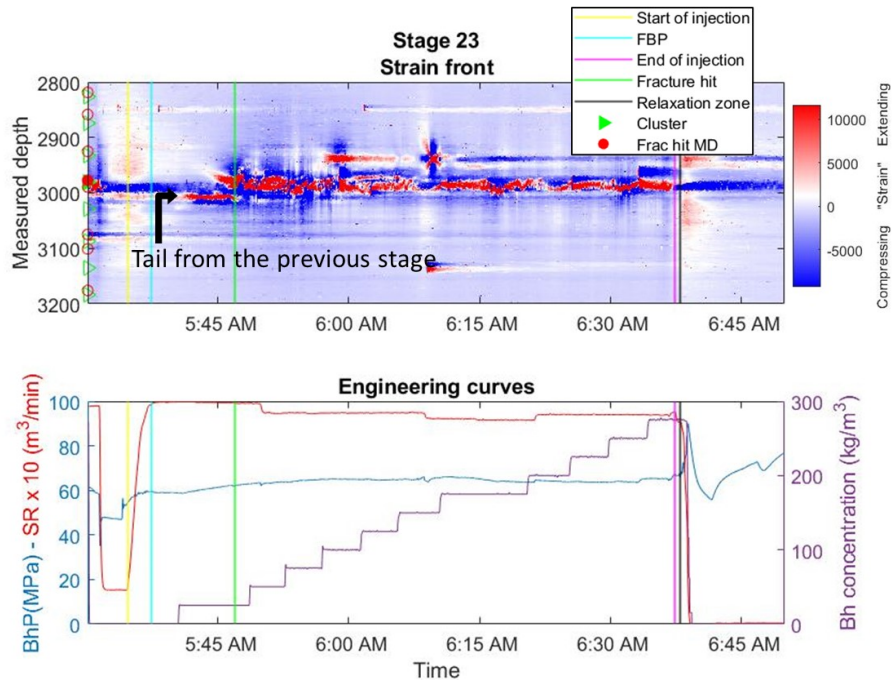


Figure 2.21: Stage 23 strain front and engineering curves. This stage is an example of a stage that has a heart-shaped tip, no FBP peak, and no antenna, but the tail of the previous stage was reopened during treatment.

2.5 DAS analysis conclusions

In this chapter, the low-frequency DAS strain fronts and the engineering curves of one hydraulic fracturing treatment were analyzed.

The low-frequency DAS strain fronts have characteristic features that provide a way to visualise hydraulic fractures propagation at the monitoring well and estimate some of its characteristics when integrated with the engineering curves. The DAS data also helps identify whether previous stages are being re-stimulated as long as the re-stimulated fracture passes through the monitoring well.

The fracture signal on the strain fronts resembles the shape of a dragonfly. If it is a newly created fracture intercepting the monitoring well, the dragonfly will have a heart-shaped tip with wings on the side. If the fracture was already opened, the dragonfly will have only an antenna that occurs almost at the start of the injection and the stress shadow surrounding the fracture will not have the characteristic wing shape. If the dragonfly presents an antenna and a heart-shaped tip, that means that a pre-existent fracture is being re-stimulated, but the injection did create a new fracture.

In this hydraulic fracturing treatment, most of the stages do not have a FBP peak, but the strain fronts present evidence that fractures are being created. It seems like the re-stimulation of previous fractures during injection lowered the FBP for the new ones.

When multiple fractures are created during one stage, they open towards the heel of the well, away from the stress shadow of the previous stage. If the fractures are created with enough spacing between them, the strain fronts present multiple dragonflies. If the fractures are close to each other, the dragonfly signals are suppressed by the main or first fracture created, but some features are still visible, like multiple heart-shaped tips, wings and/or tails.

The hydraulic fractures of this treatment propagated mostly perpendicular to the

treated well. Azimuth deviation happens mainly in the final stages and towards the heel of the well, because of the stress shadow of the previous stages.

The average speed of the hydraulic fractures is 21.13 m/min. Due to completion parameters and/or formation state, their propagation speed progressively increases.

The fractures take less time to start closing after the end of the injection towards the final stages. This indicates that the pressures and fluids are more easily dispersed into the formation and/or that the cumulative stress shadows from the previous stages induce an accelerated fracture closure.

Low-frequency DAS is effective in monitoring hydraulic fractures at the monitoring well. However, we do not know what is happening in other parts of the formation. Microseismicity can complement the DAS analysis by extending the range of information. This will be the focus of the next chapter.

References

- Asgarpour, S. (2013). The modern practices of hydraulic fracturing: A focus on Canadian resources. *52*, 83–85.
- Ballotpedia. (n.d.). *Slurry* [accessed on 2022-04-18]. <https://ballotpedia.org/Slurry>
- Becker, M., Ciervo, C., & Coleman, T. (2018). Laboratory testing of low-frequency strain measured by distributed acoustic sensing (DAS). *SEG Technical*, 3. <https://doi.org/10.1190/segam2018-2997900.1>
- Becker, M., Coleman, T., & Ciervo, C. (2020). Distributed Acoustic Sensing (DAS) as a Distributed Hydraulic Sensor in Fractured Bedrock. *Bedrock. Water Resources Research*, *56*(9), 10. <https://doi.org/10.1002/essoar.10503402.1>
- Cole, S., Karrenbach, M., Boone, K., Ridge, A., Kahn, D., Rich, J., Silver, K., & Langton, D. (2017). Effective Diffusivity Estimates from Distributed Fiber-optic Strain and Microseismic Measurements. *SEG Technical Program*, 5. <https://doi.org/10.1190/segam2017-17680716.1>
- Dutler, N., Valley, B., Gischig, V., Jalali, M., Brixel, B., Krietsch, H., Roques, C., & Amann, F. (2020). Hydromechanical insight of fracture opening and closure during in-situ hydraulic fracturing in crystalline rock. *International Journal of Rock Mechanics and Mining Sciences*, *135*, 17. <https://doi.org/10.1016/j.ijrmms.2020.104450>
- Fernandez-Ruiz, M., Soto, M., Williams, E., Martinez-Lopez, S., Zhan, Z., Gonzales-Herraez, M., & Martins, H. (2020). Distributed acoustic sensing for seismic activity monitoring. *APL Photonics*, *5*(3), 16. <https://doi.org/10.1063/1.5139602>
- Grubert, M., Li, X., & Chavarria, A. (2020). Making sense of unconventional with DAS, journal=Oilfield Technology. *13*(1), 21–24.
- Hartog, A. (2017). *An introduction to distributed optical fibre sensors*. CRC Press. <https://doi.org/10.1201/9781315119014>
- Hubbert, M. K., & Willis, D. G. (1957). Mechanics Of Hydraulic Fracturing. *Transactions of the AIME*, *210*(01), 153–168. <https://doi.org/10.2118/686-G>
- Jin, G., & Roy, B. (2017). Hydraulic-fracture geometry characterization using low-frequency DAS signal. *The Leading Edge*, *36*, 975–980.
- Jin, G., & Roy, B. (2019). Using Distributed Acoustic Sensing to Monitor Hydraulic Fracturing Operations, 5.
- Karrenbach, M., Ridge, A., Cole, S., Boone, K., Rich, J., Silver, K., & Langton, D. (2017). DAS Microseismic Monitoring and Integration With Strain Measurements in Hydraulic Fracture Profiling, 1316–1330. <https://doi.org/10.15530/urtec-2017-2670716>
- Kavousi, P., Wilson, T., Carr, T., Kumar, A., Hammack, R., & Di, H. (2018). Integrating Distributed Acoustic Sensing (DAS), Borehole 3C Geophone Array, and Surface Seismic Array Data to Identify Long-Period Long-Duration Seismic Events during Stimulation of a Marcellus Shale Gas Reservoir. *Interpretation*, *7*(1), 1–37. <https://doi.org/10.1190/int-2018-0078.1>

- Lavrov, A. (2016). Chapter 5 - Mechanisms and Diagnostics of Lost Circulation. In L. Alexandre (Ed.), *Lost Circulation* (pp. 99–162). Gulf Professional Publishing. <https://doi.org/https://doi.org/10.1016/B978-0-12-803916-8.00005-4>
- Lee, B., Lee, Y. W., & Song, M. (2006). Guided Wave Optical Components and Devices. Elsevier Academic Press. <https://doi.org/10.1016/B978-012088481-0/50027-9>
- Lellouch, A., Schultz, R., Lindsey, N., Biondi, B., & Ellsworth, W. (2020). Low-magnitude Seismicity with a Downhole Distributed Acoustic Sensing Array – examples from the FORGE Geothermal Experiment. *Journal of Geophysical Research: Solid Earth*, *27*, 20.
- Liu, Y., Wu, K., Jin, G., & Moridis, G. (2020). Rock Deformation and Strain-Rate Characterization during Hydraulic Fracturing Treatments: Insights for Interpretation of Low-Frequency Distributed Acoustic-Sensing Signals. *SPE Journal*, *25*(05), 2251–2264. <https://doi.org/10.2118/202482-PA>
- Mellors, R., Sherman, C., Fu, P., McLennan, J., Morris, J., Ryerson, F., & Morency, C. (2019). Potential Use of Distributed Acoustic Sensors to Monitor Fractures and Microseismicity at the FORGE EGS site. *44th Workshop on Geothermal Reservoir Engineering*, 6.
- Molenaar, M., & Cox, B. (2013). Field cases of hydraulic fracture stimulation diagnostics using fiber optic distributed acoustic sensing (DAS) measurements and Analyses, 10. <https://doi.org/10.2118/164030-MS>
- Muanenda, Y. (2018). Recent Advances in Distributed Acoustic Sensing Based on Phase-Sensitive Optical Time Domain Reflectometry. *Journal of Sensors*, *23*, 1–16. <https://doi.org/10.1155/2018/3897873>
- Muanenda, Y., Oton, C. J., & Di Pasquale, F. (2019). Application of Raman and Brillouin Scattering Phenomena in Distributed Optical Fiber Sensing. *Frontiers in Physics*, *7*, 155.
- Oil and gas overview. (n.d.). *Basic Hydraulic Fracturing Calculations* [accessed on 2022-04-18]. <https://oilandgasoverview.com/basic-hydraulic-fracturing-calculations/>
- Parker, T., Shatalin, S., & Farhadiroushan, M. (2014). Distributed Acoustic Sensing, A new tool for seismic applications. *First Break*, *32*, 9.
- Paschotta, R. . (n.d.). *RP PHOTONICS ENCYCLOPEDIA* [accessed on 2020-09-20]. https://www.rp-photonics.com/rayleigh_scattering.html
- Richter, P., Parker, T., Woerpel, C., Wu, Y., Rufino, R., & Farhadiroushan, M. (2019). Hydraulic fracture monitoring and optimization in unconventional completions using a high-resolution engineered fibre-optic Distributed Acoustic Sensor, 6.
- Schlumberger. (n.d.). *Breakdown pressure* [accessed on 2022-04-19]. https://glossary.oilfield.slb.com/en/terms/b/breakdown_pressure
- Sharma, J., cuny theo, t., Ogunsanwo, T., & Santos, O. (2020). Low-frequency distributed acoustic sensing for early gas detection in a wellbore. *IEEE Sensors Journal*, *PP*, 15. <https://doi.org/10.1109/JSEN.2020.3038738>
- Trenchlesspedia. (n.d.). *Bottomhole Pressure (BHP)* [accessed on 2022-04-18]. <https://www.trenchlesspedia.com>

- Ugueto, G., Todea, F., Daredia, T., Wojtaszek, M., Huckabee, P., Reynolds, A., Laing, C., & Chavarria, J. (2019). Can You Feel the Strain? DAS Strain Fronts for Fracture Geometry in the BC Montney, Groundbirch. *Proceedings of SPE Annual Technical Conference and Exhibition*, 15. <https://doi.org/10.2118/195943-MS>
- Webster, P., Cox, B., Molenaar, M., & Canada., S. (2013). Developments in Diagnostic Tools for Hydraulic Fracture Geometry Analysis. *Unconventional Resources Technology Conference, Denver, Colorado, USA*, 218–224.
- Webster, P., Wall, J., Perkins, C., & Molenaar, M. (2013b). Microseismic detection using distributed acoustic sensing, 2459–2463.
- White, M., Frieauf, K., Cramer, D., Constantine, J., Zhang, J., Schmidt, S., Long, J., Mislán, P., Spencer, J., Meier, P., & Davis, E. (2020). *One Stage Forward or Two Stages Back, What are We Treating? Identification of Internal Casing Erosion During Hydraulic Fracturing - A Montney Case Study Using Ultrasonic and Fiber-Optic Diagnostics* (Vol. Day 2 Tue, October 27, 2020) [D021S016R006]. <https://doi.org/10.2118/201734-MS>
- Yu, C., Zhan, Z., Lindsey, N., Ajo-Franklin, J., & Robertson, M. (2019). The potential of distributed acoustic sensing (DAS) in teleseismic studies: insights from the Goldstone experiment, *Journal of Geophysical Research Letters*, 10. <https://doi.org/10.1029/2018GL081195>
- Zoback, M. D., Haimson, B. C., & Jacobson, M. L. (1982). *Proceedings of Workshop XVII; workshop on hydraulic fracturing stress measurements* (Vol. 1 and 2). U.S. Geological Survey.

Chapter 3

Microseismic analysis

3.1 Microseismic monitoring of hydraulic fractures

Hydraulic fracturing stimulation produces changes in pore pressure and stress in the formation, which results in very small earthquakes, known as microseismic events (van der Baan et al., 2013). These events start shortly after the stimulation initiates and often cease soon after the stimulation stop. They propagate in a cloud-like way that indicates the rock volume affected by the stimulation (Cole et al., 2017; van der Baan et al., 2013). Monitoring of microseismic activity gives information on the propagation and geometry of hydraulic fractures by mapping their spatial and temporal pattern (Cole et al., 2017; Le Calvez et al., 2016).

Microseismic monitoring is one of the most widely used techniques for hydraulic fracture diagnostics. It is performed by deploying sensors, permanently or temporarily, in either a downhole observation well (vertical or horizontal) or on the surface (Maxwell, 2014). The first method offers better signal-to-noise characteristics due to the sensors being closer to the microseismic sources. The second method is more cost-effective and has more extensive azimuthal coverage (van der Baan et al., 2013). The microseismic monitoring for this treatment was conducted with a vertical observation well close to the DAS monitoring well around the middle of the horizontal length.

During treatment, the sensors detect the seismic waves generated by the microseismic sources, compression (P), and shear (S) waves. The information contained within

these waves is used to estimate event locations, magnitudes, and source mechanisms (Maxwell, 2014). In order to estimate these characteristics, the microseismic data undergo some processing. The first step is usually the filtering of the data to remove unwanted noise from the waveforms and so enhance the signal-to-noise ratio (Wang et al., 2016).

After the preconditioning of the data, the microseismic events are located. This step is of great importance as it helps to determine the distribution and geometry of the fractures induced by the fracturing treatment (Wang et al., 2016). The event locations are divided into two categories; travelttime-based methods, and waveform-based methods. The first one is based on the first arrivals of the P and/or S wave and requires phase identification and picking. The second one locates the source by combining the travel time, amplitude, and phase information of seismic waveforms to reconstruct and focus the source energy into an image profile (Li et al., 2020).

The magnitude is the strength of an event. Microseismic events have magnitudes of less than 0. Over the years, there have been many different magnitude scales proposed. However, most of these scales do not relate magnitude to a physical model. The only exception is the moment magnitude proposed by Hanks and Kanamori (1979), which is why is the most commonly used method to describe the size of a microseismic event (Baig & Urbancic, 2010). Moment magnitude measures the size of events in terms of how much energy they release, relating to the amount of movement by rock and the fracture surface. This scale is logarithmic and so the increase of one unit of magnitude is equivalent to an increase of 30 times the energy (Hanks & Kanamori, 1979).

Hydraulic fracture geometry dimensions and propagation properties like length, width, height, and azimuth can be interpreted visually or measured using geometric or statistical approaches (Maxwell, 2014). The simplest method would be to just measure the height, width, and length of the microseismic clouds. Maxwell (2014) proposes to fit a rectangular box to the microseismic cloud. The longest horizontal

side would determine length, the vertical side determines depth, and the shortest horizontal side would determine the width. Obtaining the linear regressions of the microseismic clouds is a good way to determine the azimuths, they are usually in good agreement with results from other more sophisticated methods used to deduce this feature (Warpinski et al., 2013).

It is important to notice that pressures and stresses propagate beyond the created hydraulic fractures and affect the surrounding formation in all directions, that is why the microseismic cloud might not relate to the fractures only, it represents a volumetric map of the extent of rock affected by the treatment (van der Baan et al., 2013). Still, using microseismic monitoring to estimate fracture geometry is possibly the most reliable method.

3.1.1 Microseismic Spatio-temporal evolution and integration with pumping information and DAS

Microseismicity also contributes to reservoir characterization, and this is done by analyzing spatio-temporal dynamics of the microseismic clouds (Shapiro & Dinske, 2009). The evolution of the microseismic cloud distance over time can uncover the underlying physical mechanisms that cause the events (Shapiro et al., 2006). The r-t plots show the distance "r" of the microseismic event from the injection point in each stage over time "t". So basically, it shows the microseismic cloud's growth. If microseismicity is a direct response to the fluid pressure then, for constant-rate injection, a triggering front that expands in distance, r , from the injection point as a function of time t should develop (Shapiro et al., 1997). The triggering front is assumed to follow the pressure front according to

$$r = \sqrt{4\pi Dt}, \tag{3.1}$$

where the distance r is linked to the time t from the injection start and the hydraulic diffusivity D . Giving different diffusivities D we can create approximations of trigger

fronts to envelope the observed microseismic events. This gives us an idea of how the microseismic cloud is expected to grow according to the different diffusivities. Figure 3.1 shows an r-t plot with the expected time-distance behavior produced by different diffusion models.

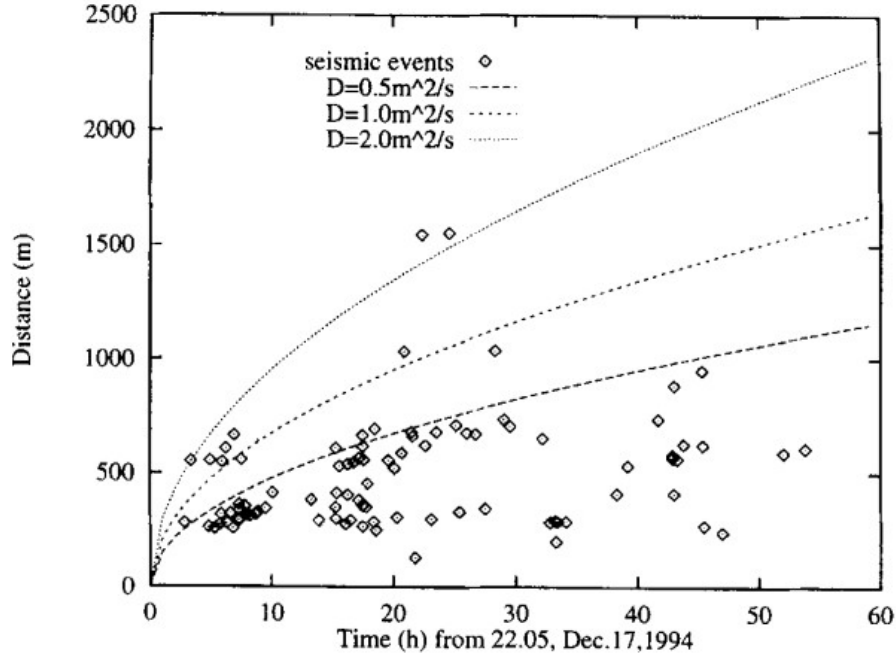


Figure 3.1: Example of an r-t plot. Distances of the MS events from the center of the injection interval versus their occurrence times. Dotted lines denote the expected distance of diffusion-controlled microseismicity (Equation (3.1)) for three different diffusivities $D= 0.5, 1,$ and $2 \text{ m}^2/\text{s}$. Retrieved from Shapiro et al. (1997).

During the beginning of the fracture growth, the triggering fronts may show a quasi-linear behavior, as seen in Figure 3.1 between 0 and 10 hours. This means that the dominant process is the fracture opening. Nevertheless, in the long term, diffusion fluid-loss processes dominate the fracture growth, and the fracture length becomes proportional to \sqrt{t} . If fractures are reopened for a second injection treatment, the triggering front exhibits linear propagation through the injection (Caffagni & Bokelmann, 2017; Shapiro & Dinske, 2009; Shapiro et al., 1997). If the events are not moving further away from the injection point in time, then the fracture stops growing.

There are instances where the events occur at a range of distances from an injection point within a short period of time. This indicates that these events are triggered by stress transfer because this takes place instantaneously, whereas the transfer of pore pressure perturbations from the injection point to the reactivated fault requires time (Shapiro & Dinske, 2009; Shapiro et al., 1997).

To sum it up, there are four development patterns found in the r-t plots. In the "normal" pattern, the microseismic events develop with a parabolic trend, the pore pressure diffusion process is driving the microseismicity. The "reactivation" pattern is displayed when there is reactivation of a pre-existent fracture, the microseismicity develops in a linear fashion. In the "halted growth" pattern, the microseismic events stop increasing in distance and concentrate within an interval, which means that the fracture stops growing. Finally, in the "stress transfer" pattern, the microseismic events occur instantaneously at different distances, meaning that the microseismicity is due to stress transfer.

Comparing the temporal rate of microseismicity to the pumping information (i.e., injection rate, bottom-hole pressure, and proppant concentration) can be used to understand fracture growth (Maxwell, 2014). Figure 3.2 shows a schematic of three different scenarios of microseismicity rate distribution relative to the engineering curves (pumping information), assuming constant injection, and the corresponding potential interpretation, proposed by Maxwell (2014). In the first scenario (Figure 3.2a) there is a high concentration of microseismic events at the beginning of the injection that decreases during the injection, this indicates fracture initiation at the formation breakdown pressure. The second scenario (Figure 3.2b) shows continuous MS occurrence during injection which indicates steady and consistent fracture growth. In the last scenario (Figure 3.2c), the microseismicity increases towards the end of the injection, this can indicate fracture blockage (e.g., proppant screen-out) or another fracture/fault activation.

When the injection stops microseismicity normally stops shortly after and these

events are mainly triggered by the process of the pressure relaxation in the fractured domain. However, sometimes this is not the case and the microseismicity continues even hours after the end of the injection. This could happen due to the release of tectonic stresses as a consequence of fault activation or due to the process of fluid pressure relaxation in the fractured domain. Some cases present an increase in microseismic events occurrence immediately at the end of injection. This might be due to increased sensitivity resulting from reduced pumping ends or to the “water hammer” effect. The water hammer effect is a phenomenon where a short-term pressure spike is caused by the stopping of the injection. This spike is associated with the removal of friction pressure losses, generating a high-pressure pulse in the hydraulic fracture (Maxwell, 2014; Shapiro et al., 2006; Shapiro & Dinske, 2009).

Figure 3.3 shows different scenarios based on pressure rates and microseismic activity during injection according to Maxwell (2014). Scenario 1 shows steady pressure and uniform MS activity meaning the fracture is growing uniformly in a homogeneous reservoir with effective proppant placement. In Scenario 2 both pressure and MS activity raise suggesting formation hardening with proppant screen out. Scenario 3 shows both pressure and MS activity dropping which means formation weakening with effective proppant placement. In Scenario 4 the pressure rises and the MS activity drops, this indicates fracture resistance with few preexisting fractures and effective proppant placement. The last scenario, Scenario 5, shows the pressure dropping and the MS activity rising, this indicates fracture compliance with fault activation and effective proppant placement.

Plotting microseismic events, based on their time and location, on the respective DAS strain fronts, is thought to give a more complete interpretation of fracture development and propagation by being able to correlate the microseismicity with respect to the perforation shot timings and locations to the strain changes in the medium. It is also believed that with this analysis is possible to compare fracture constraints obtained by DAS monitoring and microseismic monitoring. This is a relatively new research and not many studies have been done on it. The only thing known until now is that the occurrence of microseismic events strongly correlates with the largest strain changes, meaning that the fluid/rock interaction manifests itself both in the low-frequency strain field and in the microseismic activity (Cole et al., 2017; Karrenbach et al., 2017). My analysis in this chapter could give us a better understanding of the interactions between microseismicity, strain changes, hydraulic fractures, and injection rate by studying patterns among them.

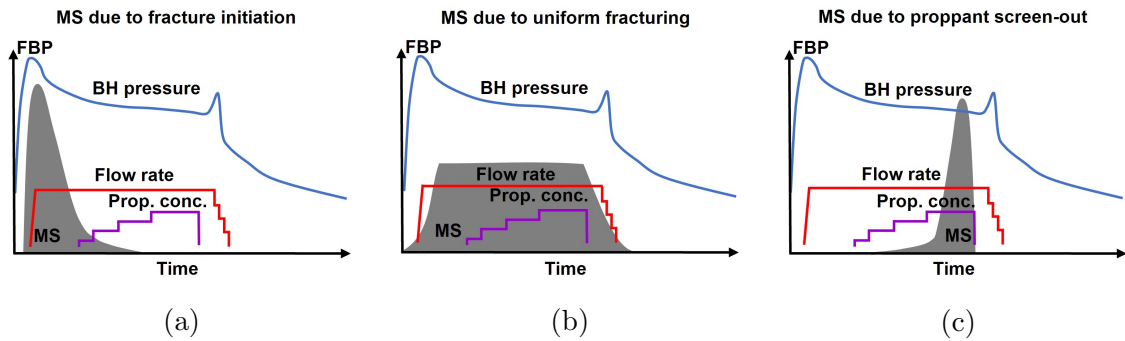


Figure 3.2: Schematic of three different scenarios of microseismicity rates (grey area) relative to the engineering curves; bottom-hole pressure (blue), injection rate (red), and proppant concentration (purple). a) High MS concentration at the beginning of injection indicates fracture initiation. b) Constant MS during injection means consistent fracture growth. c) High MS concentration towards the end of injection indicates fracture blockage or fault activation. Modified from Maxwell (2014).

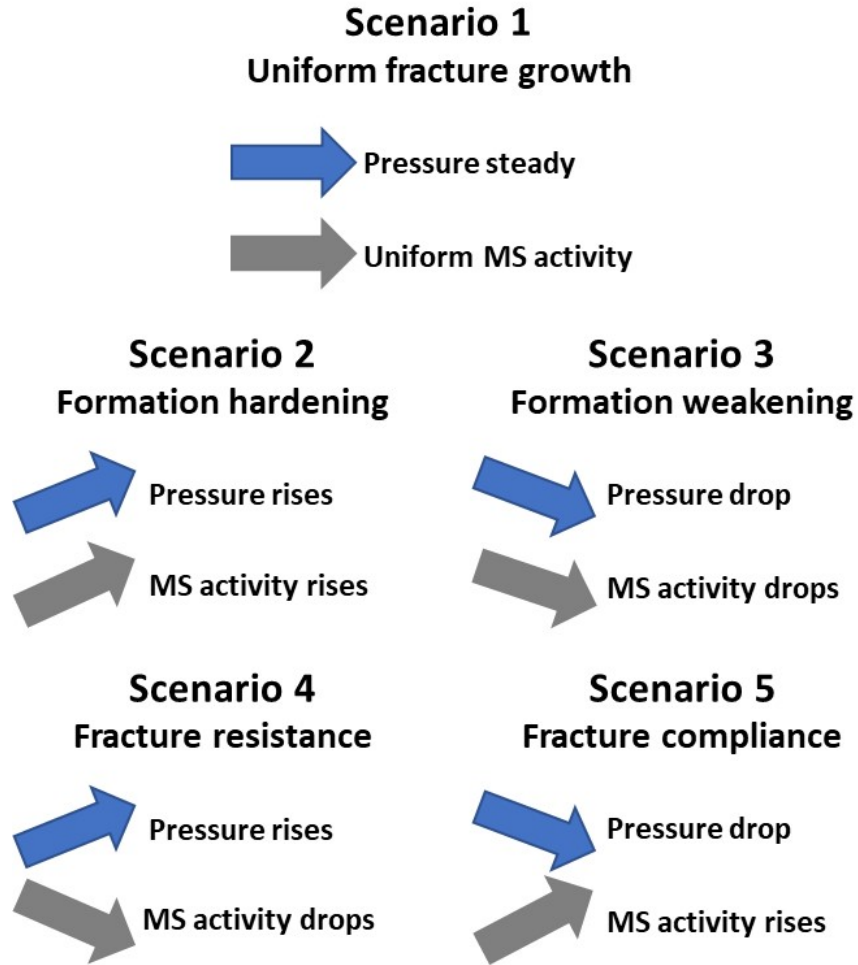


Figure 3.3: Various scenarios based on pressure and microseismic activity rates during the injection. Scenarios 1 to 5 display the behavior that shows uniform fracture growth, formation hardening, formation weakening, fracture resistance, and fracture compliance, respectively. Modified from Maxwell (2014).

3.2 Methodology

For the analysis of the microseismicity data, we first analyzed the microseismic clouds to obtain the trajectory, length, and cloud growth over time (r-t plots). Then we compared the microseismic event locations, timing, and magnitudes to the low-frequency DAS strain fronts and engineering curves.

3.2.1 Microseismic cloud analysis

As previously stated, the microseismic cloud reveals information about hydraulic fractures geometry dimensions and propagation. These characteristics can be estimated mostly visually.

First, the microseismic events were mapped in space by stage along the treated and monitoring wells. This gave us a visual of the microseismic cloud, which represents the volumetric extent of the fracture shearing, opening, and closing. No filters were applied to the data in this stage. Then, a linear regression was fitted to the cloud plane, as a function of space (coordinates x and y , as it propagates mostly in the horizontal plane), to get an approximation of fracture trajectory according to the microseismic events (Figure 3.4).

Next, the length, and height of the microseismic cloud were acquired. This was done by projecting the MS events to a line perpendicular to the treated and monitoring wells, with the treated well as the origin ($x=0$). The microseismic cloud length was obtained by measuring the distance between the treated well and the furthest event from the well on the NE. The height of the MS cloud was measured by taking the deepest event depth and subtracting the depth of the shallowest event (Figure 3.5). The microseismic lengths of all stages were plotted in a horizontal schematic of the wells. Inferred cloud lengths were plotted at the injection point perpendicular to the well (Figure 3.6). The re-stimulated stages were treated as one, the length and height chosen for these stages were from the microseismic events generated during the first injection and the second one.

Finally, the distance of the MS events to the injection point was measured and then plotted over time to create the r - t plot (Figure 3.7). This plot can help identify different diffusive patterns by looking at the cloud's growth pattern over time. For this thesis, triggering fronts were not plotted, as in this case, it was easy to identify when MS events followed different development patterns.

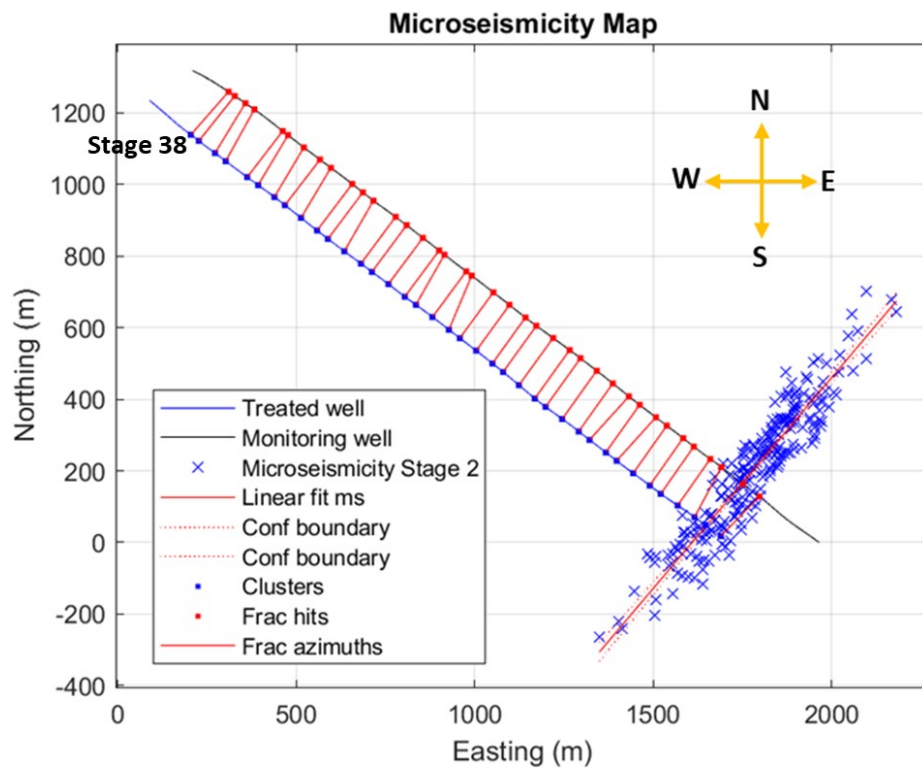


Figure 3.4: Fracture connection map with microseismic cloud and its linear regression for one stage. The microseismic events are the blue stars and the linear regression of the MS clouds is the long red line with confidence boundaries being the dotted red lines.

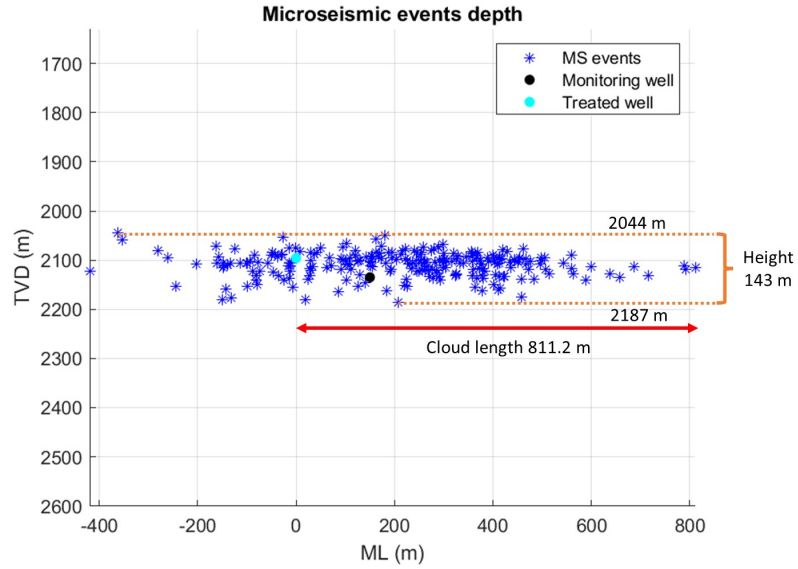


Figure 3.5: Front view of the wells with the microseismic cloud represented by the blue stars. The treated well is at the origin ($x=0$) represented by the cyan dot and the monitoring well is 150 meters apart from the treated well represented by the black dot. The MS cloud length was calculated by measuring the distance between the treated well and the last event on the right. The height of the cloud was estimated by the difference in depths between the shallowest and deepest events.

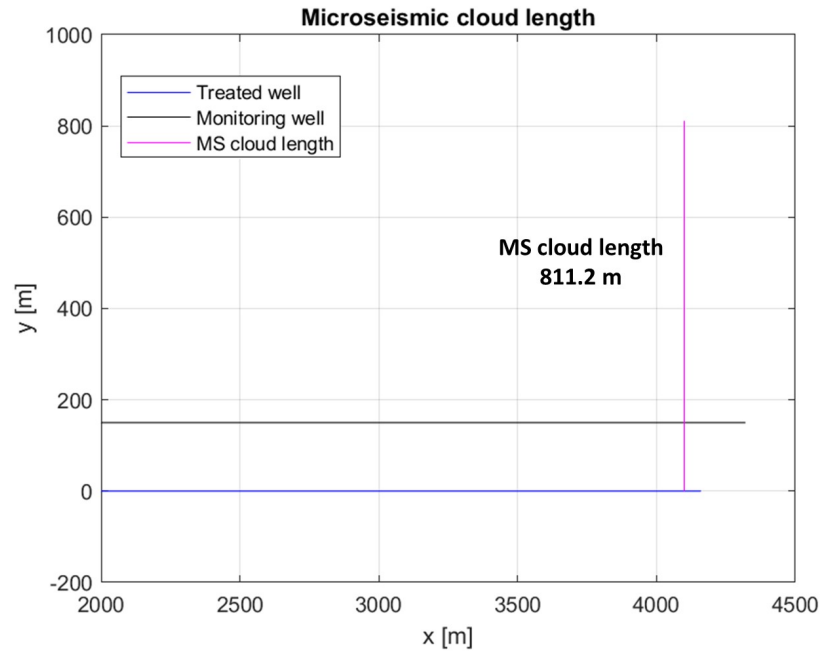


Figure 3.6: Horizontal schematic of the wells. The treated well is the blue line and the monitoring well is the black one. The MS cloud length for one stage is represented by the pink line which is placed at the stage cluster position. Fracture trajectory direction was not considered.

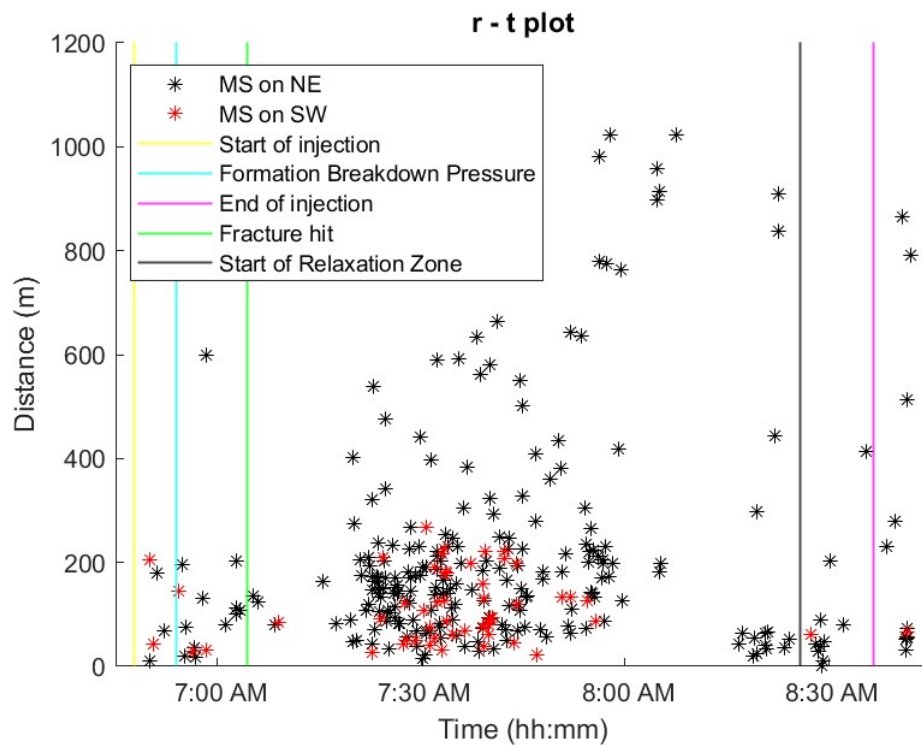


Figure 3.7: Stage r-t plot that shows the distance of the microseismic event from the injection point over time. MS events on the NE of the treated well are represented by the black stars, and the MS events on the SW are represented by the red stars. DAS characteristics and FBP are depicted by the same vertical lines and colors as in the strain fronts in Chapter 2.

3.2.2 Microseismic data integration with DAS and pumping information

To compare the microseismicity with the low-frequency DAS and the engineering curves the microseismic events were plotted on top of the strain fronts based on their time and location. The microseismic events were also plotted according to their magnitude during injection on top of the engineering curves.

First, all microseismicity that propagated away from the treatment well (SW), and those events related to different stages were eliminated using a distance and direction criterion (Figure 3.8a). Then, the remaining events were projected onto the monitoring well, using orthogonal projection, to obtain their measured depth (Figure 3.8b). Next, with their measured depth, the events were plotted on top of the strain fronts as a function of the time of their occurrence. Because these are horizontal wells, a larger measured depth indicates a position closer to the toe of the well.

Finally, the magnitudes of the MS events were plotted over time and inserted between the strain front and the engineering curves with the pumping information so the analysis between the records was easier (Figure 3.9).

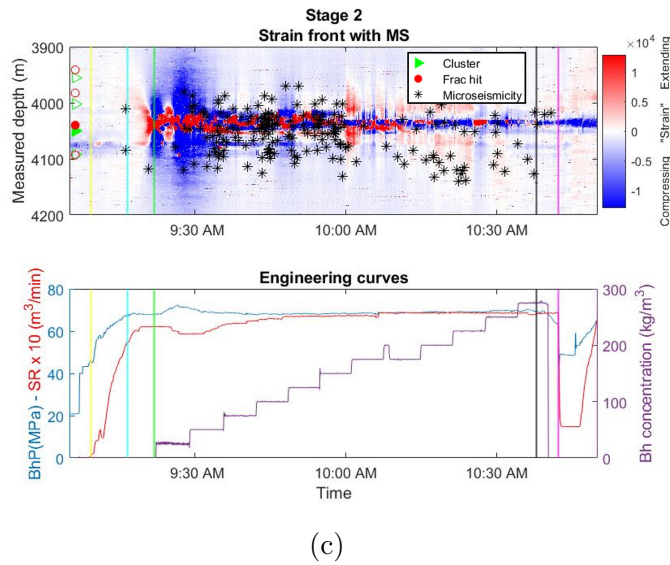
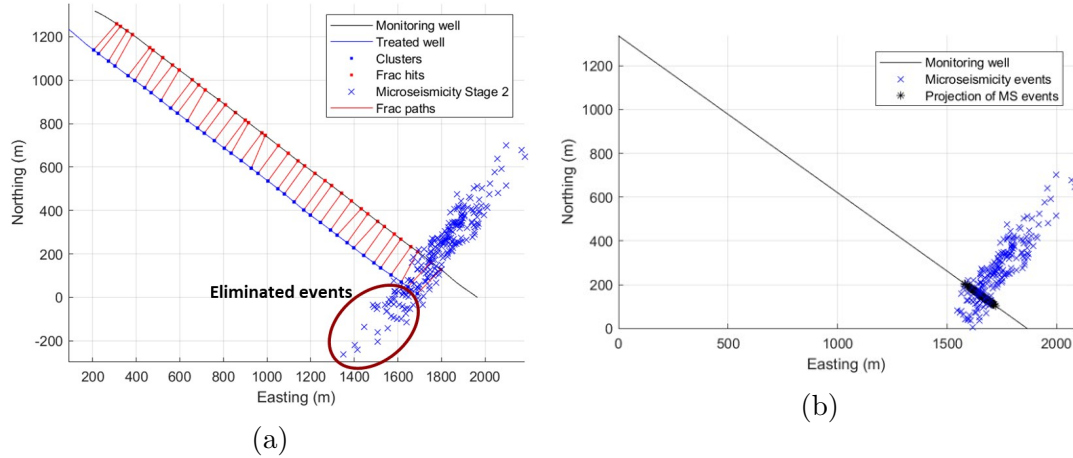


Figure 3.8: Steps to plot MS events on top of strain fronts. a) Filtering, eliminating MS events (blue stars) on the SW of the treated well (blue line). b) Projecting MS events onto the monitoring well (black line) to get their measured depth. Projected MS events are the black stars. c) Using their measured depth we plotted the MS events (black stars) on top of the strain fronts as a function of time.

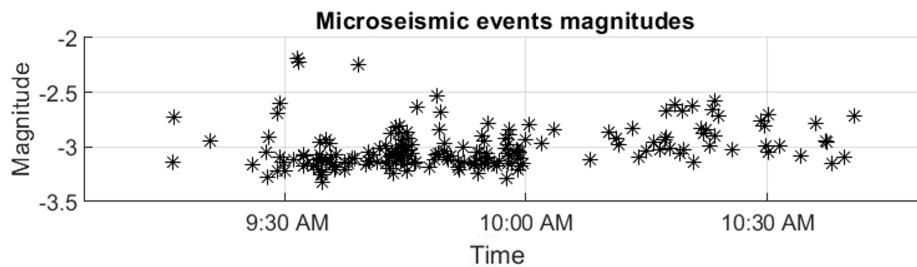


Figure 3.9: Microseismic events plotted as a function of their magnitude and the time of their occurrence.

3.3 Results and Discussion

In this section, the results of the microseismic analysis are introduced and discussed. Some multi-stage results are presented but due to the nature of the study, not all can be shown. For the first part of this analysis, we looked at the microseismic cloud to estimate fracture characteristics such as trajectory, length, height, and the cloud's growth pattern over time. For the second part of this analysis, the microseismicity data were integrated with the DAS and pumping information. The microseismic events were plotted as a function of measured depth and the time of their occurrence on top of the strain fronts after eliminating events that propagated in the opposite direction of the treated well.

3.3.1 Microseismic cloud analysis results

Fracture propagation trajectories

Figure 3.10 shows the microseismicity clouds for all stages. The linear regressions of the microseismic clouds were not included in this plot as they were not visible among all the events. Most clouds propagate towards the North-East, indicating the hydraulic fractures are propagating in that direction. However, there are some stages where they propagated towards the South-West. This is unexpected as we would anticipate bi-wing fractures, but in this treatment it is clear that the hydraulic fractures show preference for the NE.

Figures 3.11, 3.12, and 3.13 show the microseismicity clouds in groups of 4 stages. The red arrows facing right indicate the stages where the microseismic cloud propagated mostly towards the NE. The pink arrows facing left show the stages where the microseismic cloud propagated mostly towards the SW. In these plots it is noticeable that the stages that propagated towards the SW come after particularly long MS clouds or after multiple fractures propagated towards the NE, like in Stages 8 (3.11b), 24 (3.12b), 32 (3.12d). There seems to be a stress gradient that makes it

easier for fractures to propagate towards the NE. However, when the stresses in the formation towards the NE are too great or there is too much fluid/proppant in that direction the fracture changes directions and propagates in the opposite, less stressed, less full direction (SW).

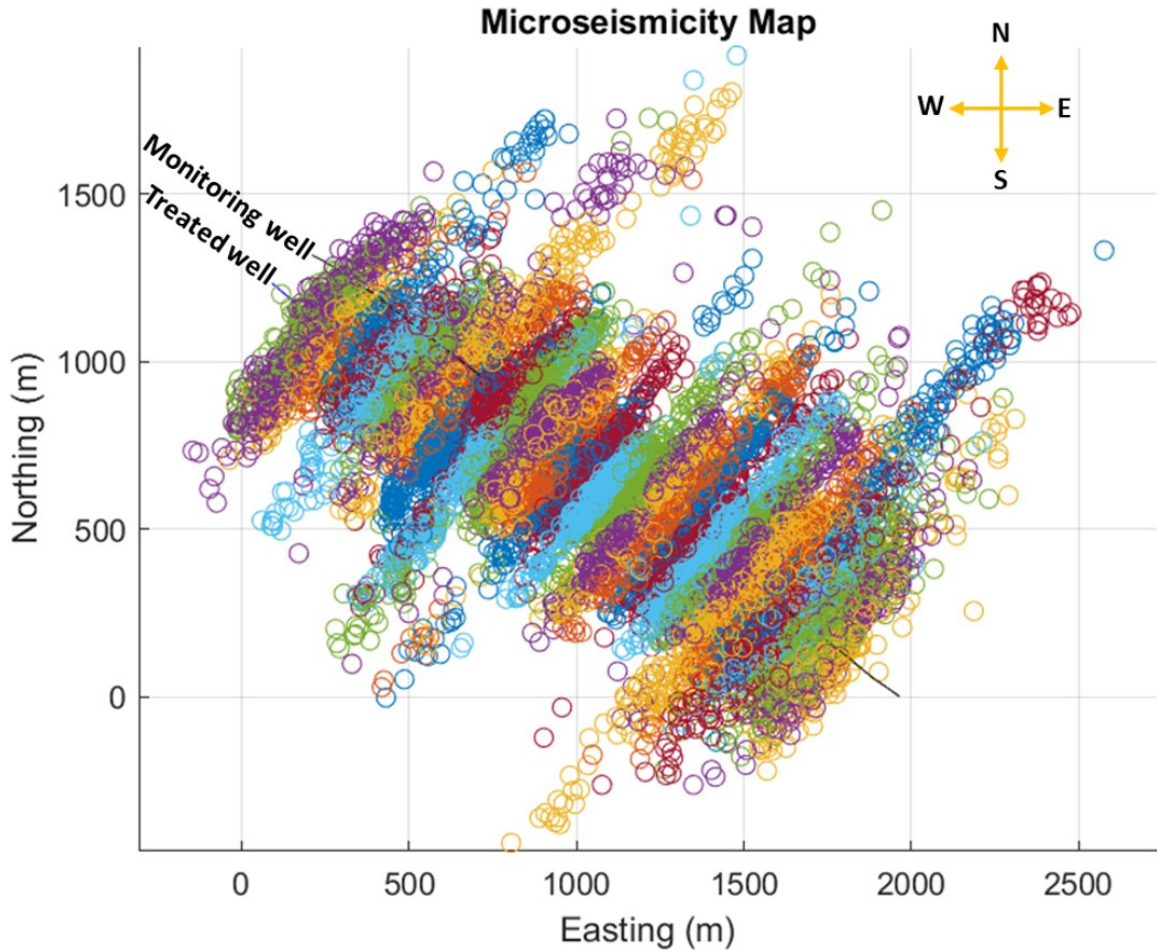


Figure 3.10: Horizontal plane of the wells with the microseismic clouds of all stages. The blue line is the treated, and the black line is the monitoring well. The microseismic clouds are shown in different colors depending on the stage. Microseismic events are propagating mostly towards the northeast.

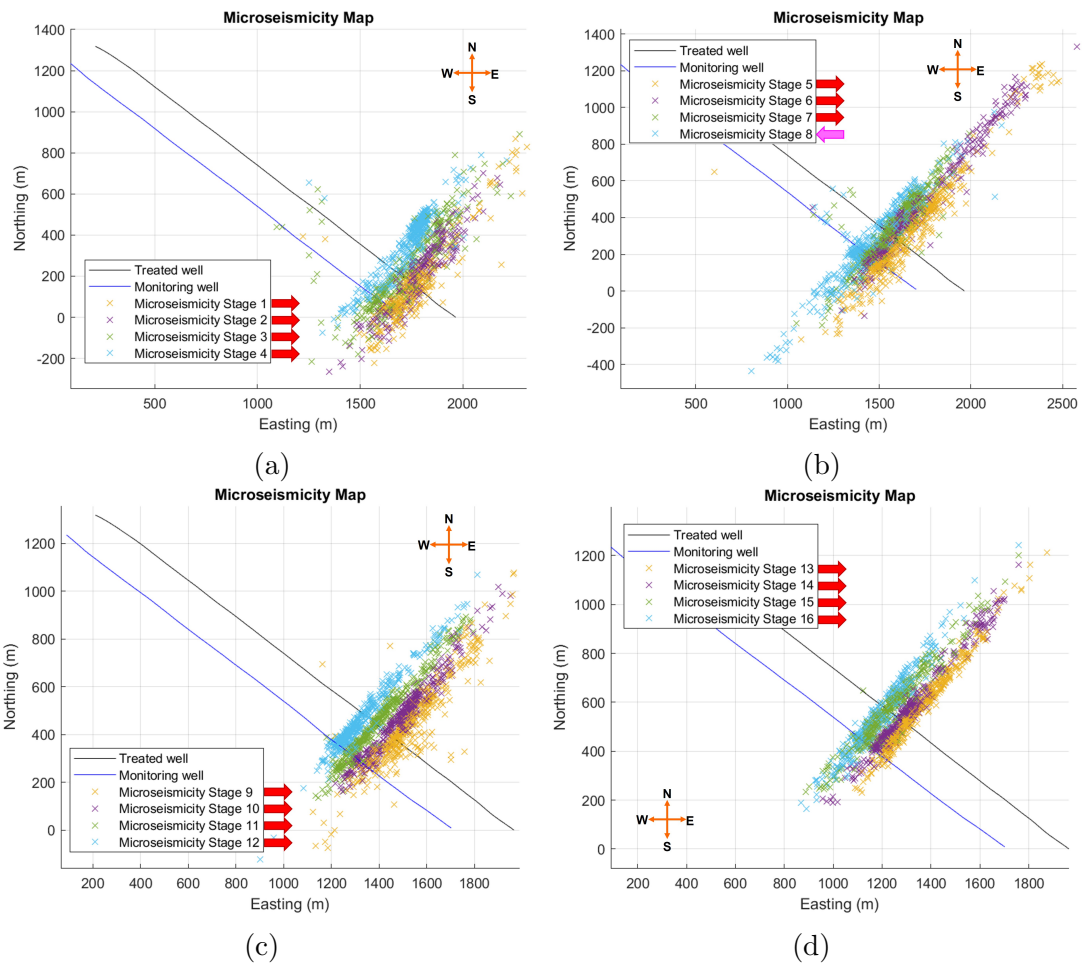


Figure 3.11: Horizontal plane of the wells with the microseismic clouds for: a) Stages 1 - 4. b) Stages 5 - 8. c) Stages 9 - 12. d) Stages 13 - 16.

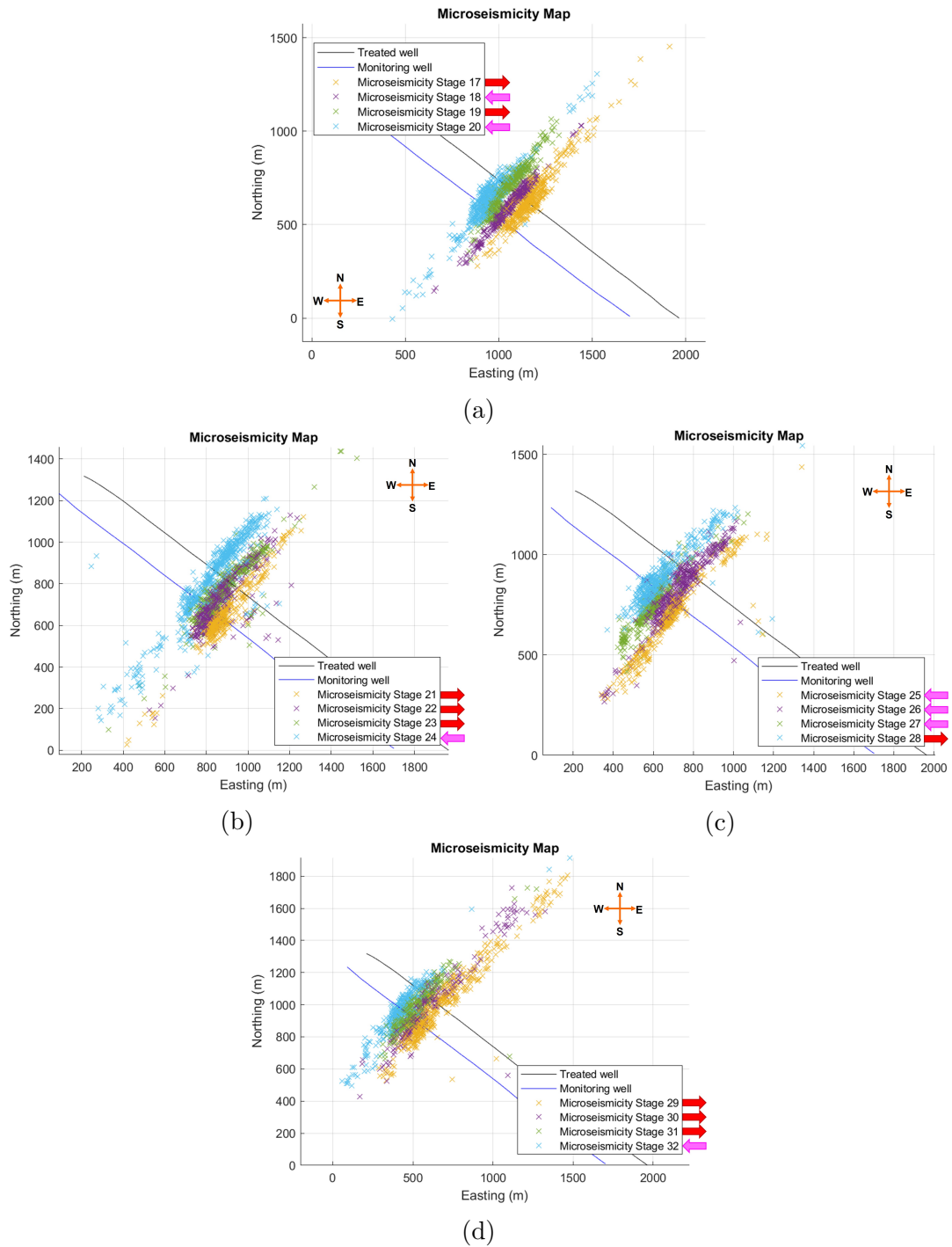
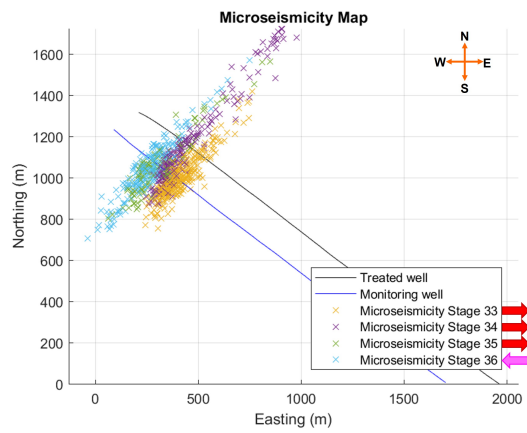
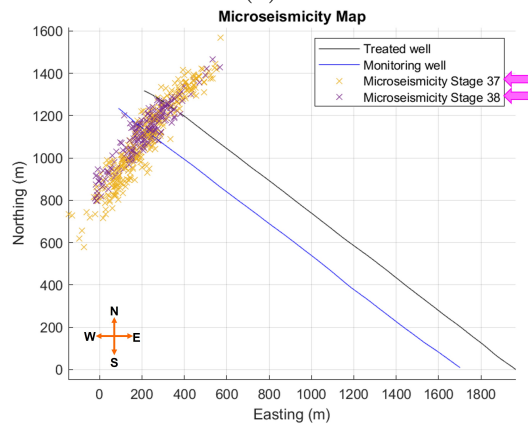


Figure 3.12: Horizontal plane of the wells with the microseismic clouds for: a) Stages 17 - 20. b) Stages 21 - 24. c) Stages 25 - 28. d) Stages 29 - 32.



(a)



(b)

Figure 3.13: Horizontal plane of the wells with the microseismic clouds for: a) Stages 33 - 36. b) Stages 37 and 38.

Fracture lengths

Figure 3.14 shows a schematic of the wells with pink lines that represent the fracture length according to the microseismic cloud length, measuring from the treated well to the NE, the length on the SW of the treated well was not considered. Inferred cloud lengths were plotted at the injection point perpendicular to the well. The purple arrows pointing down represent the stages where the microseismicity cloud propagated mainly towards the SW. The microseismic cloud lengths are longer in the early stages than in the later ones, this is because the time of injection is longer in the early stages. Even though the fractures were slower in the early stages, the injection time in these stages varies from 1:30 to 2 hours and in the later ones the injection time is of 1 hour. The lengths vary between 300 and 1386 meters.

The stages where microseismicity cloud propagated to the SW do present propagation towards the NE as well that ranges from 300 to 500 meters. They usually happen after very large fractures or after several fractures propagated towards the NE cementing the theory that they changed the direction of propagation because the NE direction presented great stresses or too much fluid/proppant.

Fracture heights

The height of the microseismic cloud was calculated as well, the results can be observed in Figure 3.15. This estimation was done because we wanted a representative treatment height for the modeling. Chapter 4 will have more information about this. The heights are mostly between 150 and 160 meters, with heights as small as 128 meters and as big as 205 meters, the average is 162.8 meters.

These were the maximum differences in heights found in the microseismic clouds between the shallowest and deepest event. Actual cloud heights vary as a function of time and position. The maximum height implies the microseismicity is contained within the Middle Montney Member between the depths of 2000 and 2215 meters. The microseismicity does not grow past these depths, which can indicate that it is

contained in a subsurface layer.

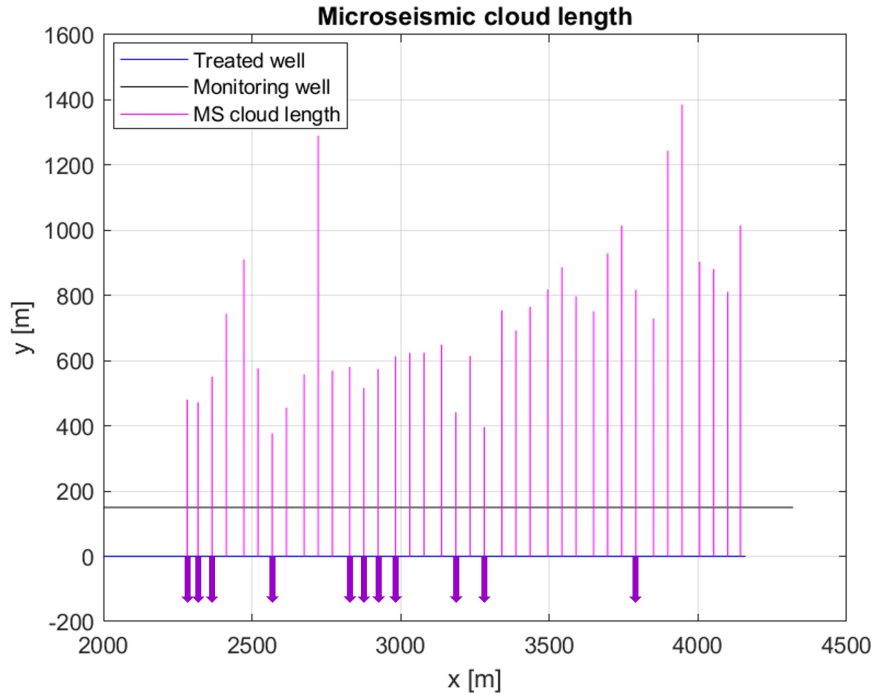


Figure 3.14: Horizontal schematic of the wells. The microseismic cloud lengths for all stages are represented by the pink lines placed at the stage cluster position. Purple arrows represent the stages where the MS cloud propagated mainly towards the SW.

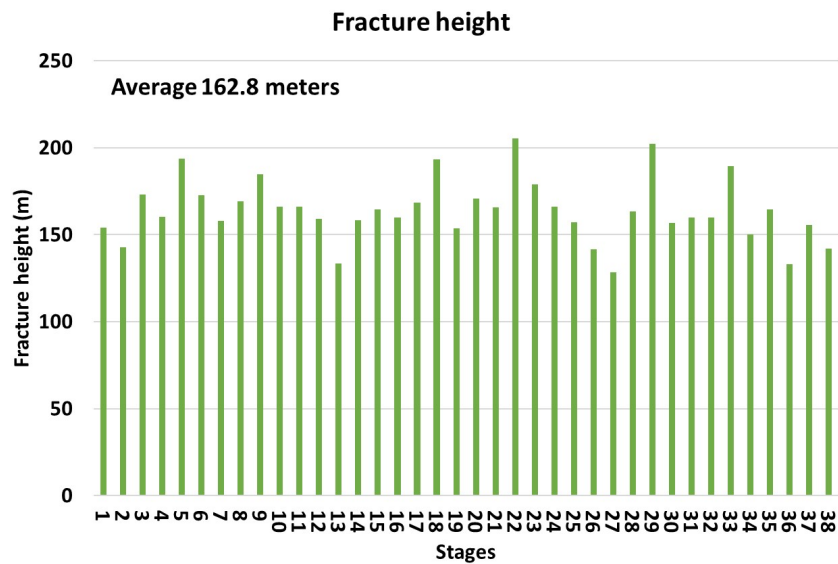


Figure 3.15: Graph that shows the measured height for all microseismic clouds which represents the fracture height for every stage. The average height is 162.8 meters.

3.3.2 Microseismic cloud growth patterns and MS-DAS integration results

The induced events exhibit complex spatial-temporal characteristics and microseismicity occurring near-instantaneously to the start of injection. Figure 3.16a shows the r-t plot of Stage 31. This stage is an example where the microseismic events developed in a "normal" pattern, the events move away monotonically from the treated well following a parabolic trend. In general, the r-t plots of the stages display this "normal" pattern, but they also present more "reactivation" and "stress transfer" patterns than in this example. In Stage 31 there is a predominance of NE propagating microseismicity (black stars). SW events (red stars) occur mostly at the beginning of the injection and close to the treated well (under 200 meters). This means the fracture stopped propagating on the SW side fairly early during injection.

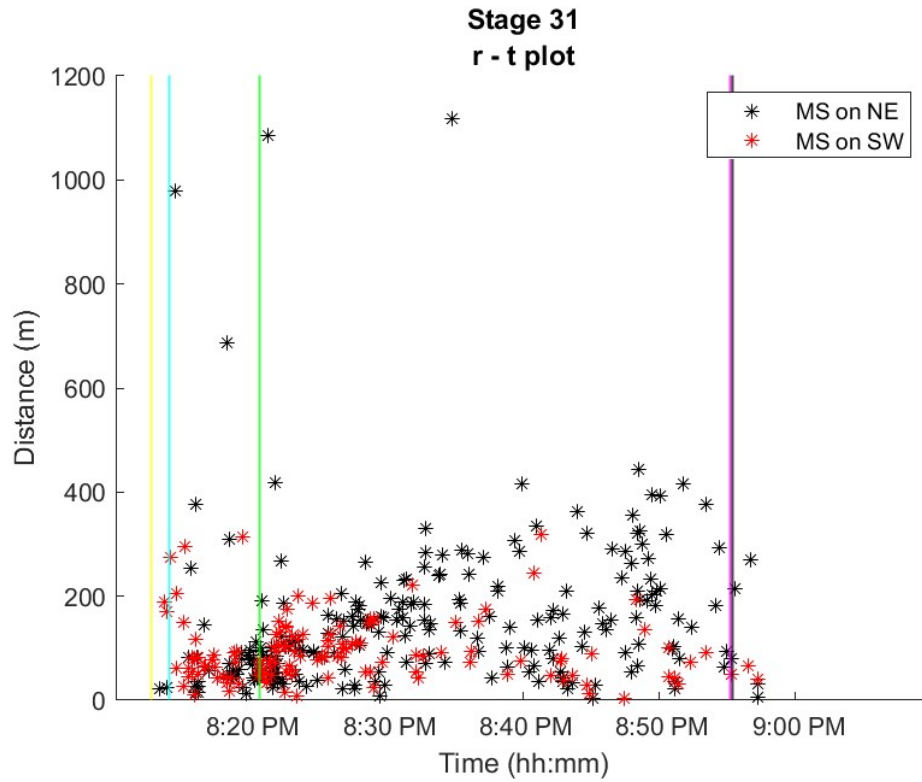
Stage 31 (Figure 3.16a) has microseismicity occurring from the start of the injection to the frac hit across different distances from the injection point. The events close to the injection point that occur immediately after the start of the injection can be associated with pore pressure diffusion. However, the events occurring further from the injection point between the start of the injection and the frac hit could mean possible fracture reactivation caused from stress transfer effects, as this occurs instantaneously. Another possible explanation for these events is continued fluid diffusion from the previous stage. Because if it is not microseismicity due to the transfer of stresses, it is not possible that pore pressure perturbations propagated that fast.

Figure 3.16b shows the DAS-MS plot of Stage 31, the strain fronts and overlaying microseismicity at the top, the microseismic events magnitude over time in the middle, and the engineering curves at the bottom. The microseismicity happens continuously during injection and is on top of the dragonfly and its surroundings. The dragonfly in the strain front has an antenna, which indicates the re-stimulation of a pre-existent fracture, that corresponds to an opening in Stage 11. The MS events that happen

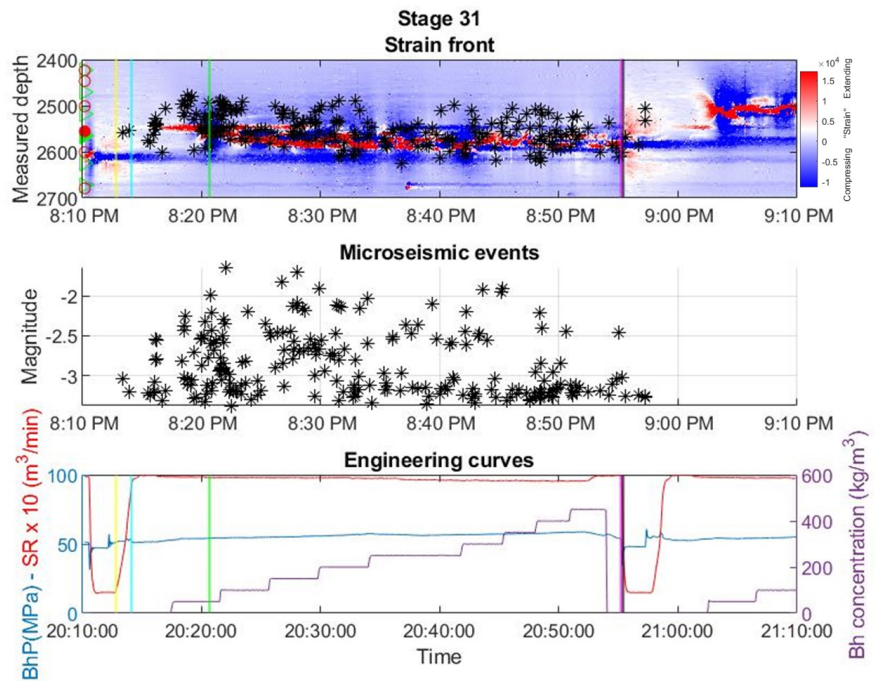
between the FBP and the frac hit far away from the injection point in the r-t plots are on top of the antenna signal. This means that these events are on the path of a re-stimulated fracture. The microseismicity between the start of the injection and the frac hit does not concentrate on the tail of the previous stage, so the events happening far away from the injection point between the FBP and the frac hit correspond to fracture reactivation caused from stress transfer effects.

Figure 3.17a shows the r-t plot of Stage 18, which displays "halted growth" development pattern. The microseismicity begins immediately when the injection starts and the events occur within a range of distances only. At the beginning, there is microseismicity happening instantaneously at different distances which is characteristic of the "stress transfer" pattern. These events might be hiding the "normal" pattern of the hydraulic fracture which stopped growing at around 350 meters. Another possible explanation is that there is fracture reactivation, but the fracture is not growing more, it is filling instead.

Figure 3.17b shows the DAS-MS plot of Stage 18. In this plot, the microseismicity concentrates on top of the strain fracture signal (dragonfly) and happens continuously during the whole injection. The dragonfly signal has an antenna and there is microseismicity on the tip of it (around the yellow line) which, looking at the r-t plot at the same time (yellow line), it happens very close to the injection point. This could enforce the theory that it is a pre-existent fracture that is not growing in length. However, there are indications in the strain front that multiple fractures were created during injection. It seems like the microseismicity of the pre-existent fracture is hiding the triggering front of the new ones, and the deviation of the fluids did not let the new fractures grow past 350 meters.

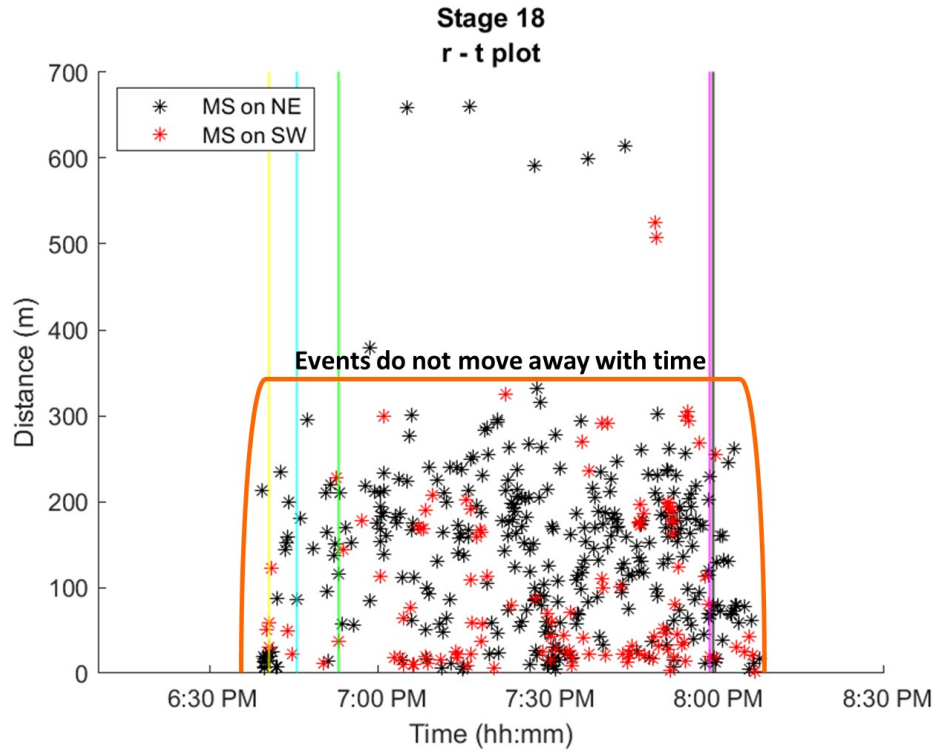


(a)

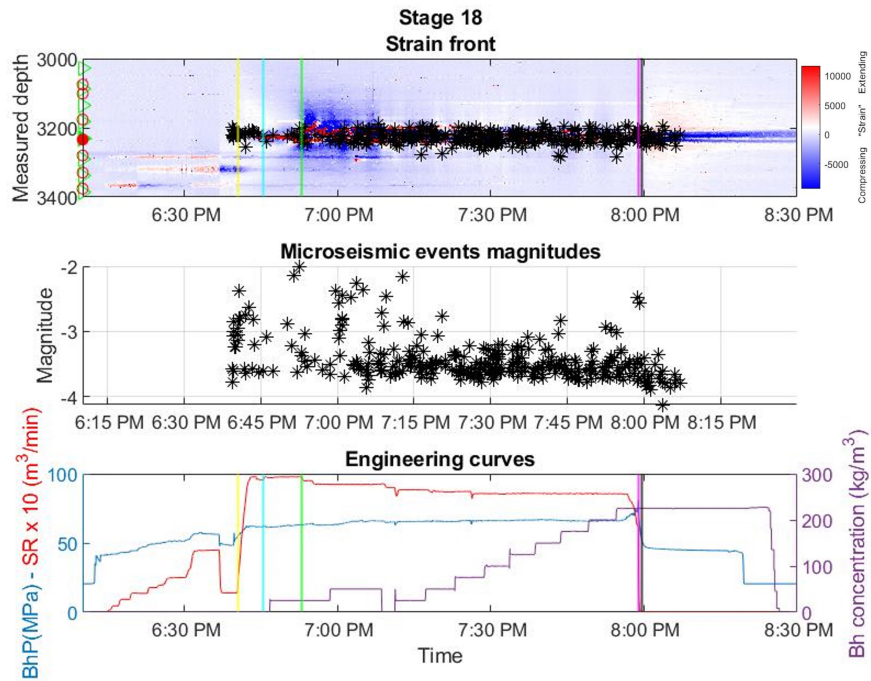


(b)

Figure 3.16: Stage 31. a) r-t plot with normal development pattern. Black stars are MS events propagating towards NE and red towards the SW. DAS characteristics and FBP are depicted as well. b) DAS-MS plot with microseismicity (black stars) on the strain front, and with the DAS characteristics and FBP depicted.



(a)



(b)

Figure 3.17: Stage 18. a) r-t plot with "halted growth" development pattern. b) DAS-MS plot. The MS events are on top of the dragonfly and happen continuously. See Figure 3.16 for the full legend.

Figure 3.18a shows the r-t plot of Stage 25. Most of the microseismicity happens towards the SW (red stars), but during the first part of the injection, there is a cluster of events (orange circle) separate from the main MS growth that is not following a linear growth as they occur around the same distance. In the DAS-MS plot (Figure 3.18b) this separate cluster of MS events happens on the same measured depth as the fracture created on Stage 25 and the tail of the fracture in Stage 24 (orange circle). One fracture in Stage 25 has an antenna that comes from Stage 21. This means that possibly the new injection causes instantaneous stress changes at the old location that opened in Stage 21 and in Stage 24.

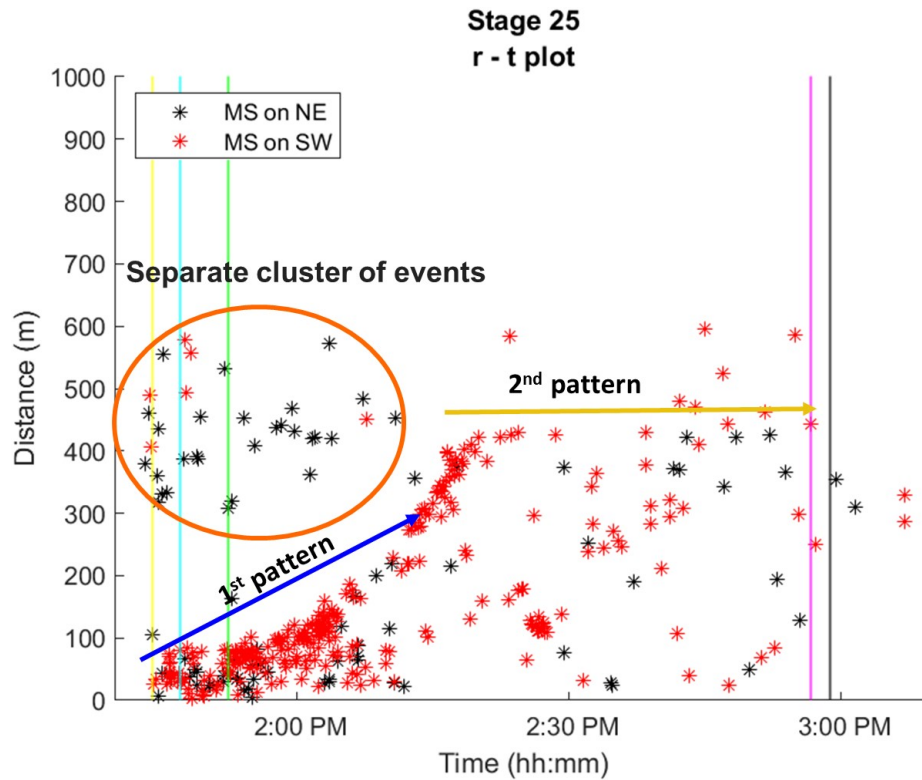
Stage 25 also seems to have two different diffusive patterns. The first one occurs from the start of injection to just before 2:15 pm, and it seems to be a "reactivation" pattern, speeding up linear growth. After that, it seems like the fracture tip stops advancing as the events do not keep moving away from the injection point but happen in a "halted growth" pattern like in Stage 18 (Figure 3.17a). It seems that the fracture stopped growing mid-treatment. Unfortunately, most of these events happened towards the SW of the treated well. It is not visible how the microseismicity is behaving on top of the strain front.

In the r-t plot for Stage 14 (Figure 3.19b) events are happening before the start of the injection and immediately after at different distances from the injection point (orange circle). Figure 3.19a shows the DAS-MS plot of Stage 14. In the strain plot, the tail of the previous stage is noticeable and there is a concentration of MS events before and immediately after the start of the injection (orange circle). In this stage microseismicity is still occurring at the previous stage due to continued pore pressure and/or stress changes, as the events at the start of the injection occur around the same distances as the events that happened before the injection for the new stage started.

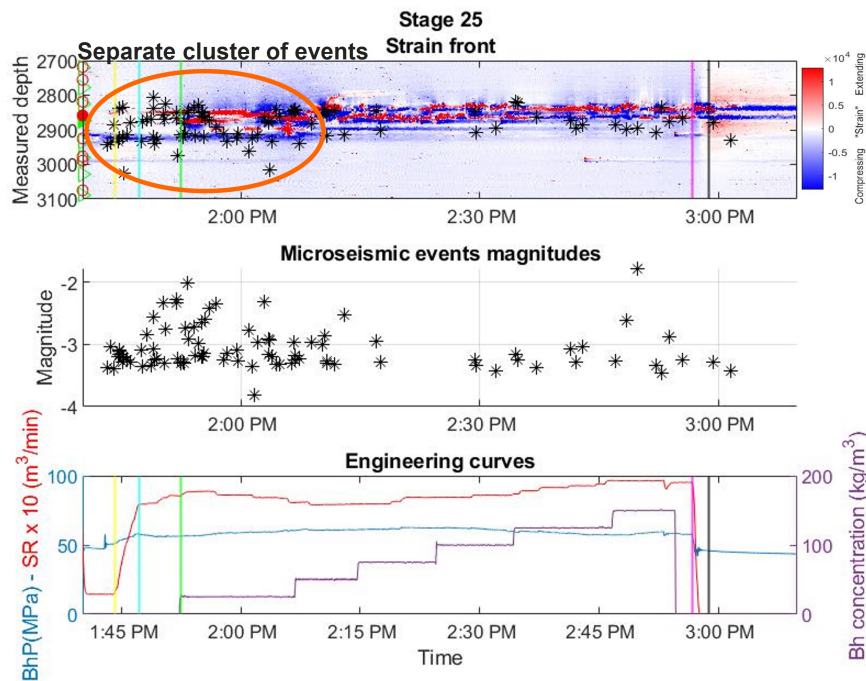
Around 11:50 am, in the r-t plot (Figure 3.19b), a series of microseismic events branch out from the main front and display "reactivation" pattern (green circle).

Meanwhile, in the DAS-MS plot (Figure 3.19a) at the same time, some microseismic events happen below the dragonfly (green circle). This means that there is fracture or fault reactivation, due to probably the movement of residual fluids in those parts, as they happen in the middle of the injection, do not extend too much, and occur only for a short period, not like in Stage 6 (Figure 3.20) where they extended until the end of injection.

Figure 3.20a shows the DAS-MS plot of Stage 6. This stage displays unexpected behavior found in Stages 5, 6 and 7 of the treatment. In this stage, the microseismicity travels towards the toe of the well (to previous stages) highlighted by an orange circle. Looking at the r-t plot of this stage (Figure 3.20b) there is a noticeable a "reactivation" pattern around the same time the microseismicity starts to travel to the previous stages in Figure 3.20a (highlighted by an orange circle). This can only mean that the fluids are moving into pre-existing fractures or faults and reactivating them. There is no strain signal in the DAS data that captures this reactivation because the reactivation occurs around 200 meters from the treated well, further away from the monitoring well (150 meters from the treated well).

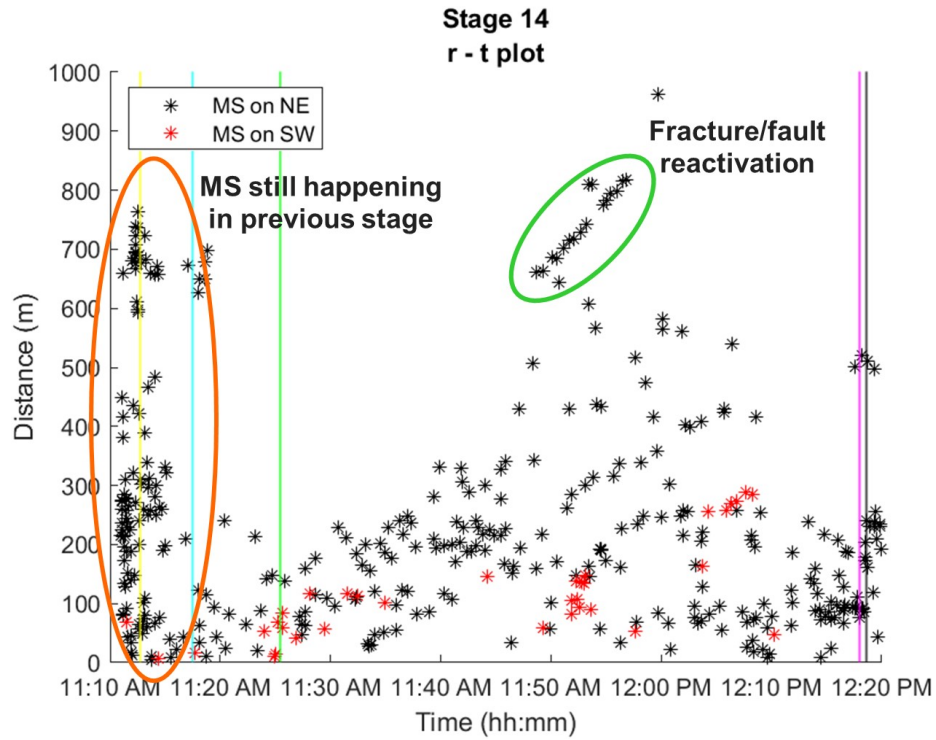


(a)

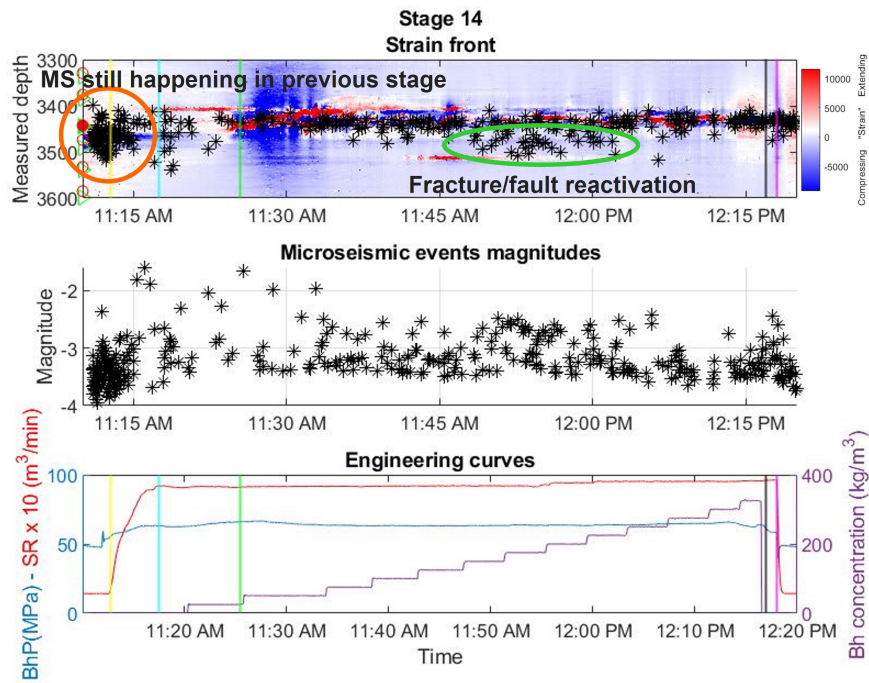


(b)

Figure 3.18: Stage 25 a) r-t plot and b) DAS-MS plot. The r-t plot uncovers a separate cluster of events from the main MS growth (orange circle). The new injection might have caused stress changes at the old location and opened a previous fracture. This stage also has two different diffusive patterns (blue and yellow arrows).

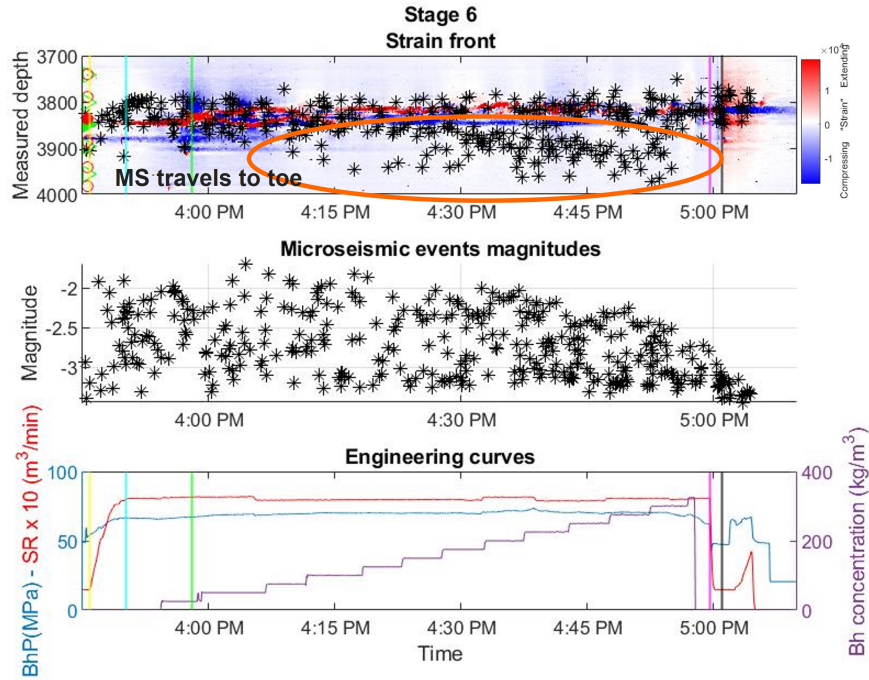


(a)

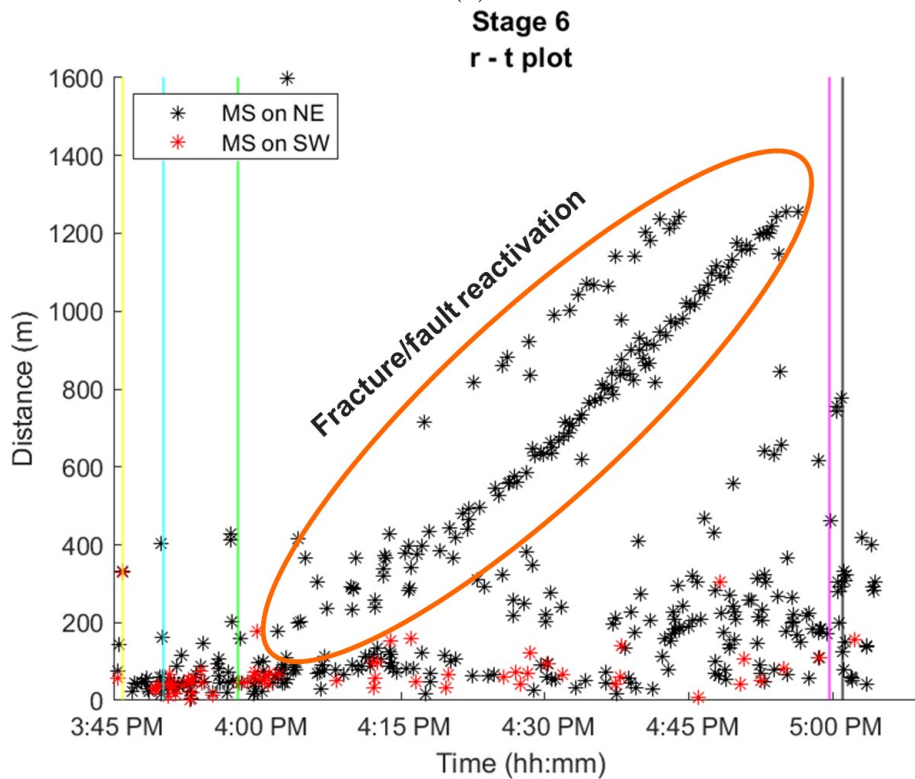


(b)

Figure 3.19: Stage 14 a) r-t plot and b) DAS-MS plot. There are clearly MS events still occurring at the previous stage which is why there is microseismicity happening immediately after the start of injection (orange circle). This stage presents fault/fracture reactivation in the middle of injection most likely due to stress changes rather than fluids (green circle).



(a)



(b)

Figure 3.20: Stage 6 a) DAS-MS plot and b) r-t plot. The MS events travel to the toe of the well during injection in the strain front (orange circle). The r-t plot presents linear MS growth around the same time (orange circle). This can be interpreted as fluids moving into pre-existing fractures or faults and reactivating them.

Stages 14 and 31 (Figures 3.19b and 3.16b) are examples of the most common response for the DAS-MS plots in this treatment. The microseismicity happens on top of the dragonfly and in the immediate surroundings, especially under the dragonfly (greater measured depth), in a mostly continuous manner. This makes sense as the pressures and stresses of the hydraulic fractures affect the surrounding formation in all directions. In this treatment, most stages present fracture/fault reactivation, meaning that the microseismicity lays on top of the antennas or tails of previous stages. Sometimes the microseismicity also shows at measured depths where there are no strain signal, indicating reactivation in parts away from the monitoring well.

In general, the injection rate and the bottom-hole pressure were stable and no big changes were observed that should affect the occurrence rates of the microseismic events. At the beginning of the treatment, in stages between 1 to 4, the microseismicity occurs mostly when the proppant enters, like in Figure 3.21. This is because during the early fracturing stages, the formation is mostly undisturbed, so it takes more time to get to the point where things are failing. When the proppant is injected the stresses in the area are affected more prominently, which causes the stress shadow to grow and cause failure. In later stages is easier to develop microseismicity because there is already a stress shadow and fluids in there. In this treatment, later stages (8 - 38) show substantial events from the beginning of the injection, like in Stages 18 and 31, Figures 3.17b and 3.16b respectively.

In most stages, the microseismic decays shortly after the end of the injection. Some stages have microseismicity conglomeration after the end of the injection like Stage 9 in Figure 3.22a, but just one of them, Stage 23, presents the pressure spike at the end of injection characteristic of the water hammer effect (Figure 3.22b). So the increase of microseismicity occurrence after the end of injection for this treatment might be due to increased sensitivity in the formation as the stresses are trying to go back to normal.

In this treatment, the strongest MS events occur from the beginning to the middle

of the injection, as seen on the DAS-MS plots of Stages 18 and 25 in Figures 3.17b and 3.18b respectively.

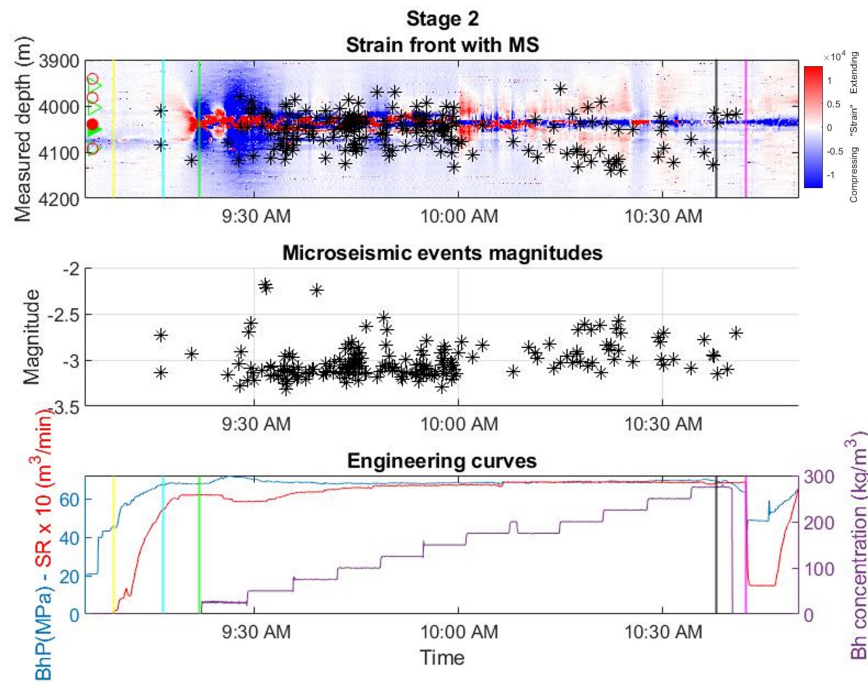


Figure 3.21: Plot with the strain front of Stage 2 with overlaying microseismicity at the top. This stage shows behavior present in the first stages of the treatment where MS occurs mostly when the proppant enters as seen on the engineering curves.

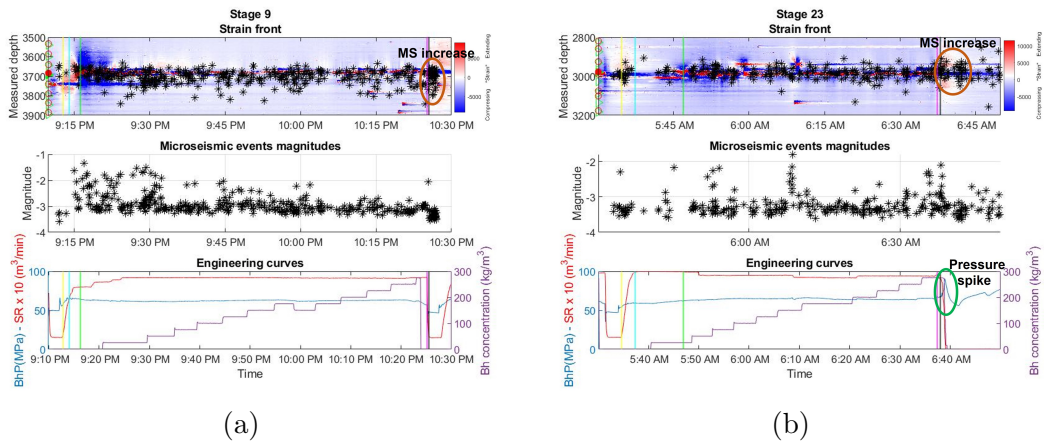


Figure 3.22: 2 cases of Stages with increased microseismicity activity after the end of the injection. a) Stage 9 increase in MS might be due to increased sensitivity resulting from the pumping ending. b) Stage 23 presents the BH pressure spike characteristic of the water hammer effect, so the increase in MS might be due to that.

MS behavior per stage

Figure 3.23 shows the fracture connection map (Figure 2.18) with different color squares on top of the fracture azimuths that stand for different microseismic behaviors present in that stage. The pink arrows indicate stages that mainly present microseismic propagation towards the SW. The green squares represent stages where the microseismicity showed a "normal" pattern in the r-t plots. The orange squares mean that in that stage, the microseismicity developed in a "halted growth" pattern. The cyan squares indicate stages with "reactivation" pattern in the microseismicity. The grey squares represent the stages with "stress transfer" patterns in the r-t plots. If a stage displays more than one dominant pattern it will have the squares of the corresponding patterns. Brown squares represent the stages where the microseismicity is not on top of the dragonfly signal in the strain front. This means that either the microseismicity travels to the previous stage or that it does not align with the dragonfly.

Stages 5, 6, 7 and 29 have brown squares because they present microseismicity travelling to previous stages in their DAS-MS plot. In Stage 16 the DAS-MS plot shows that the microseismicity is at a greater measured depth than the dragonfly, but there is an hydraulic fracture created in the stage. The r-t plot shows "halted growth" at around 600 meters. It might be that a pre-existent fracture is being re-opened past the monitoring well but it is not growing anymore. This behavior can hide the microseismicity development pattern of the new fracture.

Most stages present more than one pattern during injection. In general, the "normal" pattern is predominant in the treatment with either "reactivation" or "stress transfer" patterns. This means that in this treatment microseismicity is triggered by the pore pressure diffusion processes and there is reactivation of pre-existent fractures by either fluids ("reactivation pattern) or due to the stresses in the formation ("stress transfer" pattern). Only two stages, 4 and 25 change patterns during the injection,

from a "normal" to "halted growth" pattern and a "reactivation" to "halted growth" pattern respectively.

Looking at Figure 3.23 the stages that display halted growth pattern in the r-t plots are mostly the later ones. Besides that, there is no other noticeable pattern between these characteristics. Chapter 4 presents the PKN modelling of the hydraulic fracturing treatment. In that chapter, the length of the microseismic clouds is compared to the expected length of the fractures according to the treatment parameters and reservoir rock properties. It also compares the propagation of the microseismic clouds with the frac azimuths obtained from the DAS strain fronts. This helps to determine whether the fractures grew as much as expected and if they changed trajectories after intercepting the monitoring well. These integrated analyses with the PKN model can give a more complete picture of what is happening in these stages.

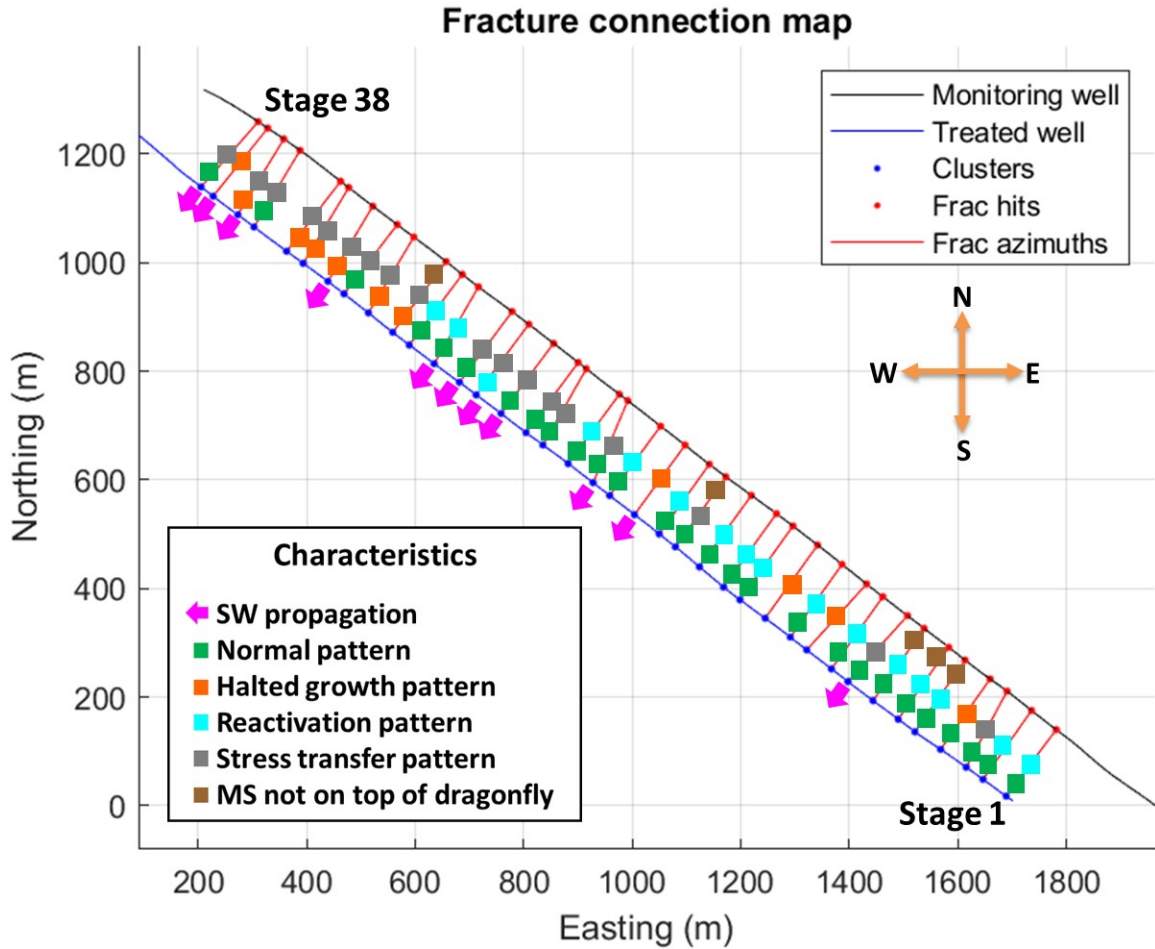


Figure 3.23: Fracture connection map for all stages, with original wells geometry. See Figure 2.18 for full legend. The squares represent characteristics present in each stage. Pink means that the fracture propagated mostly towards the SW, green means "normal" pattern in the r-t plots, orange="halted growth", cyan="reactivation", grey="stress transfer" and the brown ones mean that the MS is not on top of the dragonfly.

3.4 Microseismic analysis conclusions

In this chapter, the microseismicity generated during the hydraulic fracturing treatment was analyzed to get an estimation of hydraulic fractures geometry dimensions and propagation during injection. The microseismicity was also projected onto the strain fronts to correlate the microseismicity to the strain changes in the medium.

The microseismic clouds of most stages propagate towards the NE. The stages that

present propagation mainly towards the SW are because the NE direction presented great stresses or too much fluid/proppant and so, the fractures changed to the less stressed and full direction. Microseismicity is contained within the Middle Montney Member.

Most stages have microseismic occurrence developing with the behavior of a pore pressure diffusion-controlled triggering process. But, there is also fracture/fault reactivation by fluids or stresses in the formation. In some stages, especially in later ones, the microseismicity displays "halted growth" behavior, the events does not monotonically move away from the treated well as the hydraulic fracture grows, instead the events happen between certain distances during the whole injection, which indicates that the fracture has stopped growing. Only two stages exhibit a change in microseismicity development in the r-t plots and it is because the fracture stops propagating.

The microseismicity concentrates on top of the dragonfly signal and its immediate surroundings in the DAS-MS plots. Some stages show unexpected behaviour where the microseismicity travels to previous stages. This means that the fluids are moving to the fractures in previous stages.

In some cases, the DAS-MS plots and the r-t plots showed different behaviours. This is because the DAS data only sees what is happening at the cable. The microseismicity, however, gives a wider picture of how the fracture is propagating in the formation.

This analysis makes it clear that the microseismicity complements the low frequency DAS data and by integrating both methods, we can make a more complete interpretation. DAS does a good job of monitoring what happens at the cable location and gives details that microseismicity might not be able to pick up, such as the creation of multiple fractures. However, microseismicity is needed to monitor what happens away from the monitoring well with the DAS cable.

References

- Baig, A., & Urbancic, T. (2010). Magnitude Determination, Event Detectability, and Assessing the Effectiveness of Microseismic Monitoring Programs in Petroleum Applications. *CSEG Recorder*, 35, 5.
- Caffagni, E., & Bokelmann, G. (2017). Spatiotemporal Evolution of Microseismicity and Repeating Earthquakes in Haiti, 64.
- Cole, S., Karrenbach, M., Boone, K., Ridge, A., Kahn, D., Rich, J., Silver, K., & Langton, D. (2017). Effective Diffusivity Estimates from Distributed Fiber-optic Strain and Microseismic Measurements. *SEG Technical Program*, 5. <https://doi.org/10.1190/segam2017-17680716.1>
- Hanks, T. C., & Kanamori, H. (1979). A moment magnitude scale. *Journal of Geophysical Research: Solid Earth*, 84(B5), 2348–2350. <https://doi.org/https://doi.org/10.1029/JB084iB05p02348>
- Karrenbach, M., Ridge, A., Cole, S., Boone, K., Rich, J., Silver, K., & Langton, D. (2017). DAS Microseismic Monitoring and Integration With Strain Measurements in Hydraulic Fracture Profiling, 1316–1330. <https://doi.org/10.15530/urtec-2017-2670716>
- Le Calvez, J., Malpani, R., Xu, J., Stokes, J., & Williams, M. (2016). Hydraulic fracturing insights from microseismic monitoring. 28, 16–33. <https://doi.org/10.1190/int-2018-0078.1>
- Li, L., Tan, J., Schwarz, B., Stanek, F., Poiata, N., Shi, P., Diekmann, L., Eisner, L., & Gajewski, D. (2020). Recent Advances and Challenges of Waveform-Based Seismic Location Methods at Multiple Scales. *Reviews of Geophysics*, 47. <https://doi.org/10.1029/2019RG000667>
- Maxwell, S. (2014). *Microseismic Imaging of Hydraulic Fracturing: Improved Engineering of Unconventional Shale Reservoirs*. Society of Exploration Geophysicists. <https://doi.org/10.1190/1.9781560803164>
- Shapiro, S. A., Dinske, C., & Rothert, E. (2006). Hydraulic-fracturing controlled dynamics of microseismic clouds. *Geophysical Research Letters*, 33(14), 5. <https://doi.org/https://doi.org/10.1029/2006GL026365>
- Shapiro, S., & Dinske, C. (2009). Fluid-induced seismicity: Pressure diffusion and hydraulic fracturing. *Geophysical Prospecting*, 57(2), 301–310. <https://doi.org/https://doi.org/10.1111/j.1365-2478.2008.00770.x>
- Shapiro, S. A., Huenges, E., & Borm, G. (1997). Estimating the crust permeability from fluid-injection-induced seismic emission at the KTB site. *Geophysical Journal International*, 131(2), 15–18. <https://doi.org/10.1111/j.1365-246X.1997.tb01215.x>
- van der Baan, M., Eaton, D., & Dusseault, M. (2013). Microseismic Monitoring Developments in Hydraulic Fracture Stimulation. In A. P. Bungler, J. McLennan, & R. Jeffrey (Eds.), *Effective and Sustainable Hydraulic Fracturing* (p. 28). IntechOpen. <https://doi.org/10.5772/56444>
- Wang, H., Li, M., & Shang, X. (2016). Current developments on micro-seismic data processing. *Journal of Natural Gas Science and Engineering*, 32, 521–537. <https://doi.org/https://doi.org/10.1016/j.jngse.2016.02.058>

Warpinski, N., Mayerhofer, M., Bridges, A., & Du, J. (2013). Hydraulic-Fracture Geomechanics and Microseismic-Source Mechanisms. *SPE Journal*, 18(04), 766–780. <https://doi.org/10.2118/158935-PA>

Chapter 4

PKN modelling analysis

4.1 2D Hydraulic fracturing models

Hydraulic fracture geometry is complex and depends on different factors like reservoir stress conditions, reservoir rock properties, mechanical properties, natural fracture system, and operational parameters. Various models simplify this complicated process and define the development of fracture geometry under specific assumptions.

They are classified into 2D and 3D categories. The main two 2D models are the Perkins-Kern-Nordgren (PKN) fracture model, and the Khristianovic-Geertsma-de Klerk (KGD) fracture model. 3D models include fully 3D models and pseudo-three-dimensional (P-3D) models. The PKN and KGD models are based on the assumption that the hydraulic fracturing process occurs in a homogeneous and isotropic formation, which creates a symmetric, bi-wing fracture. They also assume that the hydraulic fracture propagation is a function of the constant injection of the Newtonian fracturing fluid (Belyadi et al., 2019; Xiang, 2012).

4.1.1 KGD model

The KGD model was developed by Khristianovitch and Zheltov (1955), and further extended by Geertsma and De Klerk (1969). It assumes that plane strain is on the horizontal plane where a vertical fracture has an elliptical horizontal cross-section and rectangular vertical cross-section. This fracture propagates horizontally with

constant fracture height that is much larger than the fracture length and has constant fracture width, independent of the fracture height. It considers that tip processes dominate fracture propagation and assumes constant flow rate in the fracture, as well as constant pressure along most of the fracture length, except for a small region close to the tips (Belyadi et al., 2019; Xiang, 2012; Zoback & Kohli, 2019). Figure 4.1a shows the schematic representation of fracture geometry in the KGD model. This model is a good choice to represent the short planar fractures created for testing purposes, like in the leak-off tests or frac-pack completions, as the fracture height is larger than fracture length (Espinoza, n.d.).

4.1.2 PKN model

The Perkins-Kern-Nordgren (PKN) model is a 2D hydraulic fracturing model created by Perkins and Kern (1961) who developed equations to compute fracture length and width with a fixed height. Later, Nordgren (1972) further improved this model by adding fluid loss to the solution. This model assumes plane-strain in the vertical plane where the fracture has an elliptical cross-section both in the horizontal and vertical directions and propagates horizontally with constant fracture height independent of and smaller than the fracture length. The width varies from zero to a maximum value at the middle of the fracture height. In the PKN model, the fracture process is assumed to be in a viscosity-dominated regime, where fracture toughness can be ignored. The fracture tip region does not play a role, and leak-off and storage were neglected in the model. Figure 4.1b shows the schematic diagram of the fracture geometry in the PKN model. The PKN model is suitable to be used for fractures that propagate longer in length than in height, which is why it can be regarded to best represent long planar fractures done for reservoir completion with well-defined bottom and top fracture barriers (Belyadi et al., 2019; Espinoza, n.d.; FrackOptima, n.d.; Garikapati et al., 2018).

The main differences between the KGD and the PKN models are: The fracture

planes are perpendicular to the vertical plane strain in the PKN model while strain is on the horizontal plane in the KGD model. In the KGD model, the fracture width is constant in the vertical direction, but it varies in the PKN model. The PKN model applies to long fractures with smaller heights, whereas the KGD model is used for short fractures with larger heights than lengths.

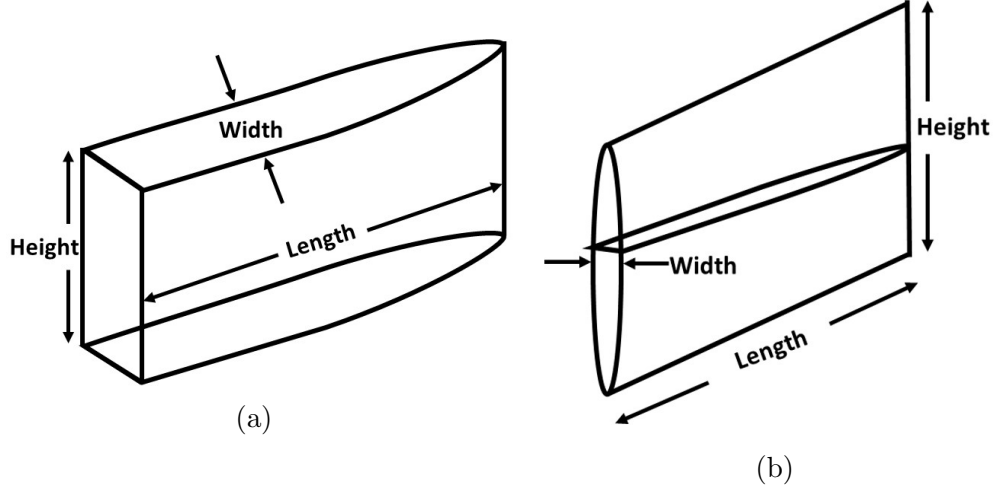


Figure 4.1: Illustration of the fracture geometry of the two main 2D hydraulic fracturing models. a) KGD fracture model, where height > length. b) PKN fracture model, where height < length. Modified from Xiao et al. (2017).

Espinoza (n.d.) comes to a simple analytical solution to calculate the fracture half-length (x_f), just on one side of the bi-wing fracture, at a certain time based on the treatment parameters. The solution is

$$x_f = 0.524 \left(\frac{q^3 E'}{\mu h^4} \right)^{\frac{1}{5}} t^{\frac{4}{5}}, \quad (4.1)$$

where x_f is fracture half-length (m), q is injection rate (m^3/s), E' is plane strain modulus (Pa), μ is fluid viscosity ($Pa*s$), h is fracture height (m) and t is injection time (s).

For this thesis, the PKN model was used as a validation tool for the low-frequency DAS data and the microseismic analysis. The results of this analysis can give insight into whether things went according to plan in the stages by comparing speeds and

fracture lengths obtained from the DAS and microseismicity results with the speeds and lengths obtained from the PKN modeling using treatment parameters and reservoir rock properties.

4.2 Methodology

For the PKN modeling analysis, we use Equation (4.1) to forecast fracture half-length growth over time. The PKN model was used to get an estimation of the fracture half-length at the end of injection and the fracture half-length at the DAS hit time. Then, the fracture half-lengths were integrated with the fracture azimuths obtained from the DAS data to compare to the propagation of the microseismic clouds.

4.2.1 Fracture half-length at the end of injection and at the DAS hit time

The PKN model was programmed to estimate how the fracture half-length evolved over time using treatment parameters and reservoir rock properties. Table 4.1 shows the values of the parameters and their selection. The Plane Strain modulus (E') is a fixed value for all stages, it and was calculated using Young's modulus from a rock sample taken around the same depth as the depth of the well. The Plane Strain modulus is defined as

$$E' = \frac{E}{1 - \nu^2}, \quad (4.2)$$

where E is Young's modulus (Pa), and ν the Poisson's ratio of the medium. The injection rate changes depending on the stage and was set equal to the average injection rate. The fluid viscosity is a fixed value and was chosen as the fluid viscosity of water as there was no record on the slickwater used. The fracture height is a fixed value and chosen as the rounded value of the 25th percentile (Q1) of the height data displayed in Figure 3.15. I decided not to change height values because I wanted to simplify and standardize the analysis. I also decided to use the Q1 value instead

of the average height, as the heights obtained for that analysis were the maximum vertical extension of the microseismic clouds, which might overestimate the fracture height as the microseismicity is clearly not related only to the hydraulic fractures. The time of injection changes depending on the stage and is the fracture propagation time from the FBP to the end of injection.

Figure 4.2 shows an example of the PKN modeling plot, the fracture half-length evolution over time is displayed and asterisks mark the fracture half-length at the end of injection (red) and at the DAS hit time (pink).

Parameter	Variability	Value	Selected from
E = plane strain (<i>Pa</i>)	Fixed value	40.5×10^9	Triaxial test
q = injection rate (m^3/s)	Changes depending on stage	-	Average injection rate
m = fluid viscosity (<i>Pa * s</i>)	Fixed value	0.001	Chosen (water viscosity)
h = fracture height (<i>m</i>)	Fixed value	155	Chosen (Q1 from fracture heights)
t = Injection time (<i>s</i>)	Changes depending on stage	-	Fracture propagation time

Table 4.1: Geomechanical and completion parameters for the PKN fracture propagation model.

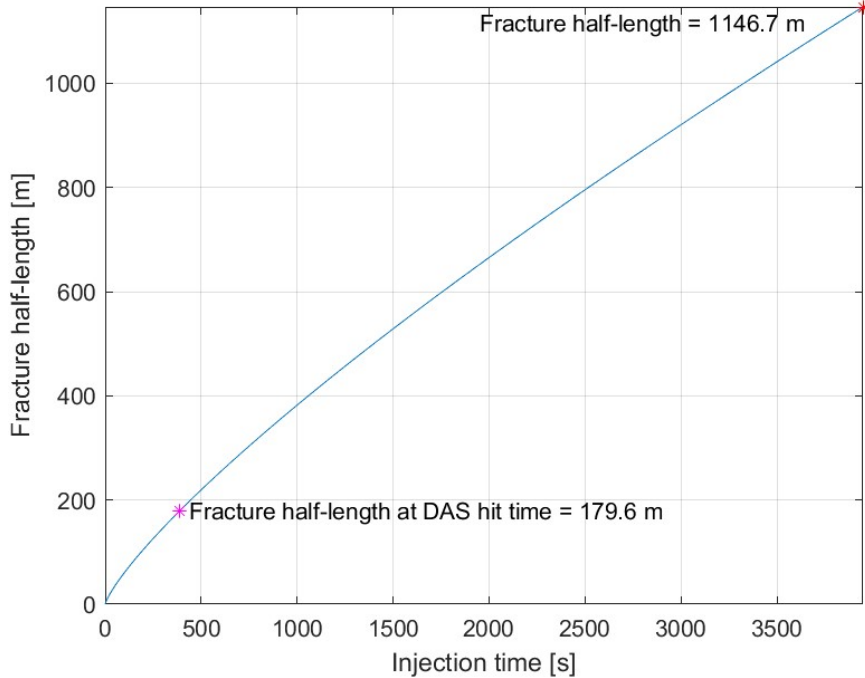


Figure 4.2: Fracture half-length evolution during injection for one stage. The fracture half-length at the end of injection and at the DAS hit time are marked in the curve with a red and pink asterisk respectively.

After obtaining the fracture half-length at the end of injection and at the DAS hit time, the values were plotted in a horizontal schematic of the wells. The fractures were positioned in the place of the clusters. Figure 4.3a shows the fracture half-length at the end of injection of one stage plotted in the position of the stage cluster and represented by the steel-blue line. These values will be compared to the microseismic cloud lengths to see if the fracture grew as much as expected by the model. Figure 4.3b shows the fracture half-length at the DAS hit time, as calculated by the PKN model, of one stage plotted in the position of the stage cluster, represented by an orange line. According to the strain fronts, it is at this time that the fracture intercepted the monitoring well, so the expected result is that the fractures half-lengths are at the monitoring well at this time, meaning their length should be around 150 meters. If they are not, this will give us an indication that something unexpected happened. A range of good agreement was placed at ± 50 meters of the monitoring well, represented by the dotted cyan lines. This range was selected because 50 meters is the Interquartile

Range (IQR) of the data. The IQR is a measure of the middle dispersion of a dataset, and it is calculated as the difference between the 25th percentile (Q1) and the 75th percentile (Q3).

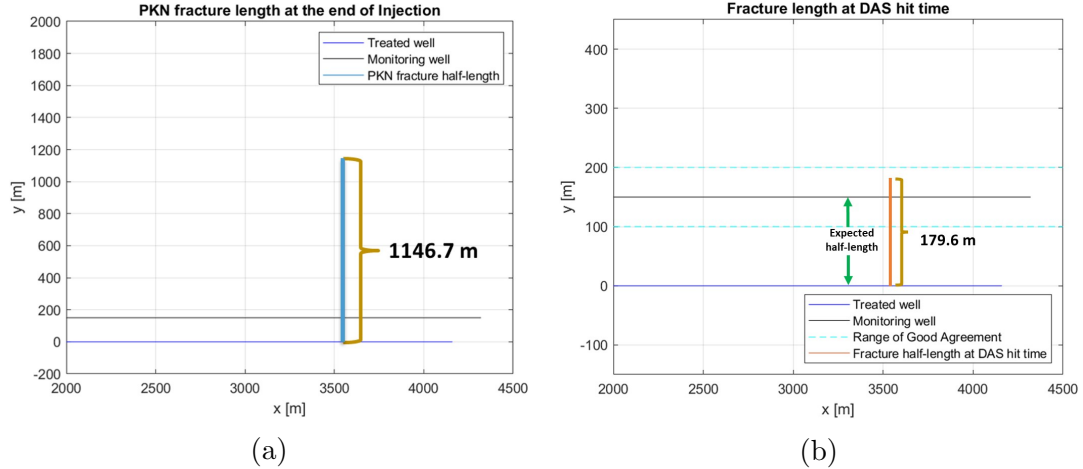


Figure 4.3: Horizontal schematic of the wells. See Figure 3.6 for full legend. a) The fracture half-length at the end of injection for one stage is represented by the steel-blue line which is placed at the stage cluster position. b) The fracture half-length at the DAS hit time for one stage (orange line) placed at the stage cluster position.

4.2.2 PKN integration with DAS to compare to the micro-seismic cloud (PKN vs MS plots)

The PKN fracture half-lengths (steel blue) were plotted next to the microseismic lengths (pink) in a horizontal schematic of the wells to compare both predictions (Figure 4.4). Next, the fracture half-lengths obtained from the PKN model were integrated with the fracture azimuths obtained from the DAS analysis to create the "PKN fracture" of every stage. The PKN fracture is a green line with length equal to the fracture half-length obtained from the PKN model for every stage, that starts at the stage's cluster position and propagates in space with the angle determined by the frac azimuth in the fracture connection map. Figure 4.5 shows a diagram of this integration. After that, the PKN fracture was plotted in space with its respective microseismic cloud (blue stars), linear regression (red line), and the wells as seen in Figure 4.6.

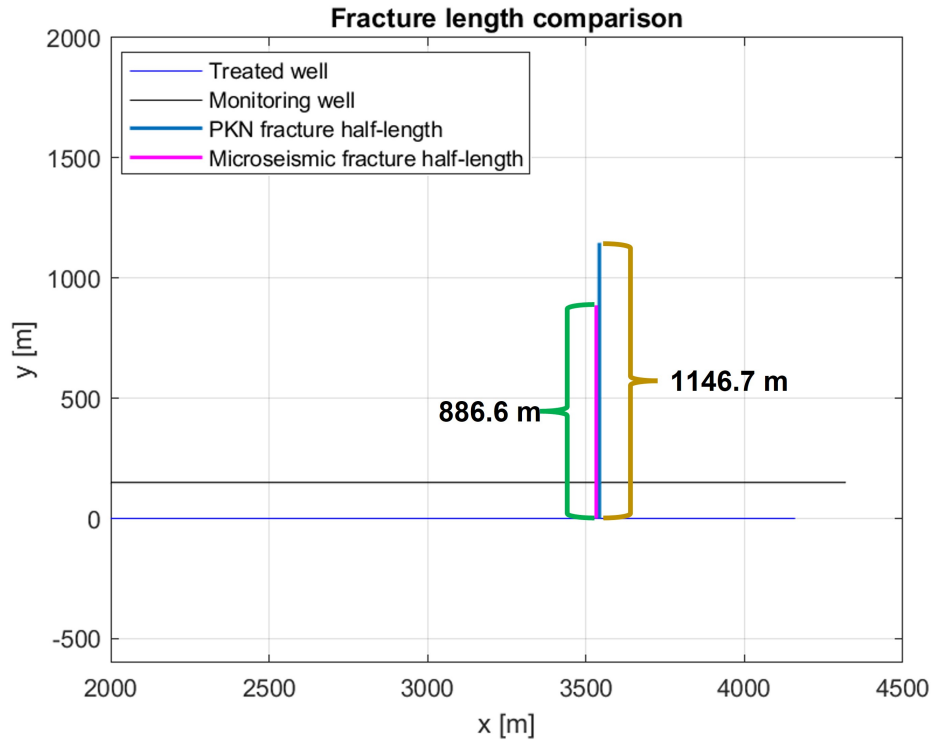


Figure 4.4: Horizontal plane of the wells with the PKN and microseismic fracture half-length for one stage. The steel blue line is the PKN fracture half-length at the end of injection (1146.7 m) and the pink line is the microseismic fracture half-length (886.6 m).

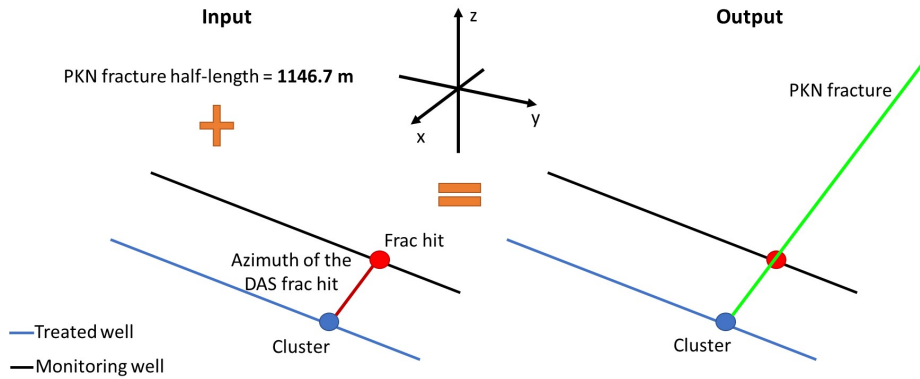


Figure 4.5: Diagram that shows the integration of the PKN fracture half-length with the DAS frac azimuth. The fracture azimuth of the stage was extended to the PKN half-length maintaining the angle of propagation to create the PKN fracture.

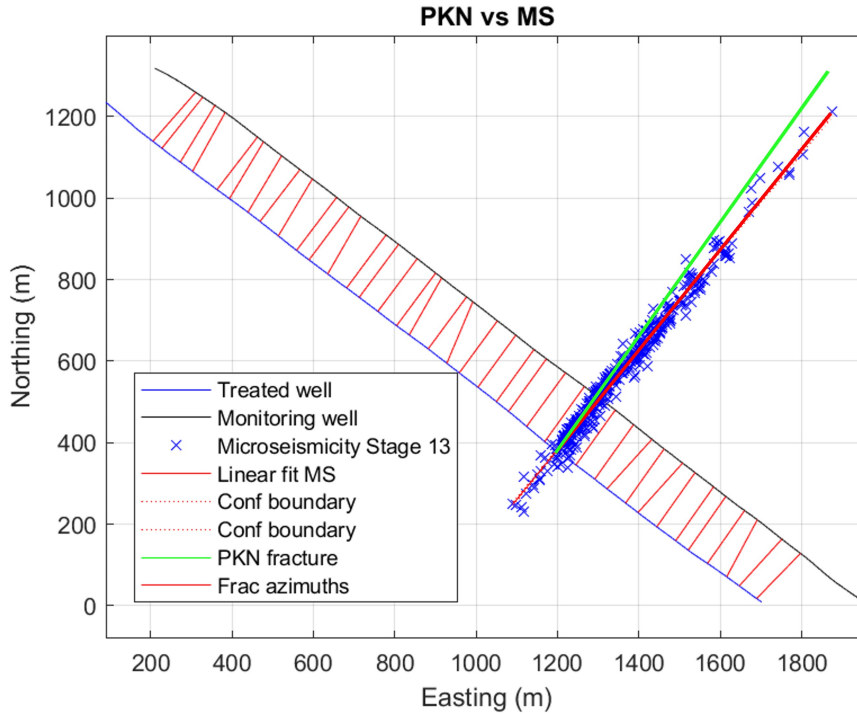


Figure 4.6: PKN vs MS plot. Fracture connection map with microseismic cloud, its linear regression for one stage and the PKN fracture (green line). See Figure 3.4 for full legend.

4.3 Results and Discussion

In this section, the results of the PKN analysis are introduced and discussed. Some multi-stage results are presented but because of the nature of the study, not all can be shown.

4.3.1 Fracture half-length at the end of injection

For the first part of the analysis, the fracture half-lengths at the end of the injection for every stage were estimated by programming the PKN model using Equation (4.1). Figure 4.7 shows the 2D horizontal plane of the wells with the PKN fracture half-length at the end of injection for all stages positioned in the place of the clusters (steel blue lines). This figure displays the variations of lengths among the stages, they vary from 310 to 1387 meters. The fractures are noticeable longer in the early stages than in later ones, even though the later ones propagate faster according to Figure 2.16.

and this is mostly because the time of injection is longer in the early stages.

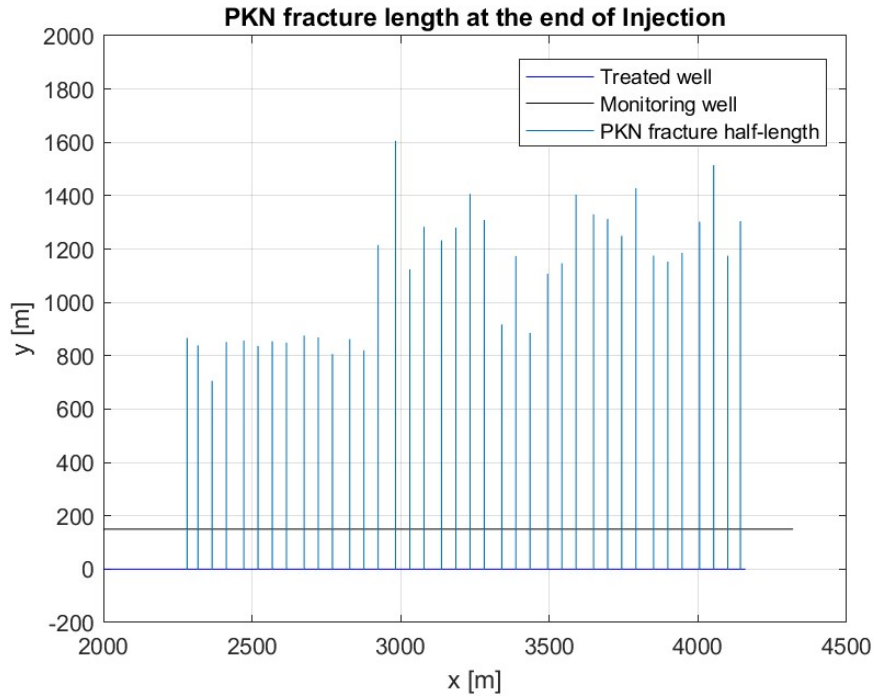


Figure 4.7: Horizontal plane of the wells with the fracture half-lengths at the end of injection for all stages (steel blue lines). See Figure 3.6 for full legend. Fractures are smaller in later stages compared to earlier ones.

4.3.2 Fracture half-length at the DAS hit time

In this phase, the fracture half-lengths at the DAS hit times were calculated as well. Figure 4.8 displays these lengths (orange lines) plotted in a 2D horizontal plane of the wells and placed at their respective cluster location. The dotted cyan lines represent the range of good agreement. The expected behavior for the fracture half-lengths at the DAS hit times would be that all these lengths are at the monitoring well at this time. As seen in Figure 4.8 most of the fractures are within the range of good agreement and close to the monitoring well, meaning that most fractures propagated with a reasonable speed. The ones that are too short or too long are indicators that something unpredicted happened at that stage. If it is too short, it means that the fracture propagated very fast, which indicates that the fracture was already there. If the length is too long, this indicates that the fracture propagated slower

than expected, which might mean that the cluster failed, and the fluid traveled along the well until it found a fracture to propagate through or something hindered the fracture's growth.

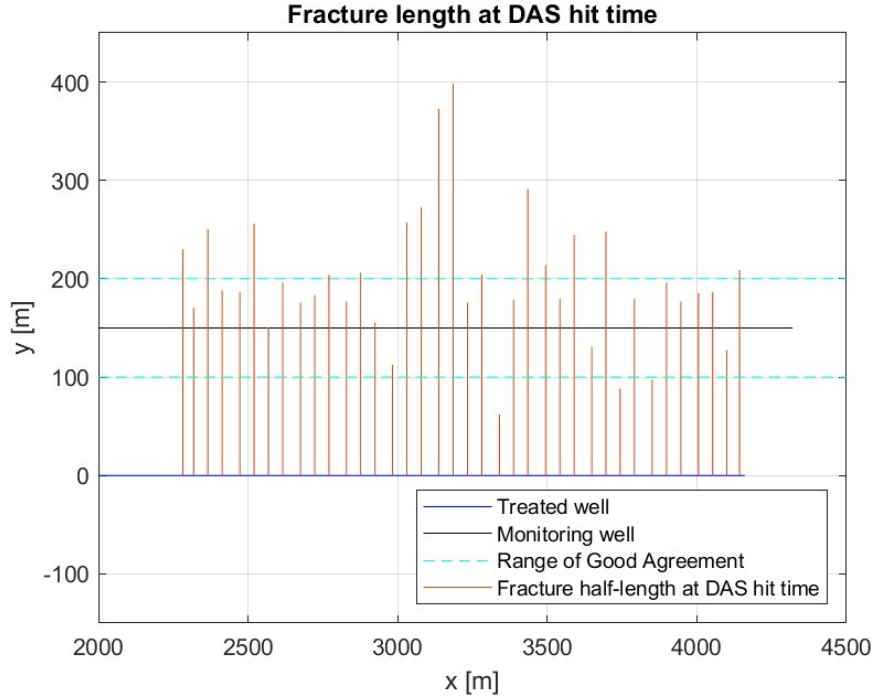


Figure 4.8: Horizontal plane of the wells, (See Figure 3.6 for full legend), with the fracture half-lengths at the DAS hit time represented by the orange lines. The range of good agreement is placed at ± 50 meters showed by the dotted cyan lines. Most fractures are within the range of good agreement and the ones that are not show that something unexpected happened during the injection.

4.3.3 PKN vs MS plots

The PKN fracture half-lengths were integrated with the fracture azimuths obtained from the DAS analysis to create the PKN fractures. These fractures allow us to compare the trajectory of the fracture azimuths to the trajectory of the microseismic clouds. Figures 4.9 and 4.10 show the PKN vs MS plots of all stages in groups of 5. For visualization purposes, the microseismic events are not included in these plots. The PKN fractures of each stage are the solid lines and the linear regressions of the MS clouds are the dotted lines of the same color. Most stages present good agreement

between both methods, only deviating minimally from each other.

Figures 4.11 and 4.12 show examples of good and poor agreement between the PKN fracture and the microseismic cloud trajectories, respectively. Stages that present poor agreement are few and this discrepancy between methods could be because the fractures intercepted the monitoring well at a certain angle and then changed trajectories because of formation complexities or stress and/or pore pressure perturbations. Another explanation is that the fluids were diverted from the stage's hydraulic fracture path to a previous stage. Figure 4.13 shows Stages 5 and 6 microseismic clouds in black circles and blue stars respectively, with the linear regression of the MS cloud, in red, and PKN fracture of Stage 6 in green. Around the start of the pink circle on the left, the microseismicity changes directions to the path of the microseismicity in Stage 5. Until that point the PKN fracture and the microseismic cloud were agreeing with each other, but the fluids are clearly diverted towards Stage 5. It also seems like the growth of the fracture in Stage 6 stopped after the fluids moved to Stage 5.

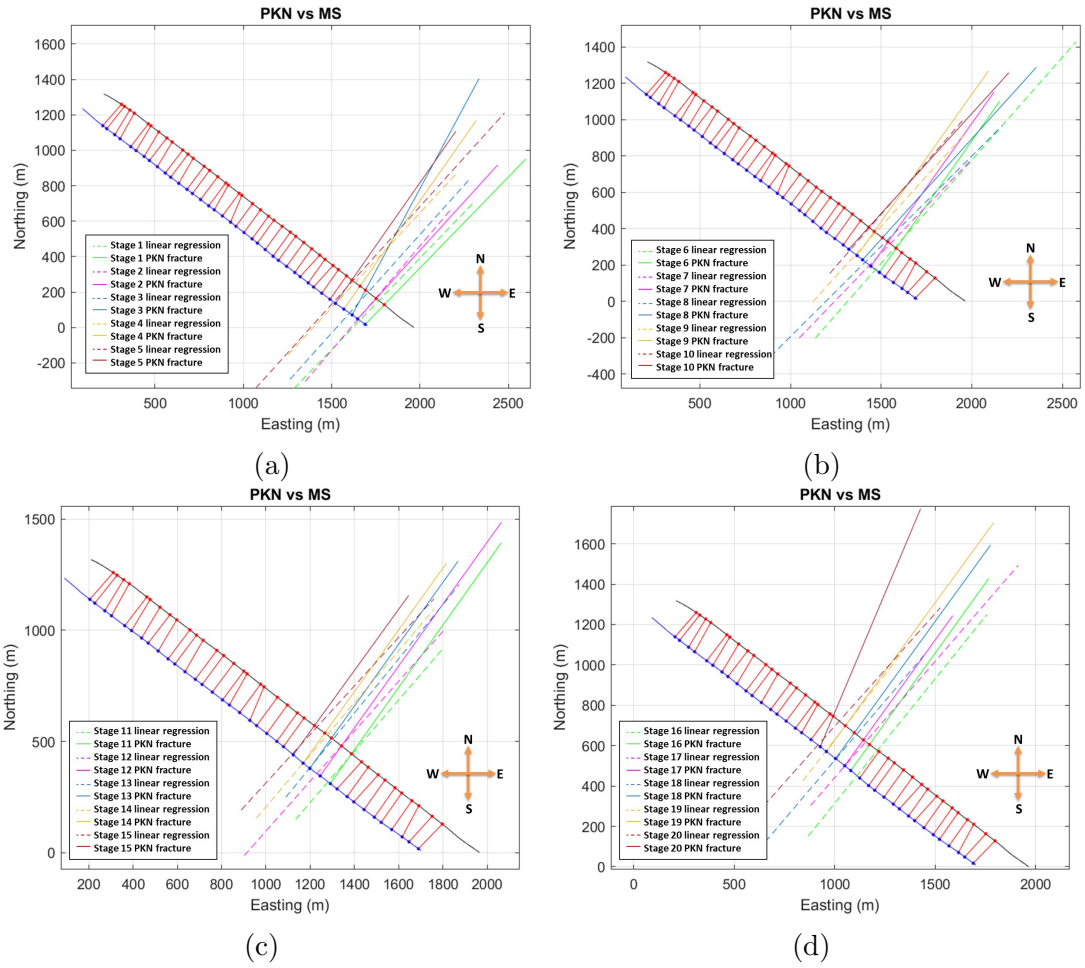
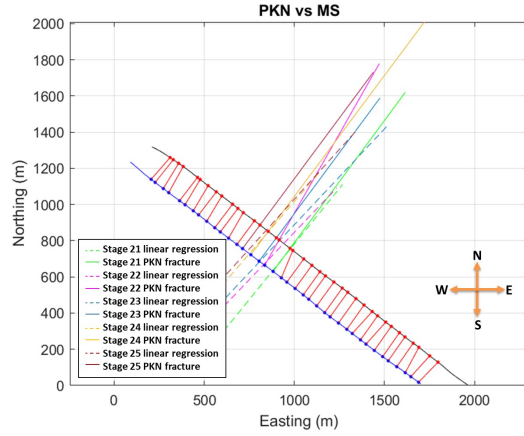
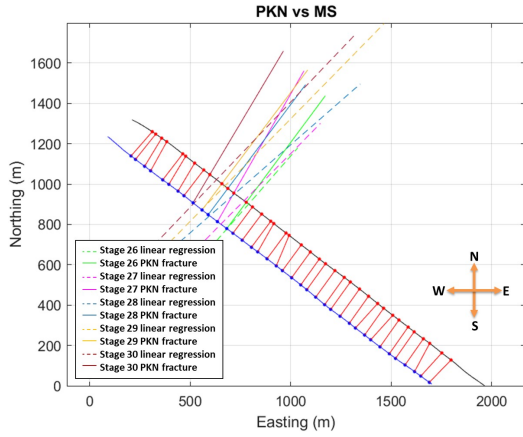


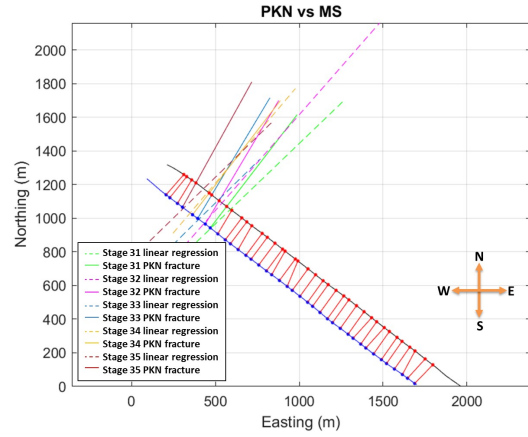
Figure 4.9: PKN vs MS plots for: a) Stages 1 - 5. b) Stages 6 - 10. c) Stages 11 - 15. d) Stages 16 - 20. PKN fractures are the solid lines and the linear regressions of the MS clouds are represented by the dotted lines.



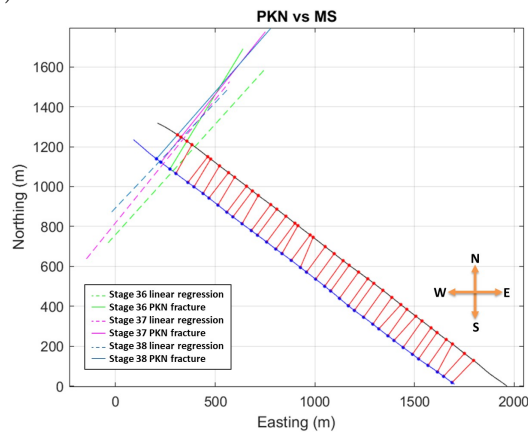
(a)



(b)



(c)



(d)

Figure 4.10: PKN vs MS plots for: a) Stages 21 - 25. b) Stages 26 - 30. c) Stages 31 - 35. d) Stages 36 - 38. PKN fractures are the solid lines and the linear regressions of the MS clouds are represented by the dotted lines.

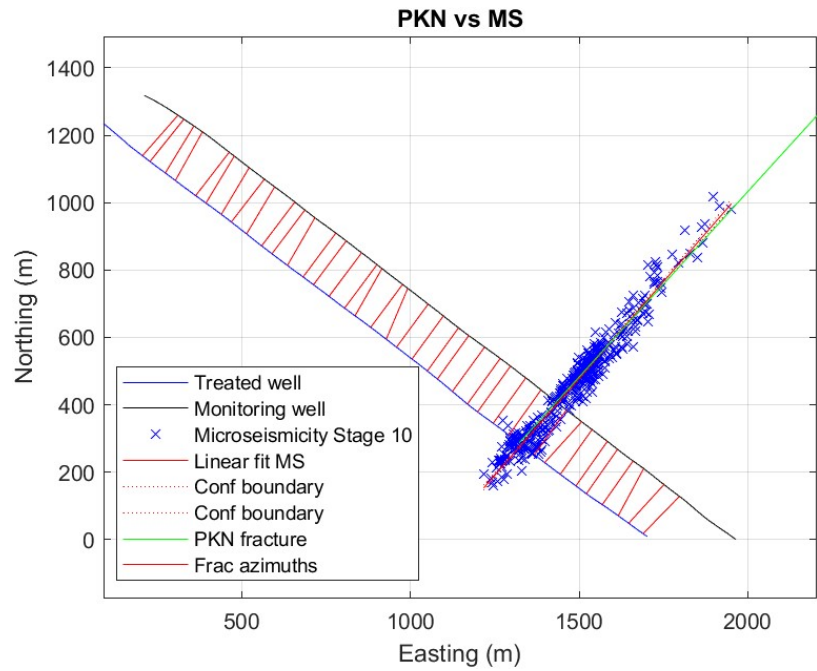


Figure 4.11: Example of good agreement between trajectories. PKN vs MS plot of Stage 10. See Figure 4.6 for full legend.

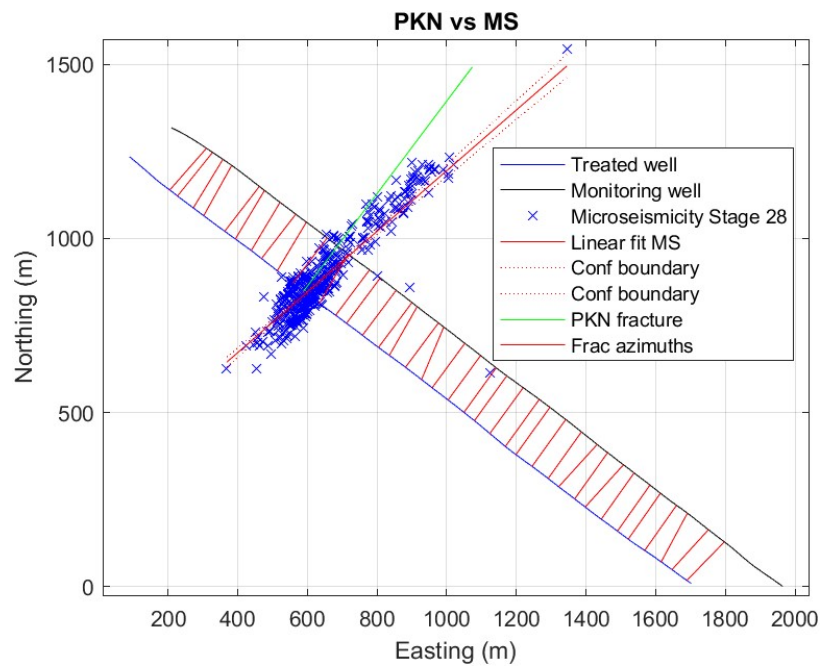


Figure 4.12: Example of bad agreement between trajectories. PKN vs MS plot of Stage 28. See Figure 4.6 for full legend.

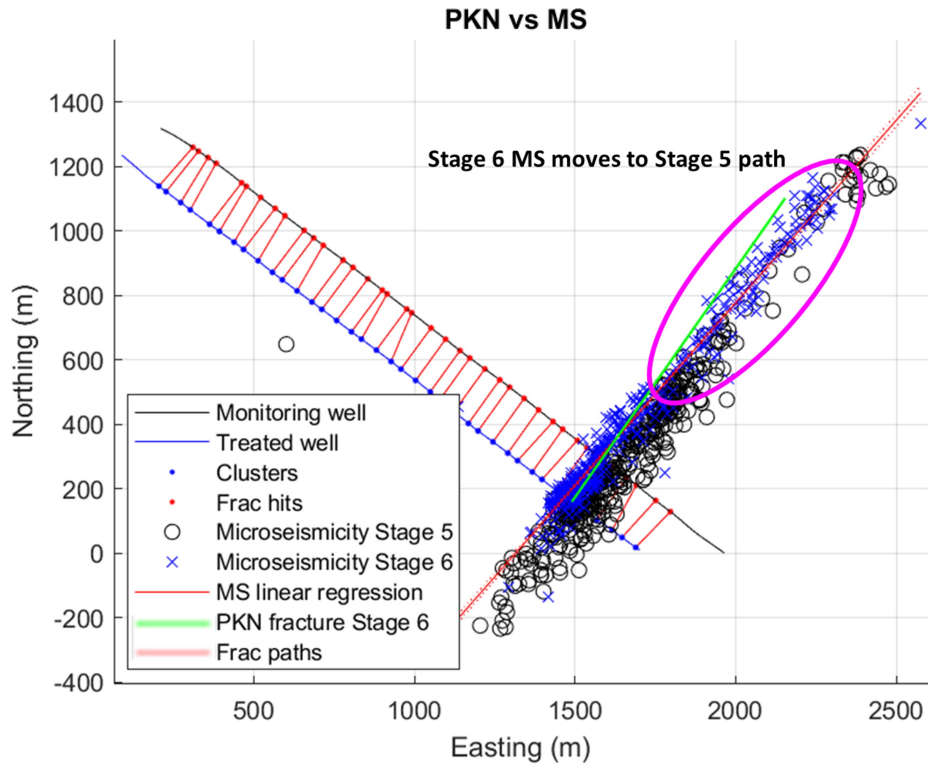


Figure 4.13: Stages 5 (black circles) and 6 (blue stars) microseismic clouds with the wells, with the linear regression of the MS cloud and the PKN fracture of Stage 6. See Figure 3.4 for full legend. The PKN fracture and MS cloud of Stage 6 had a similar trajectory until the pink circle where the MS seems to migrate towards Stage 5.

4.3.4 PKN results

For the second part of this analysis, the PKN results of the fracture half-lengths at the end of the injection were plotted side by side with the microseismic cloud lengths in Figure 4.14. The green arrows pointing down represent the stages where the microseismicity propagated mainly towards the SW. The circles at the bottom represent the stages that are not within the range of good agreement for the fractures half-length at the DAS hit time. The orange ones are the longer than expected fractures and the yellow circles the shorter ones. This plot makes a length comparison between the two methods easier. It is expected that the lengths would be similar, but large discrepancies between the two lengths might uncover issues during treatment.

A "large discrepancy" between the lengths occurs when the PKN fracture half-length estimation is 500 meters larger than the MS cloud length. These cases are indicated by the red bracket and red stars. The cases where the microseismic cloud is larger than the PKN are indicated by pink stars.

Overall, the PKN half-lengths are longer than the microseismic cloud lengths, which is not unexpected, as the model is an idealized, simplified model that does not consider all parameters that influence hydraulic fracture growth such as leak off and changing fracture heights. In the middle stages, the difference in length between both methods is bigger than in the earlier and final stages. The red bracket highlights these stages. According to the company that provided the data set, there was a problem in the middle stages and there was a change in the fluid injected in the formation, which could explain this bigger length difference. Some stages in these parts also present microseismic propagation towards the SW, which could contribute to the smaller microseismic cloud length compared to the PKN half-length. The possibility of other occurrences that limited the growth of the fractures in these stages is not discarded. Stages that present SW propagation outside the middle stages also present larger discrepancies between lengths, although not as big as the stages in the middle of the treatment. There are four stages where the MS cloud is larger than the PKN fracture. In all these stages, the further events from the treated well seem to correspond to fault/fracture re-stimulation like in Stage 6 (Figure 3.20).

The differences in the angle of propagation of the PKN fracture and the microseismic clouds in the PKN vs MS plots do not mean that it is a failed stage. In most stages, both lines intercept the monitoring well very close to each other, so the difference in azimuth means that the fracture changed directions during propagation. In Chapter 5 the results from this chapter and previous ones (Chapters 2 and 3) are integrated to look at the different analyses results for every stage. The objective is to find connections between the different results and to find properties and/or characteristic features of good and failed stages.

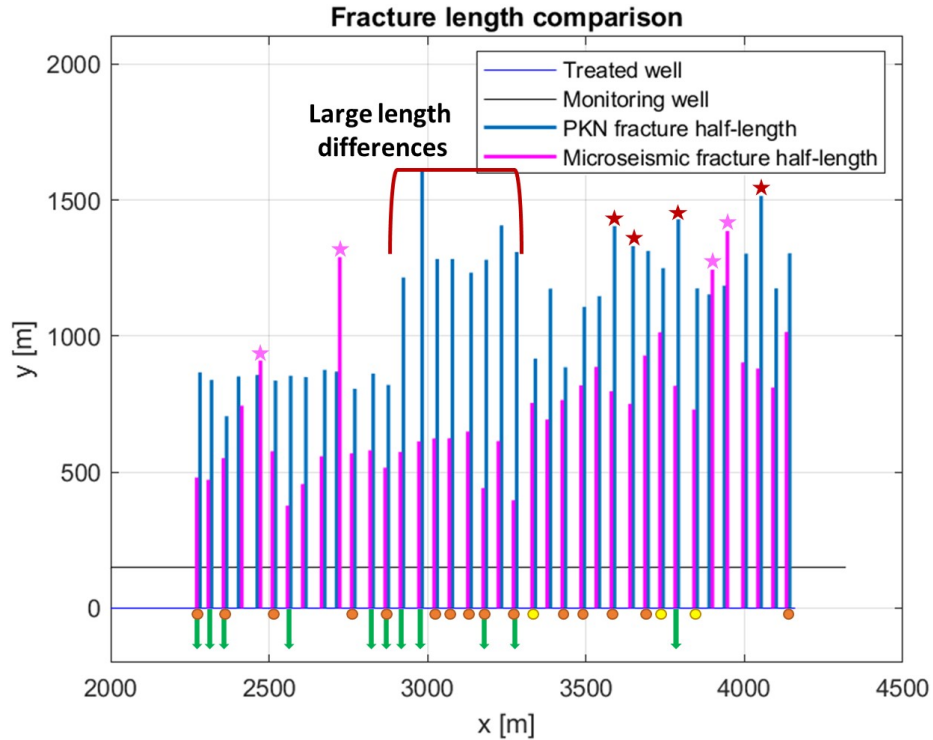


Figure 4.14: Horizontal plane of the wells, (see Figure 3.6 for full legend), with the PKN fracture half-lengths at the end of injection (steel blue) and the microseismic cloud lengths side by side (pink). The green arrows represent stages where the MS propagated SW. The orange circles show stages where the fracture half-length at the DAS hit time was longer than expected, the yellow circles show the stages where it was shorter.

4.3.5 PKN modelling conclusions

In this chapter, the PKN model was applied as a tool to find stages where things did not go as planned by comparing its results to the DAS data and microseismicity. The model was used to calculate the fracture half-length at the end of injection and the fracture half-length at the DAS hit time. The lengths at the end of the injection were compared to the lengths of the microseismic clouds, and the lengths at the DAS hit time were used to distinguish stages that propagate faster or slower than expected. Then, the fracture half-length at the end of injection was integrated with the frac azimuths to compare the trajectories to the microseismic cloud trajectories.

The PKN predicted fractures half-length that go from 310 to 1387 meters. The

fractures are longer in early stages than in later ones, probably because the injection time was longer at the beginning of the treatment and decreased with the stages, this matches with the results from Chapter 3. When comparing the lengths of the PKN model to the lengths of the microseismic clouds, the PKN model predicted longer fractures. However, this was expected as it is an idealized, simplified model, which does not capture the reality of all the processes involved, so an overestimation of fracture lengths is not considered abnormal. When the difference between the fracture lengths is higher than 500 meters, then something unexpected held back the growth of the fracture. Fractures where the microseismic cloud propagated towards the SW show significant length differences between the two methods. This difference is not as large as the differences that present stages in the middle. Around the middle of the treatment, the company reported problems in the treatment. This could be the reason the discrepancy in lengths is so large.

The use of the PKN model to calculate the fractures half-length at the DAS hit time is useful to detect the fractures that propagated slower or faster than expected. Most of the fracture lengths in this treatment are within the range of good agreement. However, the ones that are not, tend to be longer. If a fracture is longer than expected, it means that the fracture propagated slower than expected. This can be because of the cluster failing to create a fracture and the fluid traveled along the well until it found a fracture to propagate. If the fracture is shorter than expected, the fracture propagated very fast so the fracture was probably already there. Most of the fractures that are longer than expected at the DAS hit times are in the middle of the treatment, where the PKN fracture half-length and the microseismic cloud length present large length differences. This cements the idea that something unexpected happened in these stages. The analysis of all records, performed in Chapter 5, will shed some light on this.

Integrating the PKN fracture half-lengths with the frac azimuths to compare the trajectory obtained from the DAS data to the trajectory from the microseismic cloud

is a good tool for detecting when fractures changed direction. If the trajectories of the PKN fracture and the microseismic cloud differ greatly from each other, it means that the fracture changed propagation direction after the monitoring well. It could also mean that the fluids are being diverted to the previous stages. Mostly, the trajectories were very similar in the treatment stages. Eliminating events that happened far away from the microseismic cloud and on the SW side of the well can change the linear regression of the microseismic clouds, which might reveal that more stages trajectories agree with each other.

Using the PKN model is a simple way to see if things went according to plan during treatment. While using the individual heights for the fractures in the model might give more accurate fracture half-length values, I believe the results would have been similar. The stages that showed large discrepancies between the microseismic cloud and the PKN would still have large discrepancies, and the ones that agreed between methods would still agree. The same conclusion applies to the DAS hit time lengths and their proximity to the monitoring well. In the PKN model, if the plane strain modulus (E') and the injection rate (q) increase, the fracture half-length (x_f) also increases, and if they decrease, the half-length also decreases. If the fluid viscosity (μ) and the fracture height (h) increase, the fracture half-length (x_f) decreases, and when they decrease, the half-length increases. These parameters are part of a fraction calculation elevated to the power of $\frac{1}{5}$, so in this model the parameter that has a larger influence in the fracture half-length is the injection time (t). More sophisticated fracture models can be implemented to get more accurate growth predictions. For this study, the PKN model was a good tool to single out stages where the hydraulic fractures did not propagate as expected.

References

- Belyadi, H., Fathi, E., & Belyadi, F. (2019). Chapter Fifteen - Numerical simulation of hydraulic fracturing propagation. In H. Belyadi, E. Fathi, & F. Belyadi (Eds.), *Hydraulic Fracturing in Unconventional Reservoirs (Second Edition)* (Second Edition, pp. 257–272). Gulf Professional Publishing. <https://doi.org/https://doi.org/10.1016/B978-0-12-817665-8.00015-1>
- Espinoza, N. (n.d.). *Hydraulic fracture design: Single fracture completion* [accessed on 2021-09-10]. <https://dnicolasespinoza.github.io/node56.html#sec:CoupledFracProblem>
- FrackOptima. (n.d.). *PKN Hydraulic Fracturing Model* [accessed on 2021-09-10]. <http://www.frackoptima.com/userguide/theory/pkn.html>
- Garikapati, H., Verhoosel, C. C., van Brummelen, E. H., Zlotnik, S., & Diez, P. M. B. (2018). Sampling-based stochastic analysis of the PKN model for hydraulic fracturing. *Computational Geosciences*, *23*, 81–105.
- Geertsma, J., & De Klerk, F. (1969). A Rapid Method of Predicting Width and Extent of Hydraulically Induced Fractures. *Journal of Petroleum Technology*, *21*(12), 1571–1581. <https://doi.org/10.2118/2458-PA>
- Khristianovitch, S., & Zheltov, Y. (1955). *Formation of Vertical Fractures by Means of Highly Viscous Liquid* (Vol. All Days).
- Xiang, J. (2012). *A PKN Hydraulic Fracture Model Study and Formation Permeability Determination* (Master's thesis). Texas AM University.
- Xiao, C., Tian, L., Zhang, Y., Hou, T., Yang, Y., deng, Y., Wang, Y., & Chen, S. (2017). A Novel Approach To Detect Interacting Behavior Between Hydraulic Fracture and Natural Fracture by Use of Semianalytical Pressure-Transient Model. *SPE Journal*, *22*, 22. <https://doi.org/10.2118/187954-PA>
- Zoback, M. D., & Kohli, A. H. (2019). Stimulating Production from Unconventional Reservoirs. *Unconventional Reservoir Geomechanics: Shale Gas, Tight Oil, and Induced Seismicity* (pp. 231–374). Cambridge University Press.

Chapter 5

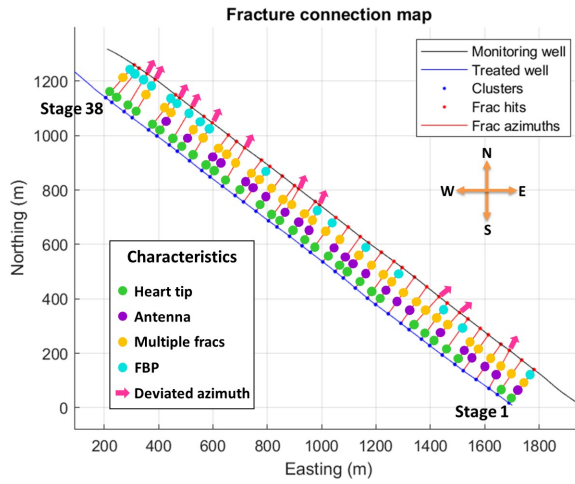
Discussion

5.1 Integrated scenarios

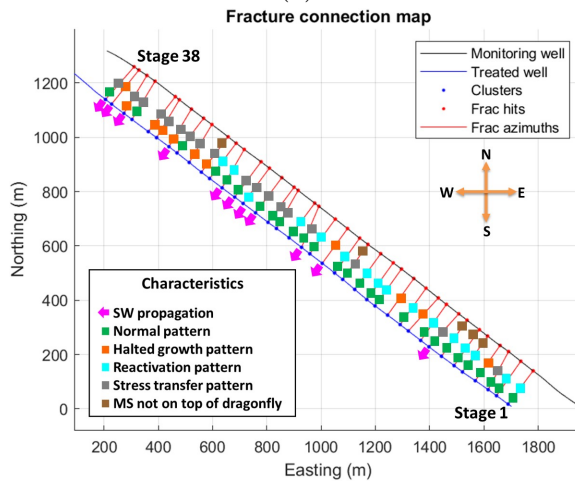
In the past chapters, low-frequency DAS, pumping information, microseismicity and the PKN model were used to study hydraulic fractures during injection. The different analyses provide complementary information that helps in the interpretation of these fractures.

Figure 5.2 shows a table with the integration of the information in Figures 2.19, 3.23, and 4.14 which show the analysis results from Chapters 2, 3, and 4 respectively (Figure 5.1). Blue means the stage has that characteristic and red that it does not have it. The characteristics cells are also colored in blue or red, blue meaning that having that characteristic is a sign that the stage worked correctly and red meaning the contrary. Stages that have an "R" after the number are stages that were re-stimulated a second time. Figure 5.3 shows the definition of the parameters to determine if a stage has or does not have that characteristic.

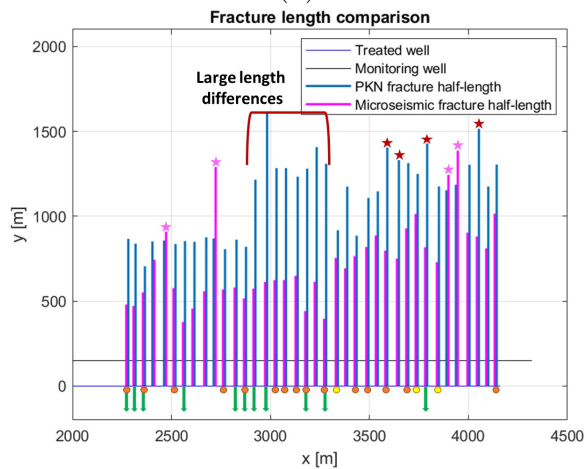
Integrating the different results can help detect stages where the hydraulic fractures did not behave as expected. In this chapter, I am going to show the expected behavior of the low-frequency DAS, engineering curves, microseismicity, and PKN for some scenarios.



(a)



(b)



(c)

Figure 5.1: Figures 2.19, 3.23, and 4.14 that present the results from Chapters 2, 3, and 4 respectively. See those figures for full legend.

Stage	Heart tip	Antenna	Multiple fracs	FBP	Perp azimuth	SW propagation	"Normal" pattern r-t plot	MS on top of dragonfly	PKN-DAS agreement	Frac changed directions	PKN-MS agreement
1							R		L		
2							R				
3							ST				
4							C (N-H)				
5							R	t			MS
6							R	t			MS
7							R	t	S		
8							ST				
9							R		S		
10							H		L		
11							R				
12							H		L		
13							R				
14							R		L		
15							R		L		
15 R							R-H		S		
16							ST				
17							R		S		
18							H		L		
19							R				
20							ST		L		
21							R		L		
22							ST		L		
23							ST		L		
24							ST				
25							C (R-H)				
25 R							R-ST		S		
26							ST		L		
27							R				
28							R		L		
29							H-ST	t			MS
30							H-ST				
31							ST				
32							H-ST				
33							H-ST		L		
34							H-ST				MS
35							ST				
36							H-ST		L		
36 R							R		S		
37							H				
38							ST		L		

Figure 5.2: Characteristics table for all stages. Blue means the stage presents that characteristic and red that it does not have it. The "R" next to the stage number means that the stage was re-stimulated. In the r-t front propagation, R = "reactivation" pattern, ST = "stress transfer" pattern, H = "halted growth" pattern, and C = the MS change patterns. In the MS overlay, characteristic "t" means the MS events travel to previous stages. In the PKN-DAS agreement row, "S" means the fracture length is shorter than expected, and "L" means the fracture length is longer than expected. In the PKN-MS agreement, "MS" means that the microseismic cloud is longer than the PKN fracture.

Heart tip	At least one heart-shaped tip present	No heart-shaped tip			
Antenna	Linear extending signal that can overlap with the heart-shaped tip	No antenna			
Multiple fracs	Multiple dragonflies or heart-shaped tips, wings and/or tails.	Single dragonfly and no multiple heart-shaped tip, wings and/or tails			
FBP	Noticeable formation breakdown pressure peak	No noticeable FBP peak			
Perp azimuth	Frac azimuth is perpendicular to the treated well	Frac azimuth shows deviation from the perpendicular			
SW propagation	The hydraulic fracture in that stage propagated mostly towards the SW	The fracture propagated towards the NE			
"Normal" pattern r-t plot	The triggering front has the "normal" pattern characteristic of a pore pressure diffusion process	R = The stage has "normal" pattern but also shows "reactivation" pattern	ST = The stage has "normal" pattern but also shows "stress transfer" pattern	C () = The stage changed patterns mid injection.	H = The stage shows "halted growth" pattern.
MS on top of dragonfly	The MS events are on top of the dragonfly and the immediate surroundings of it	The events are not on top of the dragonfly	t = means the events are travelling to a previous stage		
PKN-DAS agreement	The DAS hit time length is ±50 meters from the monitoring well	L = the fracture length at the DAS hit is long, so the fracture propagated slower than expected	S = the fracture length is short, so the fracture propagated faster than expected.		
Frac changed directions	There is a big difference in the trajectories of the microseismic cloud and the PKN fracture.	The trajectories are similar			
PKN-MS agreement	The PKN fractures are at most 500 meters larger than the MS cloud lengths	The length difference is larger than 500 meters	MS = the microseismic cloud is longer than the PKN fracture.		

Figure 5.3: Definition of the parameters to determine if a stage has or does not have a characteristic.

5.1.1 Scenario 1 - Expected stage

This scenario represents a stage where everything went according to plan and the hydraulic fracture propagated as expected. It has the expected characteristics displayed in the different observations which are displayed in Figure 5.4 and are:

- A noticeable heart-shaped tip in the dragonfly signal.
- Lack of the antenna signal in the dragonfly.
- Nice formation breakdown pressure peak in the bottom-hole curve.
- Fracture azimuth with perpendicular propagation.
- The r-t plot display "normal" development pattern.

- Microseismicity overlays mostly on top of the dragonfly on the strain fronts
- The fracture half-length at the DAS hit time is close to the monitoring well (within the boundaries).
- The PKN fracture and microseismic cloud have similar lengths.

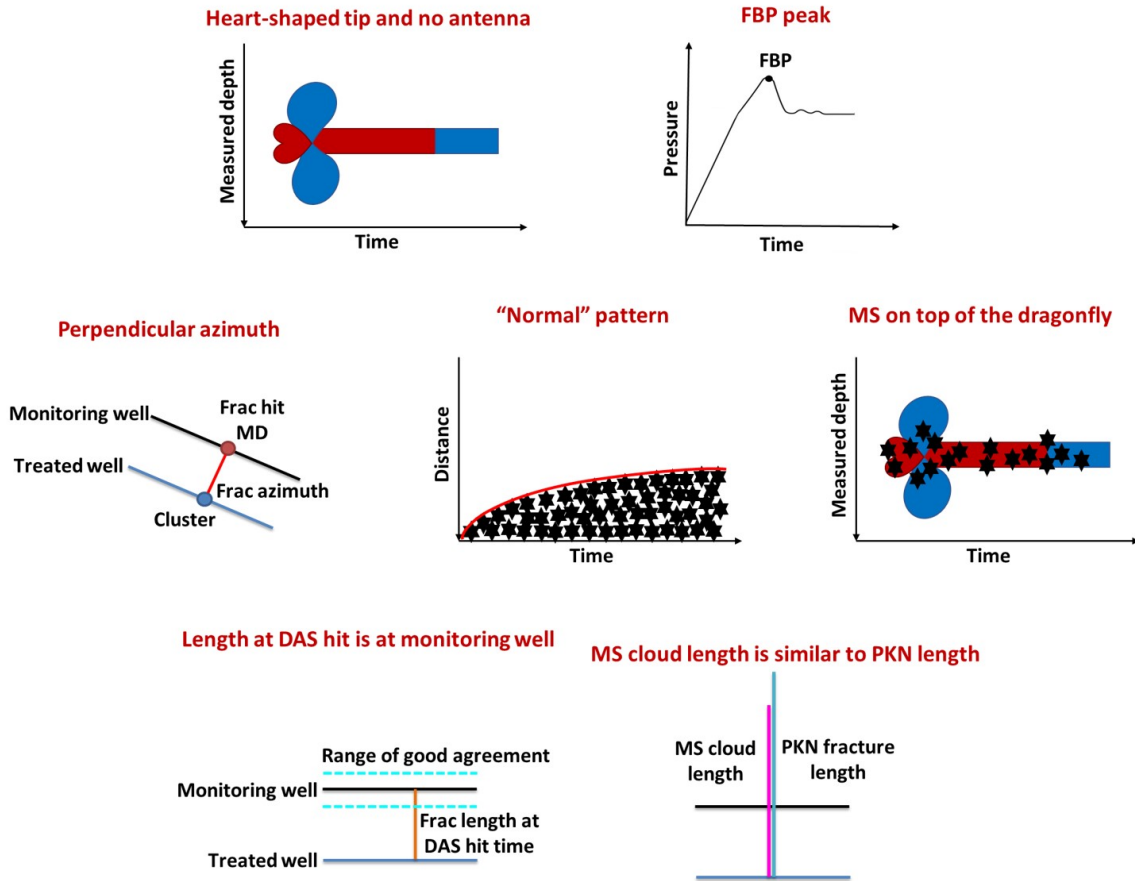


Figure 5.4: Schematic of the expected characteristics displayed in the LF DAS, engineering curves, microseismicity and PKN analyses for Scenario 1.

Fracture signal characteristics in the strain fronts

- **Heart-shaped tip**

For Scenario 1, we consider that a new hydraulic fracture will show a heart-shaped tip just before intercepting the monitoring well. Figure 5.5 shows the variations in the

local stress field caused by hydraulic fracture propagation and expansion. Tensile and shear stresses develop around the tip of the hydraulic fracture and there are compressive stresses surrounding the fracture as the formation is trying to accommodate the opening feature (Barthwal & van der Baan, 2019; Eyre & van der Baan, 2018). Past studies in LF DAS attribute the heart-shaped tip only to the tensile stress (Ugueto et al., 2019), but I believe the shear lobes contribute to the heart-shaped tip as well, because the shear will extend the cable too. The tensile stress on its own might not be able to create the heart shape characteristic of the tip but as we can see in Figure 5.5 the shear lobes on the side of the tensile stress look like a heart.

A pre-existent fracture does not present the tensile and shear stresses at the tip as the rock is already fractured and the fluids can propagate through it more easily. If this is the case, the strain signal will only show a extending passage with no heart shape tip and probably no pronounced wings, since there should not be much volumetric change in the reopening of a pre-existent fracture.

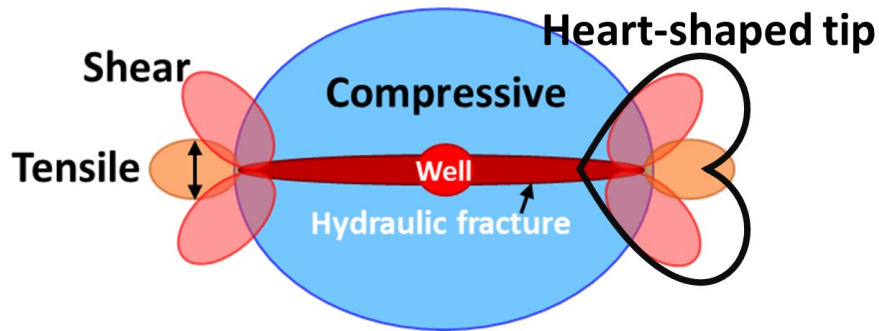


Figure 5.5: Schematic showing the stresses created by a planar propagating hydraulic fracture. Modified from Eyre and van der Baan (2018).

- **No antenna signal**

For this scenario we also do not expect to see an antenna signal, as the antenna signal means that the fluids are moving through a pre-existent fracture. It can last only a few minutes or during the whole injection, which might hinder the development of the new hydraulic fracture.

Formation Breakdown Pressure

If a new hydraulic fracture is being open, we would expect to see a noticeable FBP peak in the bottom-hole pressure curve. This is because when the injection kicks off in a fracturing stage, the pressure starts increasing up to a maximum that is known as the Formation Breakdown Pressure. This is the pressure at which the formation fractures and allows fluid to be injected. After the FBP, the pressure is expected to drop to the fracture propagation pressure, which is the pressure at which the fracture propagates as shown in Figure 5.4 (FBP peak). This is the ideal situation. However, the lack of FBP does not necessarily mean that no new fracture was created. It can also mean that there are initial cracks in the formation that helped the fluid open the hydraulic fractures more easily (Hubbert & Willis, 1957; Lavrov, 2016).

Perpendicular frac azimuth

Hydraulic fractures open in the direction of the minimum principal stress and propagate in the direction of the maximum principal stress, as shown in Figure 5.6. The horizontal well in this treatment was drilled in the direction of the minimum stress, so we would expect that the hydraulic fractures propagated perpendicular to the treated well. The geological conditions present in the area, like the presence of natural fractures and weakness planes, might interact with the hydraulic fractures and change the size and trajectory of the hydraulic fracture (Eberhardt & Amini, 2018). The stress shadows of pre-existent fractures can also cause deviation of hydraulic fractures (Wright & Weijers, 2001).

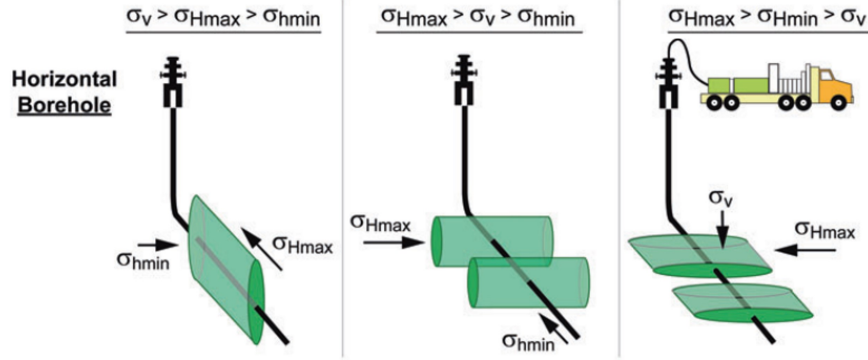


Figure 5.6: Relationship between hydraulic fracture opening and propagation directions relative to the in situ principal stresses in a horizontal well. Modified from Eberhardt and Amini (2018).

”Normal” pattern in the r-t plot

In the pore pressure triggering approach, it is assumed that some parts of the Earth’s subsurface are close to failure and so, the injection of fluids increases fluid pressure within the reservoir. This increases the pore pressure and modifies the effective normal stress which can lead to microseismicity (Angus & Verdon, 2013; Hummel & Müller, 2009).

The pore pressure induced seismicity has a parabolic development pattern in the r-t plots and this is the behavior we expect to see in hydraulic fracturing. I call it the ”normal” pattern in this work. It is displayed in Figure 5.4 (”Normal” pattern). Linear development corresponds to the reactivation of pre-existent fractures and I call it ”reactivation” pattern. If the events do not show increasing distances during injection, this means that the fracture is not growing more. I call it the ”halted growth” pattern. Instantaneous events or events that do not follow a pattern over time are originated by stress transfer and I call them ”stress transfer” pattern (Shapiro & Dinske, 2009; Shapiro et al., 1997).

MS on top of the dragonfly

The injection of fluids during hydraulic fracturing produces pressure changes and consequently deformations in the reservoir. This produces microseismic events that are related to the activation of pre-existing fractures or the creation of new fractures. The microseismic events concentrate on the fracture zone, which is the rock affected by the injection (Barthwal & van der Baan, 2019; Caffagni et al., 2016; van der Baan et al., 2013). Figure 5.7 shows a schematic diagram of the microseismicity during hydraulic fracturing.

The microseismic events are expected to happen continuously during the injection. The concentration of these events at some point in the injection reveals stimulation and/or hydraulic fracture growth issues (Maxwell, 2014). When plotting the MS events on top of the LF DAS strain fronts, we would expect that the events are on top of the dragonfly signal and in the immediate surrounding as in Figure 5.7. If the fluid changed directions or there is reactivation of a pre-existent fracture outside of the fracture zone, then the microseismicity would occur at other measured depths away from the fracture zone.

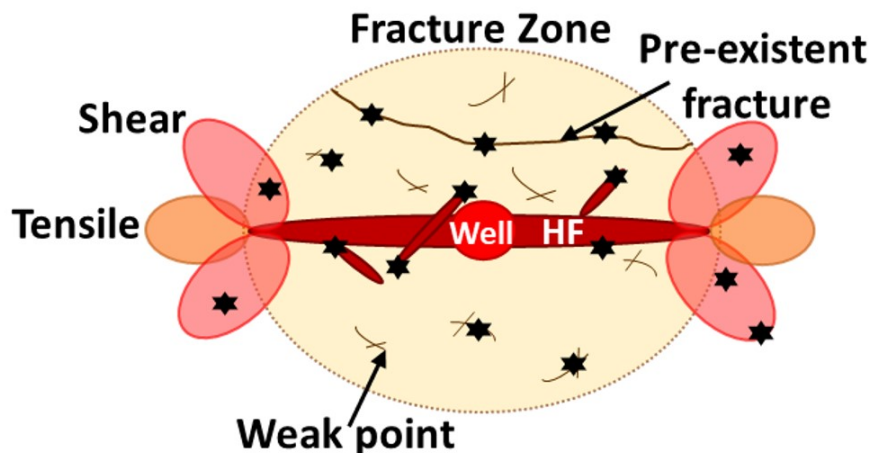


Figure 5.7: Schematic showing the stresses created by a planar propagating hydraulic fracture and the associated microseismicity. Modified from Cipolla and Wright (2002) and Eyre and van der Baan (2018).

Fracture growth is reasonably described by the PKN model.

- **Fracture half-length at the DAS hit time is at the monitoring well**

The PKN model can give an estimation of the fracture half-length at a certain time of the injection using treatment parameters and reservoir rock properties (Espinoza, n.d.). Using the time difference between the FBP and the frac hit on the DAS strain fronts, which we call the DAS hit time, I calculated the fracture half length. It is at this time that the fracture intercepted the monitoring well according to the strain fronts. So, we would expect that the fracture half-length at this time is around 150 meters, which is the separation between the treated and monitoring well with the DAS cable (Figure 5.4. Length at DAS hit is at monitoring well). If it's not, it would indicate that the fracture did not propagate with the expected speed. If it is too short, it propagated faster than expected, possibly the fracture was already there. If it is too long, it means that it propagated slower than expected. This could be because of cluster failure to create a fracture or because a pre-existent fracture was being re-stimulated, which delayed the propagation of the new hydraulic fracture.

- **PKN fracture length is similar to the microseismic cloud length**

With the PKN model, I also calculated the fracture half length at the end of injection. This represents the expected length of the fracture towards the NE direction. When compared with the length of the microseismic cloud, we would not expect both lengths to be exactly the same as the PKN is a simplified model. But we would expect that the PKN fracture is longer than the microseismic cloud and that the difference in lengths between them is not too large as we are using parameters from the treatment (Figure 5.4. MS cloud length is similar to PKN length.). If the difference in lengths is very large, it means that the fracture did not grow as expected towards the NE direction.

Stages that fall within this scenario.

No stages in this treatment were found to possess all the expected characteristics of Scenario 1. Stage 13 came close, but it has an antenna and displays "reactivation" pattern in the r-t plot. There are several indications that there is a reactivation of a pre-existent fracture. One thing I noticed during this work is that this treatment (third well fractured) presents more indications of fracture reactivation than the first and second well fractured. Meaning more antennas. The first well fractured has no antennas in their strain fronts and the second one presents only a few of them. In this well, most stages have antennas which indicates that the formation is more fractured than in previous treatments and the fluids can travel more easily.

Correlation analysis.

Figure 5.8 shows a table that exhibits the presence or absence of these expected characteristics in every stage was created. As with Figure 5.2, blue means the stage has that characteristic and red that it does not have it. The characteristics cells are also colored in blue or red, depending on if having that characteristic is good (blue) of not red) for the treatment.

After establishing what characteristics each stage posses, a correlation statistical analysis was done to the table (Figure 5.8) to find connections between the characteristics. The colors were assigned values, for blue 1 and for red -1. Table 5.1 shows the results of this analysis.

The range of values for the correlation analysis goes from -1.0 to 1.0, with -1.0 meaning perfect negative correlation and 1.0 perfect positive correlation. Negative correlation indicates that the two variables move in the opposite direction from each other and positive correlation indicates that the two variables move in the same direction. Zero indicates that there is no relationship between the two variables. Correlations between 0 and 0.3/-0.3 are considered to have a very weak relation, between 0.3/-0.3 and 0.5/-0.5 are weak, between 0.5/-0.5 and 0.7/-0.7 are considered

moderate, and $>0.7/-0.7$ have a very strong relation (Moore et al., 2013). In general, there was no significant correlation found, as observed in Table 5.1. The highest negative correlation is between the presence of the heart-shaped tip and the antenna. This makes sense, as the presence of the heart-shaped tip means the creation of a hydraulic fracture and the presence of the antenna means the re-stimulation of a pre-existent one. The highest positive correlation is between the presence of the heart-shaped tip and the FBP peak. This makes sense as if there was a new fracture being created we would expect both characteristics to be present. On that note, the presence of an antenna has a weak negative correlation with the FBP peak, this is expected as if there is an antenna this means that a pre-existent fracture is being re-stimulated or there are cracks close to the injection point that made the formation easier to fracture. We had expected to find some correlations between the characteristics. However, hydraulic fracturing is a complex process and there are a lot of variables that influence it. It is clear that the acquisition of different data types and their integrated analysis is of great value as it offers a more complete interpretation and we are able to identify issues in the fracturing stages during injection that might not be visible if only one record is used.

Stage	Heart tip	Antenna	FBP	Perp azimuth	"Normal" pattern r-t plot	MS on top of dragonfly	PKN-DAS agreement	PKN-MS agreement
1					R		L	
2					R			
3					ST			
4					C (N-H)			
5					R	t		MS
6					R	t		MS
7					R	t	S	
8					ST			
9					R		S	
10					H		L	
11					R			
12					H		L	
13					R			
14					R		L	
15					R		L	
15 R					R-H		S	
16					ST			
17					R		S	
18					H		L	
19					R			
20					ST		L	
21					R		L	
22					ST		L	
23					ST		L	
24					ST			
25					C (R-H)			
25 R					R-ST		S	
26					ST		L	
27					R			
28					R		L	
29					H-ST	t		MS
30					H-ST			
31					ST			
32					H-ST			
33					H-ST		L	
34					H-ST			MS
35					ST			
36					H-ST		L	
36 R					R		S	
37					H			
38					ST		L	

Figure 5.8: Expected characteristics table for all stages. Blue means the stage presents that characteristic and red that it does not have it. See Figure 5.2 for the full legend.

	<i>Heart tip</i>	<i>Antenna</i>	<i>FBP</i>	<i>Perp azimuth</i>	<i>"Normal" pattern r-t plot</i>	<i>MS on top of dragonfly</i>	<i>PKN-DAS agreement</i>	<i>PKN-MS agreement</i>
Heart tip	1							
Antenna	-0.40281	1						
FBP	0.326732	-0.38857	1					
Perp azimuth	0.018531	0.135359	-0.06487	1				
"Normal" pattern r-t plot	0.239434	0.093761	-0.12477	0.172537	1			
MS on top of dragonfly	-0.01757	-0.12832	0.01107	-0.25394	-0.11118	1		
PKN-DAS agreement	-0.07188	-0.06918	0.1691	0.035806	-0.01757	-0.23277	1	
PKN-MS agreement	0.271304	-0.33091	0.306373	-0.04152	-0.08403	0.140222	-0.1691	1

Table 5.1: Correlations between the expected characteristics.

5.1.2 Scenario 2 - Re-stimulation of a pre-existent fracture

This scenario represents a stage where the fluids are re-stimulating a pre-existent fracture, so the injection did not create a new hydraulic fracture. The characteristics are displayed in Figure 5.9 and are:

- No heart-shaped tip in the dragonfly. presence of antenna only.
- The wings are broader.
- No formation breakdown pressure.
- "Reactivation" pattern in the r-t plot.
- Fewer microseismic events on top of the dragonfly.
- The fracture half-length at the DAS hit time very short.

If a pre-existent fracture is being re-stimulated, we do not expect to see the heart-shaped tip in the fracture signal of the strain fronts. This is because there are no stresses at the tip of the hydraulic fracture as the fracture is already open and the fluid is not trying to crack the rock. The wings also are mostly absent. There is

compression surrounding the fracture, but it does not look like the expected wings. The region extends longer in time. This is because there is little volumetric change as the fracture is already open.

No FBP is expected as the fracture is already open, and the fluid does not need to break the formation. We would expect less microseismic events because the fluid is moving through an open fracture, so the stresses affecting the surrounding formation would not be as large as the ones in a new hydraulic fracture. Their development in the r-t plots should correspond to the "reactivation" pattern and we would expect them to be mostly on top of the dragonfly and in its immediate surroundings.

The fracture half-length at the DAS hit time will be very short, as this indicates the fracture propagated very fast which would happen if the injection does not have to open the path. I did not add an expected behavior of the PKN vs MS plots because this will depend on the fracture growing further with the injection or not and on the length of this fracture before injection.

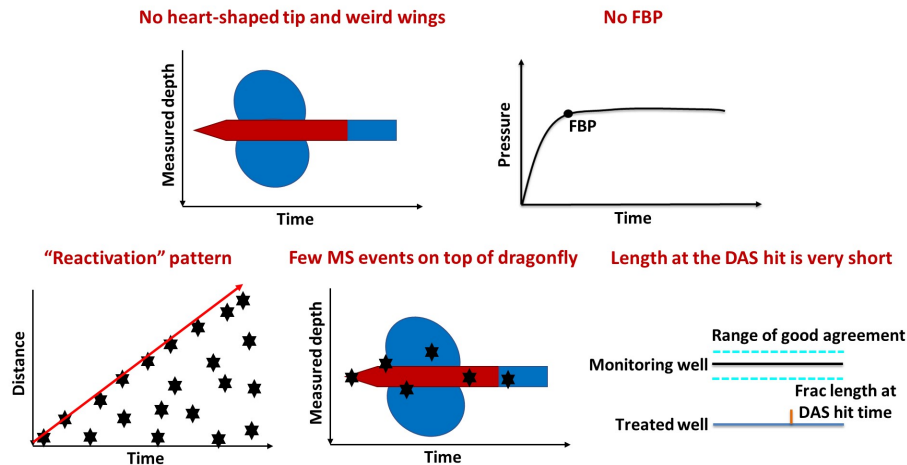


Figure 5.9: Schematic of the expected characteristics displayed in the LF DAS, engineering curves, microseismicity and PKN analyses for Scenario 2.

Stages that fall within this scenario.

The re-stimulated stage, Stage 25, is a good example of this scenario (Figure 5.10). It does not have a heart-shaped tip, the wings do not have the expected shape and

seem broader. There is also no FBP and the fracture half-length at the DAS hit time is very short (not shown as it is not visible in the schematic of the wells). The microseismic events are very few and they are on top of the dragonfly. Due to the small number of MS events, there is no clear pattern in the r-t plot, but there seems to be "stress transfer" before the injection starts and then, when it starts, the MS events grow rapidly.

The re-stimulated stages for Stages 15 and 36 also display most of these characteristics. Stage 15 shows more microseismicity than expected though. It develops in a clear "reactivation" pattern, so there could be another fracture being reactivated and growing away from the monitoring well, and that is why there is no strain signal in the strain front. Stage 36 does not have a heart-shaped tip in the dragonfly that corresponds to the hydraulic fracture from the first injection, but later on, there is a new dragonfly signal. This re-stimulation created a new hydraulic fracture and, because of this, there is more microseismicity than expected, but it develops in the "reactivation" pattern as well.

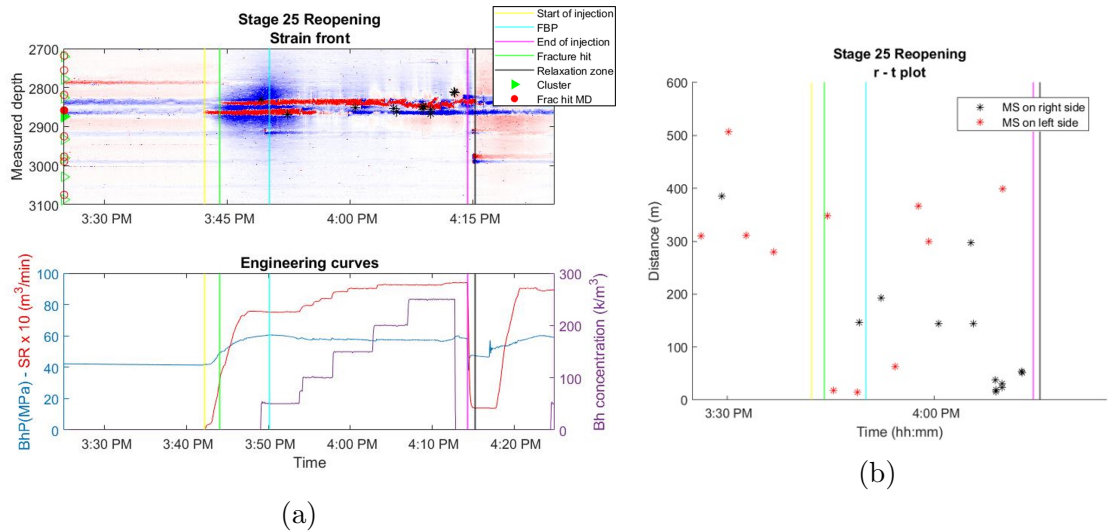


Figure 5.10: Re-stimulation of Stage 25: a) DAS-MS plot. b) r-t plot. Fracture signal in strain front does not have a heart-shaped tip and the r-t plot shows "reactivation" and "stress transfer" patterns.

Stages 3, 4, 5, 11, and 12 have antennas but do not present heart-shaped tips. It

might seem like stages where the injection did not create a fracture. However, all these stages also present indications that multiple fractures were created. We can see this clearly in Stage 11. Figure 5.11 shows the strain front with the DAS-MS plot (Figure 5.11a) and the r-t plot (Figure 5.11b). Stage 11 presents two pairs of wings and two tails in the strain front. The r-t plot shows "reactivation" pattern (red solid line) but there also seems to be microseismic events that developed with the "normal" pattern (red dotted line). The stress shadow of the re-opened fracture responsible for the antenna might have suppressed the heart-shaped tip of the new hydraulic fracture.

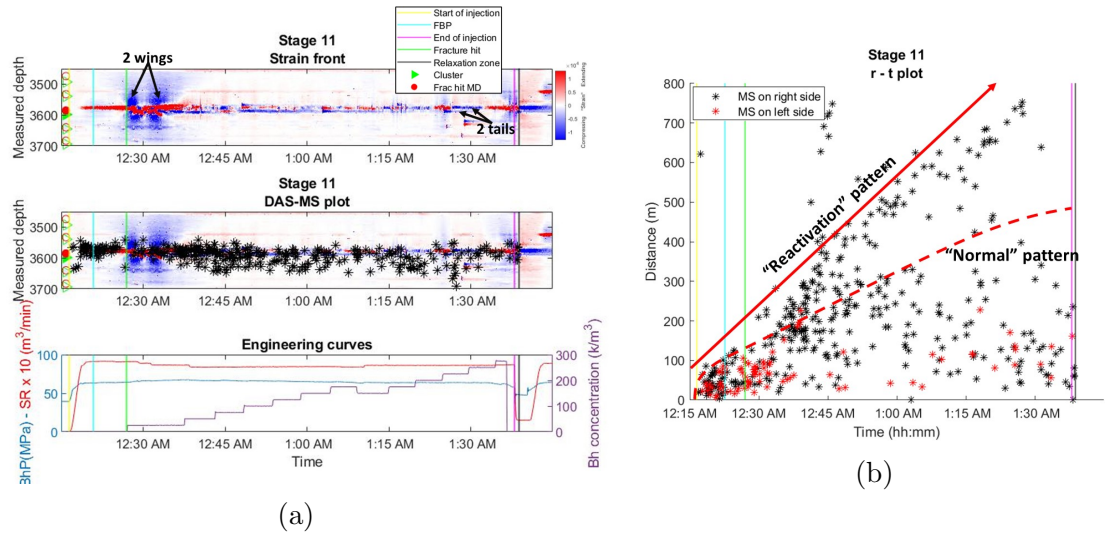


Figure 5.11: Stage 11: a) Strain front with DAS-MS plot. b) r-t plot. The fracture signal does not have a heart-shaped tip and presents the "reactivation" pattern. But there are multiple fractures propagating so the stage is not a failed one.

Stages 7, 9 and 17 have small fracture-half lengths at the DAS hit time, meaning they propagated faster than expected. But they all have heart-shaped tips. This is surprising, as we would expect them to be the reopening of a pre-existent fracture and have only an antenna. Figure 5.12 shows the DAS strain front of Stage 9 (5.12a) and the fracture half-length at the DAS hit time in the schematic of the wells (5.12b). The dragonfly has a clear heart-shaped tip, but the length at the DAS hit time is out of the range of good agreement. One thing I noticed is that these three stages are

not as fast as the re-stimulated stages, so there was probably a pre-existent fracture that did not intercept the monitoring well, and the injection of the fluid helped the fracture to keep growing and intercept the monitoring well. That is why they have heart-shaped tips.

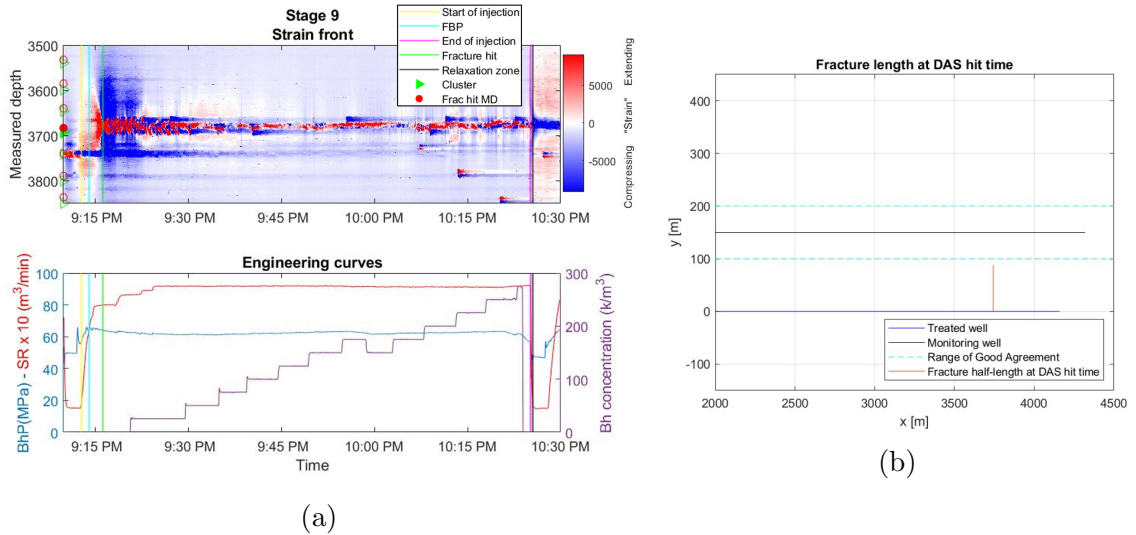


Figure 5.12: Stage 9: a) strain front and b) fracture half-length at the DAS hit time (orange line) in the schematic of the wells. The hydraulic fracture propagated faster than expected but has a heart-shaped tip.

5.1.3 Scenario 3 - Re-stimulation of a pre-existent fracture with new hydraulic fracture

This scenario represents a stage where the fluids are re-stimulating a pre-existent fracture, but the injection did create a new hydraulic fracture later in the injection. The characteristics are displayed in Figure 5.13 and are:

- heart-shaped tip and antenna in the dragonfly.
- No formation breakdown pressure.
- The fracture half-length at the DAS hit time is a bit longer than expected.

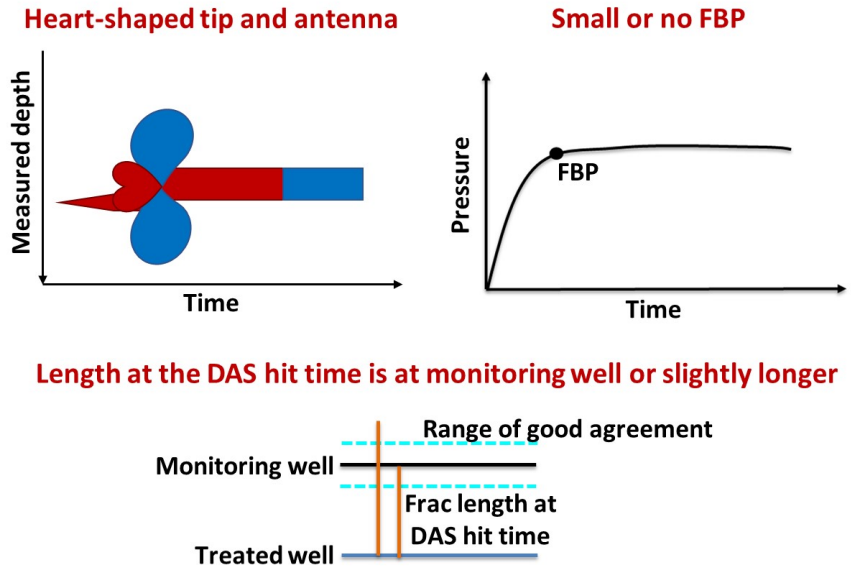


Figure 5.13: Schematic of the expected characteristics displayed in the LF DAS, engineering curves, and PKN analysis for Scenario 3.

When a pre-existent fracture is re-stimulated during the injection, but the fluid also created a hydraulic fracture, we expect that the LF DAS fracture signal has an antenna and a heart-shaped tip happening later in the injection. This is because, if the injection point is close to a pre-existent fracture, at the start of the injection the fluid finds the opening and, as the rock in other parts resist to break, the fluid moves through the pre-existent fracture. Eventually, the injection does create a hydraulic fracture, and the fluid starts going mostly through it. The antenna signal could carry for most of the injection, meaning the fluids are actively flowing through the pre-existent fracture, or be a couple of minutes long and stop as the new hydraulic fracture intercepts the monitoring well. The last explanation could be due to a pulse of fluids that go through the pre-existent fracture before the rock breaks and starts taking the fluid.

We also do not expect to see large FBPs, because if there is a fracture so close to the injection point, that its signal overlaps with the heart-shaped tip of the hydraulic fracture, then there can be cracks very close to the injection point that make it easier

for the fluid to break the rock and so we do not get large FBPs. The fracture half-length at the DAS hit time might be longer than expected because the fluid is first going to the pre-existent fracture, which might delay the creation of the new hydraulic fracture. Unless it is just a pulse of fluid.

Stages that fall within this scenario.

Stages 1, 6, 8, 13, 15, 16, 17, 18, 20, 21, 22, 24, 26, 28, 29, 31, and 33 have heart-shaped tips and antennas. Most of these cases do not have a FBP peak, and all of them have indications of having created multiple fracture. Stages 1, 15, 18, 20, 21, 22, 26, 28 and 33 have longer than expected fractures half-lengths at the DAS hit time. It seems like the re-stimulation of the pre-existent fractures and the creation of multiple fractures slowed down the propagation of these hydraulic fractures.

Figure 5.14 shows the strain front (5.14a) and the fracture half-length at the DAS hit time (5.14b) of Stage 15. This stage has an antenna that corresponds to either a natural fracture or to the hydraulic fracture of a past treatment, as it does not come from the previous stage. The antenna signal shows for all the treatment. It seems like the fluids in this stage went mostly through it. However, at the green line, we can see a small heart-shaped tip, meaning the injection did create a new hydraulic fracture. There is competition between both fractures, but it seems like the pre-existent fracture is the predominant one as its signal is continuous during the injection while the hydraulic fracture seems to close for a portion of it (12:40 pm).

In Figure 5.14b we can see that the fracture half-length at the DAS hit time is out of the range of good agreement, it propagated slower than expected. This can be because the pre-existent fracture is taking most of the fluid and so the new hydraulic fracture did not propagate as expected. This is, however, not the rule for every stage that has an antenna and a heart-shaped tip.

Stage 13 shown in Figure 5.15 has an antenna and a heart-shaped tip in the fracture signal. It has also a noticeable FBP peak in the engineering curves. The antenna in

this stage seems to be short. It appears shortly after the start of the injection and disappears when the hydraulic fracture intercepts the monitoring well (green line). It is possible that this antenna is due to a fluid pulse that found the opened passage and propagated through it before the fluid cracked the rock and created the new hydraulic fracture. The fracture half length at the DAS hit time is a bit past the monitoring well, but it is within the range of good agreement. It looks like the re-stimulation of the pre-existent fracture was not enough to delay the propagation of the hydraulic fracture, as in Stage 15.

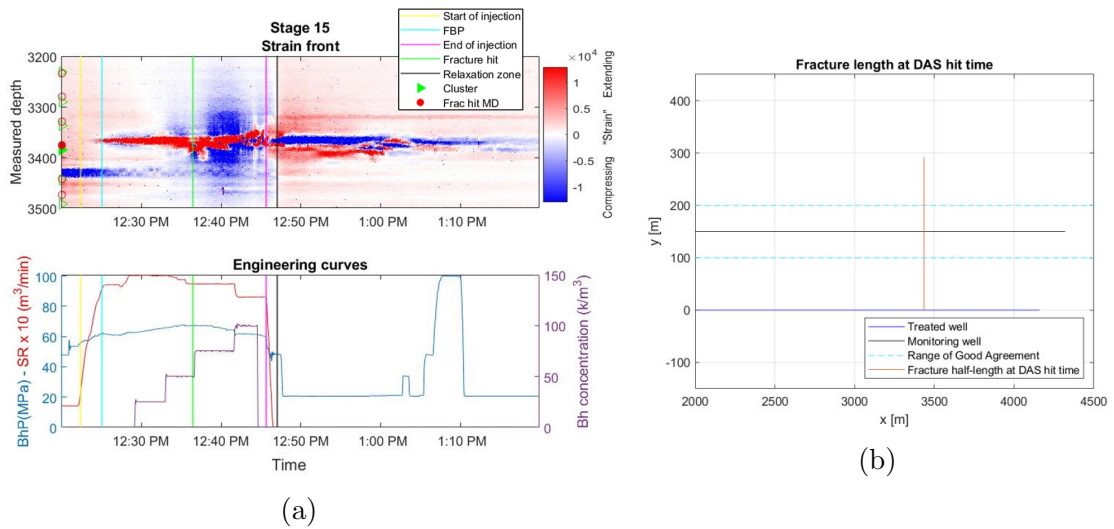


Figure 5.14: Stage 15: a) strain front and b) fracture half-length at the DAS hit time (orange line) in the schematic of the wells. The hydraulic fracture has an antenna and propagated slower than expected

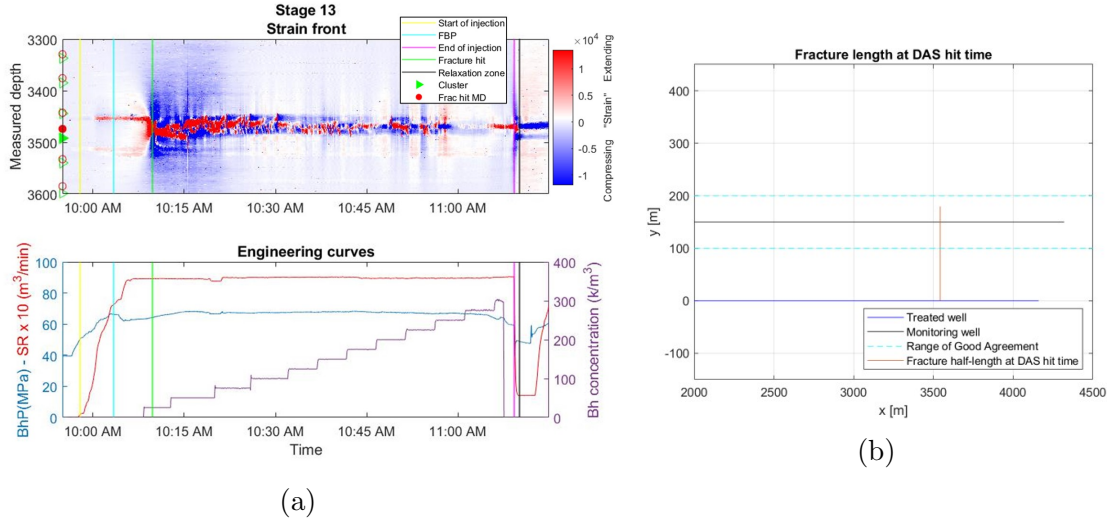


Figure 5.15: Stage 13: a) strain front and b) fracture half-length at the DAS hit time (orange line) in the schematic of the wells. The hydraulic fracture has an antenna and propagated as expected.

5.1.4 Scenario 4 - Fracture deviation

The fracture connection map (Figure 5.16, created in Chapter 2) shows that some stages did not propagate perpendicular to the treated well (pink arrows). It is worth to note that these deviations are not too acute. This scenario is for stages that do not have a perpendicular frac azimuth.

Usually, the deviation of the expected frac azimuth in hydraulic fractures is due to the presence of fractures and weakness planes in the formation that divert the hydraulic fracture from its predicted direction. However, the stress shadow of a pre-existent fracture can also divert the hydraulic fracture from its predicted direction. If the hydraulic fracture is close enough to a pre-existent fracture, their stress shadows can overlap, and this influences the propagation and geometry of hydraulic fractures.

For this scenario we would expect that the stage exhibits the following characteristics (Figure 5.17):

- Frac azimuth deviation
- Expected or slightly shorter fracture half-length at the DAS hit time.

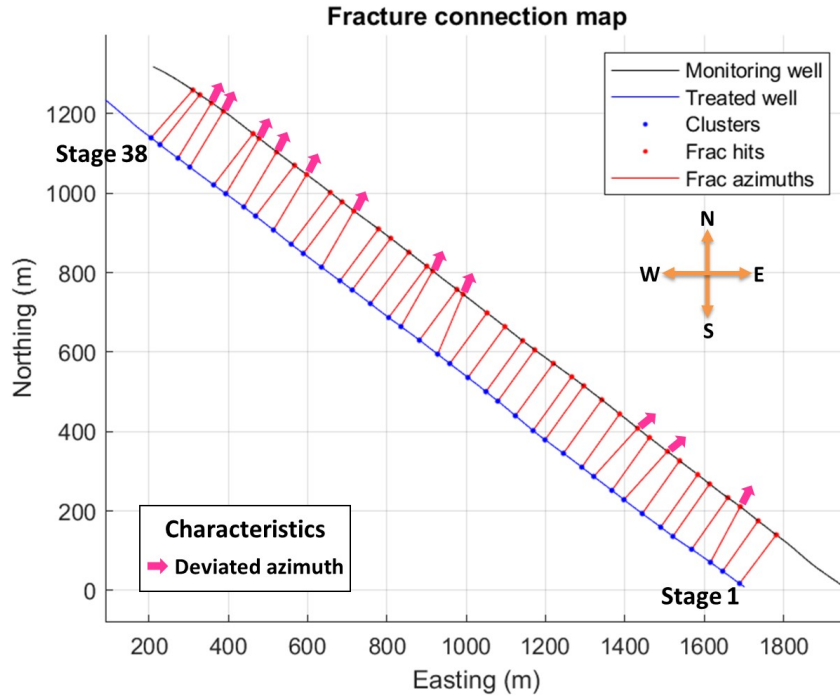


Figure 5.16: Fracture connection map for all stages, with original wells geometry See Figure 2.10 for full legend. Displays the direction of fracture propagation.



Figure 5.17: Schematic of the expected characteristics displayed in the fracture connection map, and PKN analysis for Scenario 4.

For this scenario, we would have a frac azimuth deviation, the fracture did not propagate perpendicular to the treated well and we expect to have either an expected or shorter fracture half-length at the DAS hit time. This depends on if the hydraulic fracture propagates along the natural fracture and then comes out from the tip of the natural fracture, or if the hydraulic fracture deflects into the natural fracture and re-initiates at some weak point along the natural fracture. If the fracture was deviated by the stress shadow of a pre-existent fracture, we would expect a fracture half-length at the DAS hit time within the range of good agreement as well.

Stages that fall within this scenario.

Stages 3, 8, 27, 30, 32, and 35 have deviated frac azimuth but their fracture half length at the DAS hit time is within the range of good agreement. Stages 10, 20, 22, 33 and 36 present deviated azimuths, but they have long DAS hit lengths. This is not what was expected. From these stages, Stages 20, 22, and 33 have antennas. Stage 36 does not have an antenna, but there is a clear reopening of the tail of the previous stage with enough spacing between the tail and the dragonfly to not be considered an antenna.

Figure 5.18 shows Stage 20 DAS strain front (5.18a), and the schematic of the wells with the fracture half-length at the DAS hit time (5.18b). Figure 5.18b shows that this fracture propagated slower than expected. It is out of the range of good agreement. The strain front has an antenna that comes from a fracture created in Stage 19. The antenna is in line with the Stage 20 cluster (green filled triangle) and later in the injection, a new hydraulic fracture with a heart-shaped tip is seen at a shallower measured depth than the cluster. It seems like in these cases the fracture took longer to propagate because the previous stage was taking most of the fluid and the deviation is because the stress shadow of the re-stimulated fracture is pushing the new fracture towards the heel of the well, as seen in Stage 20 (Figure 5.18a).

Stage 10 does not have an antenna, FBP, and it propagated slower than expected. This stage might have not formed a fracture, but the fluid traveled along the well until it found an opening to propagate through that was not intercepting the monitoring well before the injection. This would explain why there is no FBP, no antenna and it presents deviated azimuth.

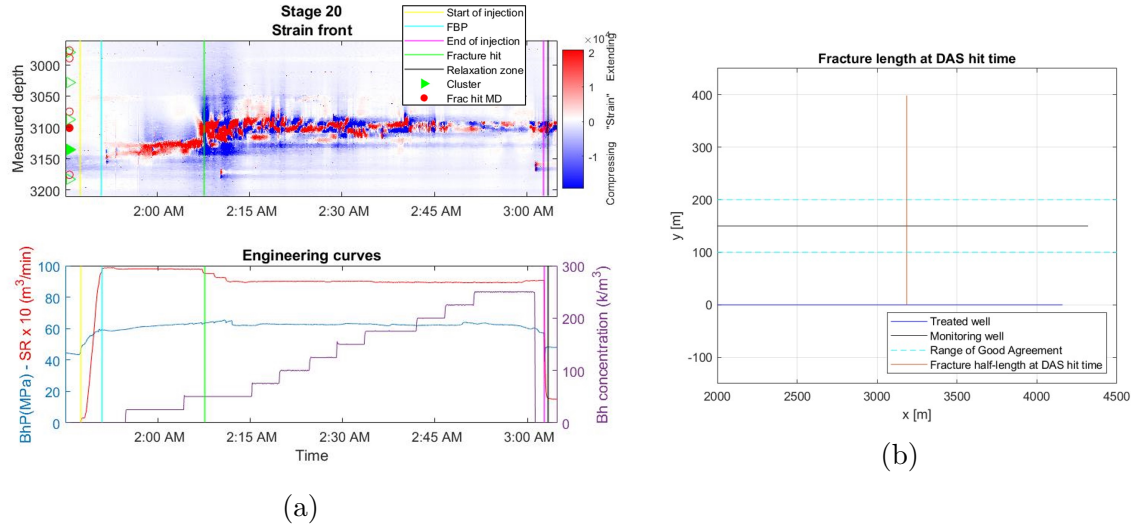


Figure 5.18: Stage 20: a) strain front and b) the fracture half-length at the DAS hit time.

5.1.5 Scenario 5 - MS cloud longer than expected

The PKN model was used to calculate the expected fracture half length at the end of injection according to treatment and geological parameters. The expected result is that the PKN fracture is longer than the microseismic cloud and that the difference in lengths between them is not too large. This scenario is for stages where the MS cloud is longer than the PKN fracture. We would expect that the stage exhibits the following characteristics (Figure 5.19):

- MS cloud longer than the PKN fracture.
- Microseismicity travels to previous stages in the DAS-MS plots.
- r-t plot shows "reactivation" pattern.

If the microseismic cloud is longer than the PKN fracture, it means that the fracture propagated longer than expected. The explanation for this could be that the hydraulic fracture intercepted a pre-existent fracture, and therefore, the hydraulic fracture is longer than expected. So, we would expect to see microseismic events not on top of the dragonfly in the DAS-MS plots and "reactivation" pattern in the r-t plots.

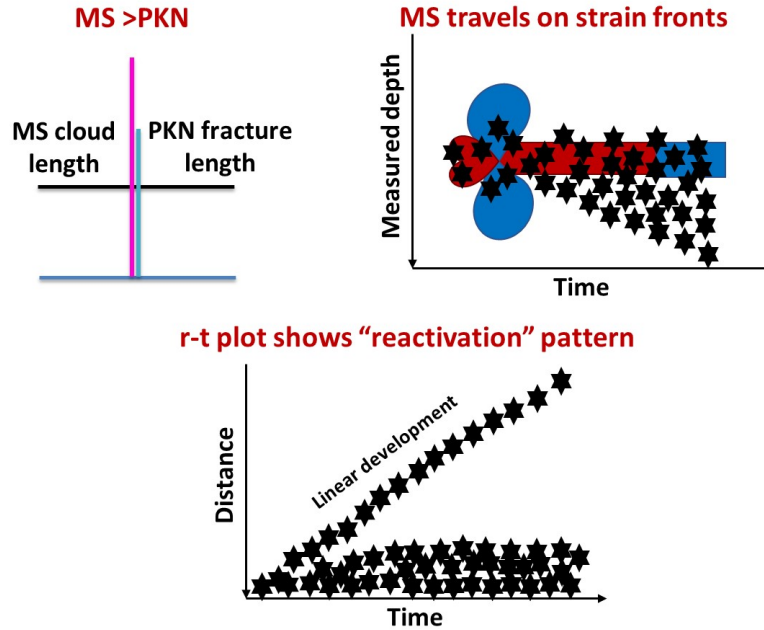


Figure 5.19: Schematic of the expected characteristics displayed in the PKN vs MS comparison, DAS-MS plot, and r-t plot for Scenario 5.

Stages that fall within this scenario.

There are four stages where their microseismic clouds are longer than their PKN fractures, Stages 5, 6, 29 and 34 shown in Figure 5.20. The first three stages also show MS traveling to previous stages in the DAS-MS plots and the r-t plots show clear fracture reactivation. Figure 5.21 shows the DAS-MS plot of Stage 6 (5.21a), the r-t plot (5.21b), and the wells with the microseismic cloud of Stage 5 (black circles) and Stage 6 (blue crosses), the linear regression and the PKN fracture of Stage 6 (5.21c). The DAS-MS plot of Stage 6 (Figure 5.21a) shows that the microseismicity moves towards the previous stages (orange circle). The r-t plot (Figure 5.21b) shows linear growth of the microseismicity around the same time the microseismicity starts to travel to the previous stages in the DAS-MS plot (orange circle). The main triggering front seems to grow only 400 meters until the end of the injection, but the reactivation of the fracture in Stage 5 made the MS cloud to grow longer. The microseismic cloud of Stage 6 corroborates this, if we look at Figure 5.21c) we can notice how after a

certain distance the events deviate towards the microseismic cloud of Stage 5 (pink circle). The fluids injected in Stage 6 are being diverted to the fracture created in Stage 5 after the monitoring well.

Stage 34 does not have MS moving to a previous stage in the DAS-MS plot (Figure 5.22a). However, the r-t plot shows reactivation of a previous fracture at greater distances than the main triggering front (orange circle in Figure 5.22b). It seems like there is a fracture being reactivated that is at the same measured depth as the fractures created in Stage 34 but is farther away from the monitoring well, so there is no strain signal in the strain front. The reactivation of pre-existent fractures in these four stages made the microseismicity to extend longer than expected.

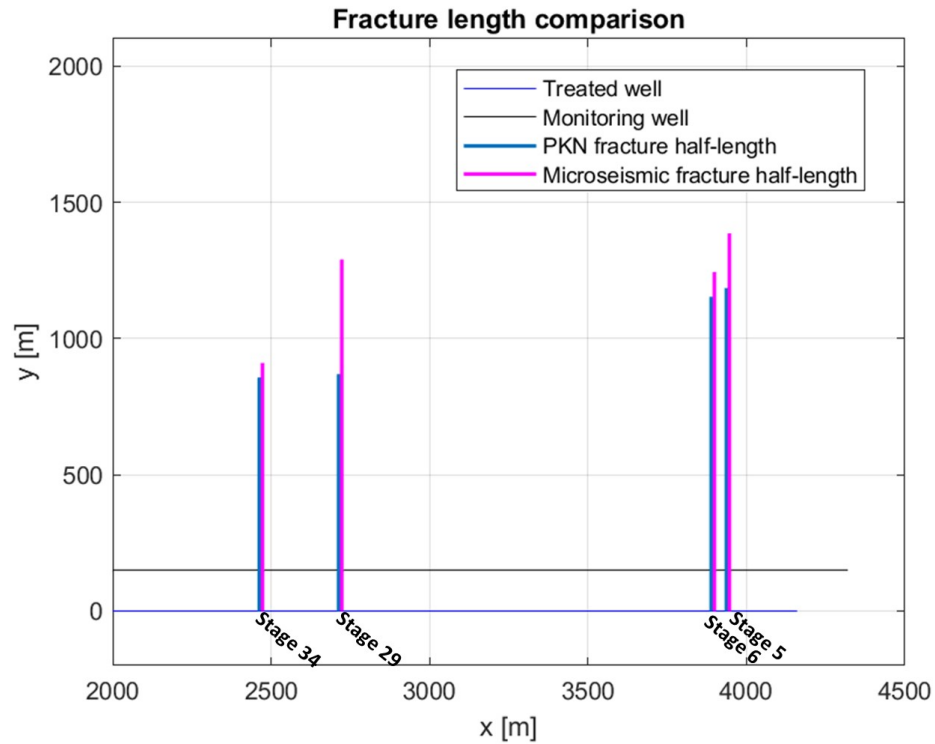
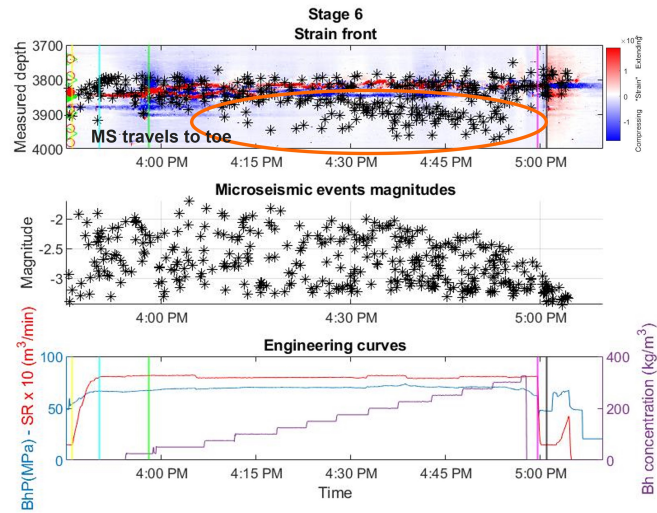
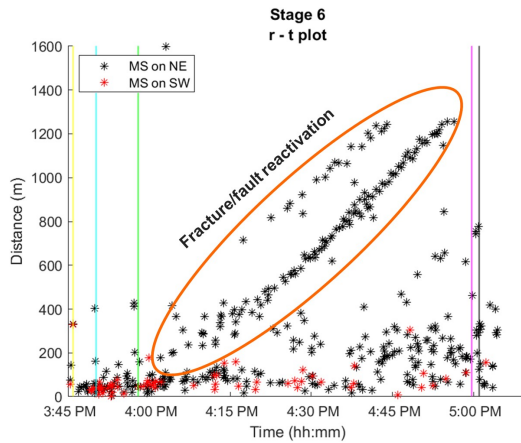


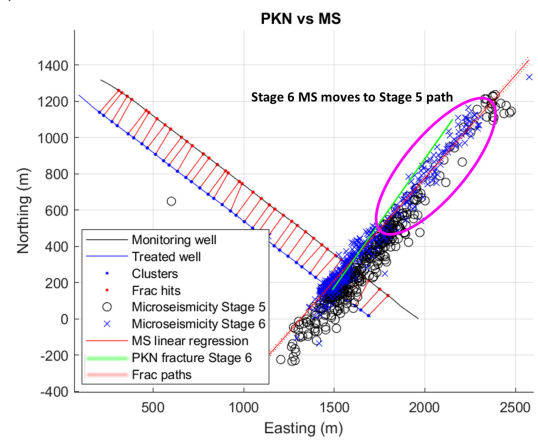
Figure 5.20: Schematic of the well with the PKN fracture (blue line) and the microseismic cloud (pink line) lengths side by side.



(a)



(b)



(c)

Figure 5.21: Stage 6: a) DAS-MS plot, b) r-t plot and c) Stages 5 (black circles) and 6 (blue stars) microseismic clouds with the wells, the linear regression of the MS cloud and the PKN fracture of Stage 6. Orange and pink circles in the three figures highlight the microseismicity moving to the previous stage.

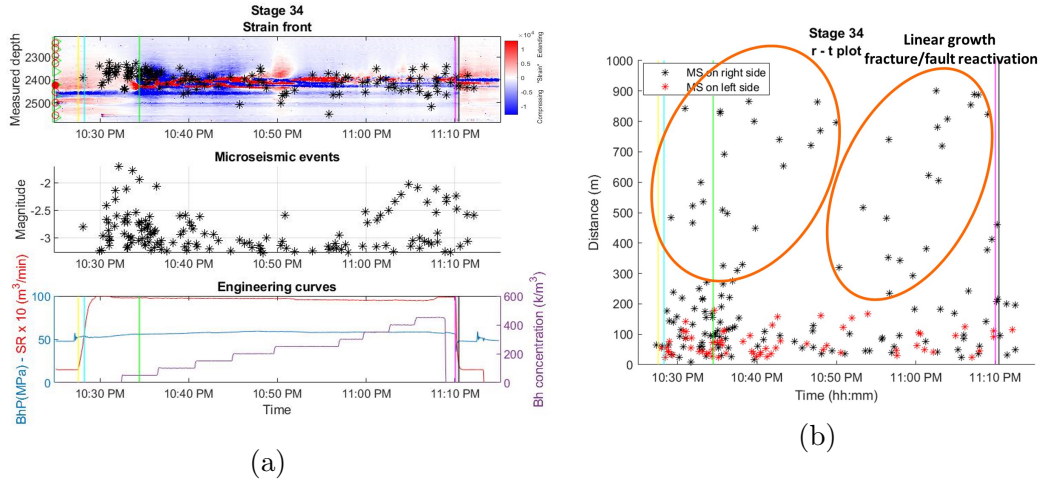


Figure 5.22: Stage 34: a) DAS-MS plot, and b) r-t plot, orange circle highlights the fracture/fault reactivation happening in the stage which seems to be at the same measured depth as the fractures created in Stage 34.

References

- Angus, D., & Verdon, J. (2013). Using Microseismicity to Estimate Formation Permeability for Geological Storage of CO₂. *ISRN Geophysics, 2013*, 1–7. <https://doi.org/10.1155/2013/160758>
- Barthwal, H., & van der Baan, M. (2019). Role of fracture opening in triggering microseismicity observed during hydraulic fracturing. *GEOPHYSICS, 84*(3), 105–118. <https://doi.org/10.1190/geo2018-0425.1>
- Caffagni, E., Eaton, D. W., Jones, J. P., & van der Baan, M. (2016). Detection and analysis of microseismic events using a Matched Filtering Algorithm (MFA). *Geophysical Journal International, 206*(1), 644–658. <https://doi.org/10.1093/gji/ggw168>
- Cipolla, C. L., & Wright, C. A. (2002). Diagnostic Techniques To Understand Hydraulic Fracturing: What? Why? and How? *SPE Production and Facilities, 17*(01), 23–35. <https://doi.org/10.2118/75359-PA>
- Eberhardt, E., & Amini, A. (2018). Hydraulic Fracturing. In P. Bobrowsky & B. Marker (Eds.), *Encyclopedia of Engineering Geology* (pp. 1–6). Springer International Publishing. https://doi.org/10.1007/978-3-319-12127-7_159-1
- Espinoza, N. (n.d.). *Hydraulic fracture design: Single fracture completion* [accessed on 2021-09-10]. <https://dnicolasespinoza.github.io/node56.html#sec:CoupledFracProblem>
- Eyre, T. S., & van der Baan, M. (2018). Microseismic insights into the fracturing behavior of a mature reservoir in the Pembina field, Alberta. *GEOPHYSICS, 83*(5), 289–303. <https://doi.org/10.1190/geo2017-0639.1>
- Hubbert, M. K., & Willis, D. G. (1957). Mechanics Of Hydraulic Fracturing. *Transactions of the AIME, 210*(01), 153–168. <https://doi.org/10.2118/686-G>
- Hummel, N., & Müller, T. M. (2009). Microseismic signatures of non-linear pore-fluid pressure diffusion. *Geophysical Journal International, 179*(3), 1558–1565. <https://doi.org/10.1111/j.1365-246X.2009.04373.x>
- Lavrov, A. (2016). Chapter 5 - Mechanisms and Diagnostics of Lost Circulation. In L. Alexandre (Ed.), *Lost Circulation* (pp. 99–162). Gulf Professional Publishing. <https://doi.org/https://doi.org/10.1016/B978-0-12-803916-8.00005-4>
- Maxwell, S. (2014). *Microseismic Imaging of Hydraulic Fracturing: Improved Engineering of Unconventional Shale Reservoirs*. Society of Exploration Geophysicists. <https://doi.org/10.1190/1.9781560803164>
- Moore, D. S., Notz, W., & Fligner, M. A. (2013). *The basic practice of statistics*. W.H. Freeman.
- Shapiro, S., & Dinske, C. (2009). Fluid-induced seismicity: Pressure diffusion and hydraulic fracturing. *Geophysical Prospecting, 57*(2), 301–310. <https://doi.org/https://doi.org/10.1111/j.1365-2478.2008.00770.x>
- Shapiro, S. A., Huenges, E., & Borm, G. (1997). Estimating the crust permeability from fluid-injection-induced seismic emission at the KTB site. *Geophysical Journal International, 131*(2), 15–18. <https://doi.org/10.1111/j.1365-246X.1997.tb01215.x>
- Ugueto, G., Todea, F., Daredia, T., Wojtaszek, M., Huckabee, P., Reynolds, A., Laing, C., & Chavarria, J. (2019). Can You Feel the Strain? DAS Strain Fronts for

- Fracture Geometry in the BC Montney, Groundbirch. *Proceedings of SPE Annual Technical Conference and Exhibition*, 15. <https://doi.org/10.2118/195943-MS>
- van der Baan, M., Eaton, D., & Dusseault, M. (2013). Microseismic Monitoring Developments in Hydraulic Fracture Stimulation. In A. P. Bunger, J. McLennan, & R. Jeffrey (Eds.), *Effective and Sustainable Hydraulic Fracturing* (p. 28). IntechOpen. <https://doi.org/10.5772/56444>
- Wright, C. A., & Weijers, L. (2001). Hydraulic fracture reorientation: Does it occur? does it matter? *The Leading Edge*, 20(10), 1185–1189. <https://doi.org/10.1190/1.1487252>

Chapter 6

Conclusions

Hydraulic fracturing is a multistage well-stimulation technique used to enable the extraction of hydrocarbons from unconventional reservoirs. Large quantities of fluid and proppants are injected at high pressures into the formation to crack the rock and create fractures that allow the trapped hydrocarbons to flow from the reservoir into the wellbore.

Understanding the geometry of these fractures is critical for designing successful unconventional reservoir completions. Distributed Acoustic Sensing is an emerging technology that measures the strain changes in the formation along a fiber optic cable by an interrogator unit, sending light pulses into the fiber and measuring the phase changes of the backscattered light. The low-frequency band of the DAS signal can be used to monitor hydraulic fractures geometry and propagation during injection.

Low-frequency DAS is very useful for monitoring hydraulic fractures during injection, but there is a clear spatial constraint as the DAS only takes strain measurements at the cable location. The integration of the LF DAS with pumping information and microseismicity helps to make a more complete interpretation of hydraulic fractures geometry and propagation, and the use of a fracture model like the PKN helps to detect stages where things did not go according to plan.

The motivation of this thesis was to study hydraulic fracture propagation at temporal and spatial scales using low-frequency DAS and pumping information as a

base and complementing the interpretation with microseismic monitoring and fracture modeling. We wanted to understand the relationship between strain changes, injection rates, microseismic events, and hydraulic fracture, as well as to identify properties and/or characteristic features of failed stages across all these analyses.

First, we analyzed the low-frequency DAS strain fronts and the pumping information for one hydraulic fracturing treatment. We determined stages that created multiple fractures, propagation direction, propagation speed, and stages where pre-existent fractures were re-stimulated.

Next, we analyzed the microseismic clouds of every stage in the treatment to get an estimation of hydraulic fractures length, height, depth, trajectory, and growth evolution. The microseismicity was projected onto the strain fronts as well in order to correlate the microseismicity to the strain changes in the medium.

Then, we used the PKN model as a detection tool to find stages where the fractures did not grow and propagate with the trajectory and speed expected. This was done by comparing the model to the results from the LF DAS and microseismicity analyses.

Finally, the expected characteristics for every one of these analyses were established, and a correlation analysis was performed. Although no correlation was found between these characteristics, it is clear that the absence of any of these characteristics indicates that something did not go according to plan. By determining the expected characteristics, we could create models of different scenarios where the hydraulic fractures did not propagate and/or grow as anticipated. The expected characteristics displayed in the different observations are:

- A noticeable heart-shaped tip in the dragonfly signal.
- Lack of the antenna signal in the dragonfly.
- Nice formation breakdown pressure peak in the bottom-hole curve.
- Fracture azimuth with perpendicular propagation.

- The r-t plot display "normal" development pattern.
- Microseismicity overlays mostly on top of the dragonfly on the strain fronts
- The fracture half-length at the DAS hit time is close to the monitoring well (within the boundaries).
- The PKN fracture and microseismic cloud have similar length.

In this treatment, it seems like all stages created new hydraulic fractures. The propagation speed of these fractures increases with the stages, but the fractures are shorter in the later stages because the injection time was reduced significantly. They also seem to close faster in later stages than in early ones. So this with the increased speeds in the later stages might indicate that the formation is more fractured towards the heel of the well, which makes it easier for fractures to propagate and for the fluids to leak into the formation.

Most hydraulic fractures propagated perpendicular from the treated well, but there are some stages where the fractures were a bit diverted due to geological and stress conditions in the formation. The stress shadows of pre-existent fractures seem to have a particularly strong relation with this, and we can see this when multiple fractures are created in the stage with enough space to see multiple dragonflies. They are created towards the heel of the well, away from the stress shadow of the previous hydraulic fracture.

There seems to be a stress gradient that makes it easier for the fractures to propagate towards the NE, but the horizontal stresses are very similar, so when the NE direction is too stressed the hydraulic fractures change directions towards the SW. This was the third well fractured in a four well operation and it is noticeable in most of the analyses (the presence of antennas in the strain fronts, and the "reactivation" pattern in the r-t plots).

From this study, we learned that acquiring different records during hydraulic fracturing is necessary to make a suitable interpretation of hydraulic fractures. DAS data analysis benefits from being supported by other diagnostic tools. The integrated observations give us estimations on fracture propagation speed, length, and trajectory. These integrated observations show good agreement between them in many cases, however, in some cases, they exhibit modest to poor agreement. This gives us an idea that something unexpected happened during the stage.

6.1 Suggested future research

In this work, the fracture characteristics present in the strain fronts were visually picked out. The development of an algorithm that detects these characteristics can be very useful in making the selection more precise and less time-consuming.

The modelling of strain responses of hydraulic fractures with different parameters and characteristics can help to determine what causes the dragonfly shapes and so help in the interpretation of the strain fronts. This is very important as there are a lot of characteristics on the strain fronts that we do not know what produces them.

The computation of the injected energy per stage could be very useful to compare with the number of events per stage, or cumulative radiated energy to see seismic efficiency. Also, the comparison of the microseismic events magnitudes with the strain values can give us information of the relationship between them.

The PKN model is very useful for detecting stages where the hydraulic fractures did not grow and/or propagate as expected. However, the use of a more sophisticated model that takes into consideration more parameters can improve accuracy.

In future works, we can integrate more records available of this treatment like Distributed Temperature Sensing (DTS), to keep building on the interpretation and learning more about LF DAS.

Bibliography

- Alberta Energy Regulator. (n.d.). *Hydraulic Fracturing* [accessed on 2022-04-12]. <https://www.aer.ca/providing-information/by-topic/hydraulic-fracturing>
- Angus, D., & Verdon, J. (2013). Using Microseismicity to Estimate Formation Permeability for Geological Storage of CO₂. *ISRN Geophysics, 2013*, 1–7. <https://doi.org/10.1155/2013/160758>
- API HF1. (2009). Hydraulic Fracturing Operations, Well Construction and Integrity Guidelines. *American Petroleum Institute, 36*.
- Asgarpour, S. (2013). The modern practices of hydraulic fracturing: A focus on canadian resources. *52*, 83–85.
- Baig, A., & Urbancic, T. (2010). Magnitude Determination, Event Detectability, and Assessing the Effectiveness of Microseismic Monitoring Programs in Petroleum Applications. *CSEG Recorder, 35*, 5.
- Ballotpedia. (n.d.). *Slurry* [accessed on 2022-04-18]. <https://ballotpedia.org/Slurry>
- Barthwal, H., & van der Baan, M. (2019). Role of fracture opening in triggering microseismicity observed during hydraulic fracturing. *GEOPHYSICS, 84*(3), 105–118. <https://doi.org/10.1190/geo2018-0425.1>
- Becker, M., Ciervo, C., & Coleman, T. (2018). Laboratory testing of low-frequency strain measured by distributed acoustic sensing (DAS). *SEG Technical, 3*. <https://doi.org/10.1190/segam2018-2997900.1>
- Becker, M., Coleman, T., & Ciervo, C. (2020). Distributed Acoustic Sensing (DAS) as a Distributed Hydraulic Sensor in Fractured Bedrock. *Bedrock. Water Resources Research, 56*(9), 10. <https://doi.org/10.1002/essoar.10503402.1>
- Belyadi, H., Fathi, E., & Belyadi, F. (2019a). Chapter Eleven - Horizontal well multistage completion techniques. In H. Belyadi, E. Fathi, & F. Belyadi (Eds.), *Hydraulic Fracturing in Unconventional Reservoirs (Second Edition)* (Second Edition, pp. 177–189). Gulf Professional Publishing. <https://doi.org/https://doi.org/10.1016/B978-0-12-817665-8.00011-4>
- Belyadi, H., Fathi, E., & Belyadi, F. (2019b). Chapter Fifteen - Numerical simulation of hydraulic fracturing propagation. In H. Belyadi, E. Fathi, & F. Belyadi (Eds.), *Hydraulic Fracturing in Unconventional Reservoirs (Second Edition)* (Second Edition, pp. 257–272). Gulf Professional Publishing. <https://doi.org/https://doi.org/10.1016/B978-0-12-817665-8.00015-1>
- Caffagni, E., & Bokelmann, G. (2017). Spatiotemporal Evolution of Microseismicity and Repeating Earthquakes in Haiti, 64.

- Caffagni, E., Eaton, D. W., Jones, J. P., & van der Baan, M. (2016). Detection and analysis of microseismic events using a Matched Filtering Algorithm (MFA). *Geophysical Journal International*, 206(1), 644–658. <https://doi.org/10.1093/gji/ggw168>
- Cipolla, C. L., & Wright, C. A. (2002). Diagnostic Techniques To Understand Hydraulic Fracturing: What? Why? and How? *SPE Production and Facilities*, 17(01), 23–35. <https://doi.org/10.2118/75359-PA>
- Cole, S., Karrenbach, M., Boone, K., Ridge, A., Kahn, D., Rich, J., Silver, K., & Langton, D. (2017). Effective Diffusivity Estimates from Distributed Fiber-optic Strain and Microseismic Measurements. *SEG Technical Program*, 5. <https://doi.org/10.1190/segam2017-17680716.1>
- Davey, H. (2012). *Geomechanical characterization of the Montney Shale northwest Alberta and northeast British Columbia, Canada* (Doctoral dissertation). Colorado School of Mines.
- Davies, G. R. (1997). The Triassic of the Western Canada Sedimentary Basin: Tectonic and Stratigraphic Framework, Paleogeography, Paleoclimate and Biota. *Bulletin of Canadian Petroleum Geology*, 45, 434–460.
- Davies, G. R., Moslow, T. F., & Sherwin, M. D. (1997). The Lower Triassic Montney Formation, West-Central Alberta. *Bulletin of Canadian Petroleum Geology*, 45, 474–505.
- Djabelkhir, N. (2020). *Simulation Of Notch Driven Hydraulic Fracture In Open Hole Completion* (Doctoral dissertation). University of North Dakota.
- Duenas, C., Davis, T., & Damico, D. (2014). *Understanding Rock Quality Heterogeneity Using Combined Multicomponent Seismic Inversion and Well Log Cluster Analysis. Montney Shale Reservoir, Pouce Coupe Field, Alberta, Canada*. <https://doi.org/10.15530/urtec-2014-1921332>
- Dutler, N., Valley, B., Gischig, V., Jalali, M., Brixel, B., Krietsch, H., Roques, C., & Amann, F. (2020). Hydromechanical insight of fracture opening and closure during in-situ hydraulic fracturing in crystalline rock. *International Journal of Rock Mechanics and Mining Sciences*, 135, 17. <https://doi.org/10.1016/j.ijrmms.2020.104450>
- Eaton, D. W. (2018). Stress Measurement and Hydraulic Fracturing. *Passive Seismic Monitoring of Induced Seismicity: Fundamental Principles and Application to Energy Technologies* (pp. 95–126). Cambridge University Press. <https://doi.org/10.1017/9781316535547.005>
- Eberhardt, E., & Amini, A. (2018). Hydraulic Fracturing. In P. Bobrowsky & B. Marker (Eds.), *Encyclopedia of Engineering Geology* (pp. 1–6). Springer International Publishing. https://doi.org/10.1007/978-3-319-12127-7_159-1
- Espinoza, N. (n.d.). *Hydraulic fracture design: Single fracture completion* [accessed on 2021-09-10]. <https://dnicolasespinoza.github.io/node56.html#sec:CoupledFracProblem>
- Eyre, T. S., & van der Baan, M. (2018). Microseismic insights into the fracturing behavior of a mature reservoir in the Pembina field, Alberta. *GEOPHYSICS*, 83(5), 289–303. <https://doi.org/10.1190/geo2017-0639.1>
- Fernandez-Ruiz, M., Soto, M., Williams, E., Martinez-Lopez, S., Zhan, Z., Gonzales-Herraez, M., & Martins, H. (2020). Distributed acoustic sensing for seismic

- activity monitoring. *APL Photonics*, 5(3), 16. <https://doi.org/10.1063/1.5139602>
- FrackOptima. (n.d.). *PKN Hydraulic Fracturing Model* [accessed on 2021-09-10]. <http://www.frackoptima.com/userguide/theory/pkn.html>
- Garikapati, H., Verhoosel, C. C., van Brummelen, E. H., Zlotnik, S., & Diez, P. M. B. (2018). Sampling-based stochastic analysis of the PKN model for hydraulic fracturing. *Computational Geosciences*, 23, 81–105.
- Geertsma, J., & De Klerk, F. (1969). A Rapid Method of Predicting Width and Extent of Hydraulically Induced Fractures. *Journal of Petroleum Technology*, 21(12), 1571–1581. <https://doi.org/10.2118/2458-PA>
- Grubert, M., Li, X., & Chavarria, A. (2020). Making sense of unconventional with DAS, journal=Oilfield Technology. 13(1), 21–24.
- Hanks, T. C., & Kanamori, H. (1979). A moment magnitude scale. *Journal of Geophysical Research: Solid Earth*, 84(B5), 2348–2350. <https://doi.org/https://doi.org/10.1029/JB084iB05p02348>
- Hartog, A. (2017). *An introduction to distributed optical fibre sensors*. CRC Press. <https://doi.org/10.1201/9781315119014>
- Hubbert, M. K., & Willis, D. G. (1957). Mechanics Of Hydraulic Fracturing. *Transactions of the AIME*, 210(01), 153–168. <https://doi.org/10.2118/686-G>
- Hummel, N., & Müller, T. M. (2009). Microseismic signatures of non-linear pore-fluid pressure diffusion. *Geophysical Journal International*, 179(3), 1558–1565. <https://doi.org/10.1111/j.1365-246X.2009.04373.x>
- Jalili, S., & Ahangari, K. (2017). Effects of different stress regimes on hydraulic fracture geometry: a particle flow code approach. *Innovative Infrastructure Solutions*, 2, 6. <https://doi.org/10.1007/s41062-017-0096-1>
- Jin, G., & Roy, B. (2017). Hydraulic-fracture geometry characterization using low-frequency DAS signal. *The Leading Edge*, 36, 975–980.
- Jin, G., & Roy, B. (2019). Using Distributed Acoustic Sensing to Monitor Hydraulic Fracturing Operations, 5.
- Karrenbach, M., Ridge, A., Cole, S., Boone, K., Rich, J., Silver, K., & Langton, D. (2017). DAS Microseismic Monitoring and Integration With Strain Measurements in Hydraulic Fracture Profiling, 1316–1330. <https://doi.org/10.15530/urtec-2017-2670716>
- Kavousi, P., Wilson, T., Carr, T., Kumar, A., Hammack, R., & Di, H. (2018). Integrating Distributed Acoustic Sensing (DAS), Borehole 3C Geophone Array, and Surface Seismic Array Data to Identify Long-Period Long-Duration Seismic Events during Stimulation of a Marcellus Shale Gas Reservoir. *Interpretation*, 7(1), 1–37. <https://doi.org/10.1190/int-2018-0078.1>
- Kendall, D. R. (1999). Sedimentology and stratigraphy of the lower triassic Montney formation, Peace River basin, subsurface of northwestern Alberta. <https://doi.org/10.11575/PRISM/10182>
- Khrstianovitch, S., & Zheltov, Y. (1955). *Formation of Vertical Fractures by Means of Highly Viscous Liquid* (Vol. All Days).
- Kim, J., Um, E., & Moridis, G. (2014). Fracture Propagation Fluid Flow and Geomechanics of Water Based Hydraulic Fracturing in Shale Gas Systems and

- Electromagnetic Geophysical Monitoring of Fluid Migration, 18. <https://doi.org/10.2118/168578-MS>
- Lavrov, A. (2016). Chapter 5 - Mechanisms and Diagnostics of Lost Circulation. In L. Alexandre (Ed.), *Lost Circulation* (pp. 99–162). Gulf Professional Publishing. <https://doi.org/https://doi.org/10.1016/B978-0-12-803916-8.00005-4>
- Le Calvez, J., Malpani, R., Xu, J., Stokes, J., & Williams, M. (2016). Hydraulic fracturing insights from microseismic monitoring. *28*, 16–33. <https://doi.org/10.1190/int-2018-0078.1>
- Lee, B., Lee, Y. W., & Song, M. (2006). *Guided Wave Optical Components and Devices*. Elsevier Academic Press. <https://doi.org/10.1016/B978-012088481-0/50027-9>
- Lellouch, A., Schultz, R., Lindsey, N., Biondi, B., & Ellsworth, W. (2020). Low-magnitude Seismicity with a Downhole Distributed Acoustic Sensing Array – examples from the FORGE Geothermal Experiment. *Journal of Geophysical Research: Solid Earth*, *27*, 20.
- Li, L., Tan, J., Schwarz, B., Stanek, F., Poiata, N., Shi, P., Diekmann, L., Eisner, L., & Gajewski, D. (2020). Recent Advances and Challenges of Waveform-Based Seismic Location Methods at Multiple Scales. *Reviews of Geophysics*, *47*. <https://doi.org/10.1029/2019RG000667>
- Liu, Y., Wu, K., Jin, G., & Moridis, G. (2020). Rock Deformation and Strain-Rate Characterization during Hydraulic Fracturing Treatments: Insights for Interpretation of Low-Frequency Distributed Acoustic-Sensing Signals. *SPE Journal*, *25*(05), 2251–2264. <https://doi.org/10.2118/202482-PA>
- Mahmoud, A., Gowida, A., Aljawad, M., Al R., M., & Ibrahim, A. (2021). Advancement of Hydraulic Fracture Diagnostics in Unconventional Formations. *Geofluids*, *2021*, 17. <https://doi.org/10.1155/2021/4223858>
- Maxwell, S. (2014). *Microseismic Imaging of Hydraulic Fracturing: Improved Engineering of Unconventional Shale Reservoirs*. Society of Exploration Geophysicists. <https://doi.org/10.1190/1.9781560803164>
- Mellors, R., Sherman, C., Fu, P., McLennan, J., Morris, J., Ryerson, F., & Morency, C. (2019). Potential Use of Distributed Acoustic Sensors to Monitor Fractures and Microseismicity at the FORGE EGS site. *44th Workshop on Geothermal Reservoir Engineering*, 6.
- Molenaar, M., & Cox, B. (2013). Field cases of hydraulic fracture stimulation diagnostics using fiber optic distributed acoustic sensing (DAS) measurements and Analyses, 10. <https://doi.org/10.2118/164030-MS>
- Moore, D. S., Notz, W., & Fligner, M. A. (2013). *The basic practice of statistics*. W.H. Freeman.
- Muanenda, Y. (2018). Recent Advances in Distributed Acoustic Sensing Based on Phase-Sensitive Optical Time Domain Reflectometry. *Journal of Sensors*, *23*, 1–16. <https://doi.org/10.1155/2018/3897873>
- Muanenda, Y., Oton, C. J., & Di Pasquale, F. (2019). Application of Raman and Brillouin Scattering Phenomena in Distributed Optical Fiber Sensing. *Frontiers in Physics*, *7*, 155.
- Nolen, R. (2013). Elements of hydraulic fracturing. *Oilfield Review*, *25*, 51–52.

- Oil and gas overview. (n.d.). *Basic Hydraulic Fracturing Calculations* [accessed on 2022-04-18]. <https://oilandgasoverview.com/basic-hydraulic-fracturing-calculations/>
- Parker, T., Shatalin, S., & Farhadiroushan, M. (2014). Distributed Acoustic Sensing, A new tool for seismic applications. *First Break*, 32, 9.
- Paschotta, R. . (n.d.). *RP PHOTONICS ENCYCLOPEDIA* [accessed on 2020-09-20]. https://www.rp-photonics.com/rayleigh_scattering.html
- Prenoslo, D., Furlong, C. M., Gingras, M., Playter, T., & Zonneveld, J. (2018). The sedimentology, stratigraphy and reservoir characteristics of the Montney D1 and D2 horizons in the Greater Pouce Coupe area. *Bulletin of Canadian Petroleum Geology*, 66, 338–358.
- Richter, P., Parker, T., Woerpel, C., Wu, Y., Rufino, R., & Farhadiroushan, M. (2019). Hydraulic fracture monitoring and optimization in unconventional completions using a high-resolution engineered fibre-optic Distributed Acoustic Sensor, 6. Schlumberger. (n.d.). *Breakdown pressure* [accessed on 2022-04-19]. https://glossary.oilfield.slb.com/en/terms/b/breakdown_pressure
- Shapiro, S. A., Dinske, C., & Rothert, E. (2006). Hydraulic-fracturing controlled dynamics of microseismic clouds. *Geophysical Research Letters*, 33(14), 5. <https://doi.org/https://doi.org/10.1029/2006GL026365>
- Shapiro, S., & Dinske, C. (2009). Fluid-induced seismicity: Pressure diffusion and hydraulic fracturing. *Geophysical Prospecting*, 57(2), 301–310. <https://doi.org/https://doi.org/10.1111/j.1365-2478.2008.00770.x>
- Shapiro, S. A., Huenges, E., & Borm, G. (1997). Estimating the crust permeability from fluid-injection-induced seismic emission at the KTB site. *Geophysical Journal International*, 131(2), 15–18. <https://doi.org/10.1111/j.1365-246X.1997.tb01215.x>
- Sharma, J., cuny theo, t., Ogunsanwo, T., & Santos, O. (2020). Low-frequency distributed acoustic sensing for early gas detection in a wellbore. *IEEE Sensors Journal*, PP, 15. <https://doi.org/10.1109/JSEN.2020.3038738>
- Smith, T. M., Sayers, C. M., & Sondergeld, C. H. (2009). Rock properties in low-porosity/low-permeability sandstones. *The Leading Edge*, 28(1), 48–59. <https://doi.org/10.1190/1.3064146>
- Trenchlesspedia. (n.d.). *Bottomhole Pressure (BHP)* [accessed on 2022-04-18]. <https://www.trenchlesspedia.com>
- Ugueto, G., Todea, F., Daredia, T., Wojtaszek, M., Huckabee, P., Reynolds, A., Laing, C., & Chavarria, J. (2019). Can You Feel the Strain? DAS Strain Fronts for Fracture Geometry in the BC Montney, Groundbirch. *Proceedings of SPE Annual Technical Conference and Exhibition*, 15. <https://doi.org/10.2118/195943-MS>
- van der Baan, M., Eaton, D., & Dusseault, M. (2013). Microseismic Monitoring Developments in Hydraulic Fracture Stimulation. In A. P. Bunger, J. McLennan, & R. Jeffrey (Eds.), *Effective and Sustainable Hydraulic Fracturing* (p. 28). IntechOpen. <https://doi.org/10.5772/56444>

- Wang, H. (2019). Hydraulic fracture propagation in naturally fractured reservoirs: Complex fracture or fracture networks. *Journal of Natural Gas Science and Engineering*, 68, 14. <https://doi.org/10.1016/j.jngse.2019.102911>
- Wang, H., Li, M., & Shang, X. (2016). Current developments on micro-seismic data processing. *Journal of Natural Gas Science and Engineering*, 32, 521–537. <https://doi.org/10.1016/j.jngse.2016.02.058>
- Warpinski, N., Mayerhofer, M., Bridges, A., & Du, J. (2013). Hydraulic-Fracture Geomechanics and Microseismic-Source Mechanisms. *SPE Journal*, 18(04), 766–780. <https://doi.org/10.2118/158935-PA>
- Webster, P., Cox, B., Molenaar, M., & Canada, S. (2013). Developments in Diagnostic Tools for Hydraulic Fracture Geometry Analysis. *Unconventional Resources Technology Conference, Denver, Colorado, USA*, 218–224.
- Webster, P., Wall, J., Perkins, C., & Molenaar, M. (2013b). Microseismic detection using distributed acoustic sensing, 2459–2463.
- White, M., Frieauf, K., Cramer, D., Constantine, J., Zhang, J., Schmidt, S., Long, J., Mislan, P., Spencer, J., Meier, P., & Davis, E. (2020). *One Stage Forward or Two Stages Back, What are We Treating? Identification of Internal Casing Erosion During Hydraulic Fracturing - A Montney Case Study Using Ultrasonic and Fiber-Optic Diagnostics* (Vol. Day 2 Tue, October 27, 2020) [D021S016R006]. <https://doi.org/10.2118/201734-MS>
- Wright, C. A., & Weijers, L. (2001). Hydraulic fracture reorientation: Does it occur? does it matter? *The Leading Edge*, 20(10), 1185–1189. <https://doi.org/10.1190/1.1487252>
- Xiang, J. (2012). *A PKN Hydraulic Fracture Model Study and Formation Permeability Determination* (Master's thesis). Texas AM University.
- Xiao, C., Tian, L., Zhang, Y., Hou, T., Yang, Y., deng, Y., Wang, Y., & Chen, S. (2017). A Novel Approach To Detect Interacting Behavior Between Hydraulic Fracture and Natural Fracture by Use of Semianalytical Pressure-Transient Model. *SPE Journal*, 22, 22. <https://doi.org/10.2118/187954-PA>
- Yu, C., Zhan, Z., Lindsey, N., Ajo-Franklin, J., & Robertson, M. (2019). The potential of distributed acoustic sensing (DAS) in teleseismic studies: insights from the Goldstone experiment, *Journal of Geophysical Research Letters*, 46. <https://doi.org/10.1029/2018GL081195>
- Zoback, M. D., Haimson, B. C., & Jacobson, M. L. (1982). *Proceedings of Workshop XVII; workshop on hydraulic fracturing stress measurements* (Vol. 1 and 2). U.S. Geological Survey.
- Zoback, M. D., & Kohli, A. H. (2019). Stimulating Production from Unconventional Reservoirs. *Unconventional Reservoir Geomechanics: Shale Gas, Tight Oil, and Induced Seismicity* (pp. 231–374). Cambridge University Press.